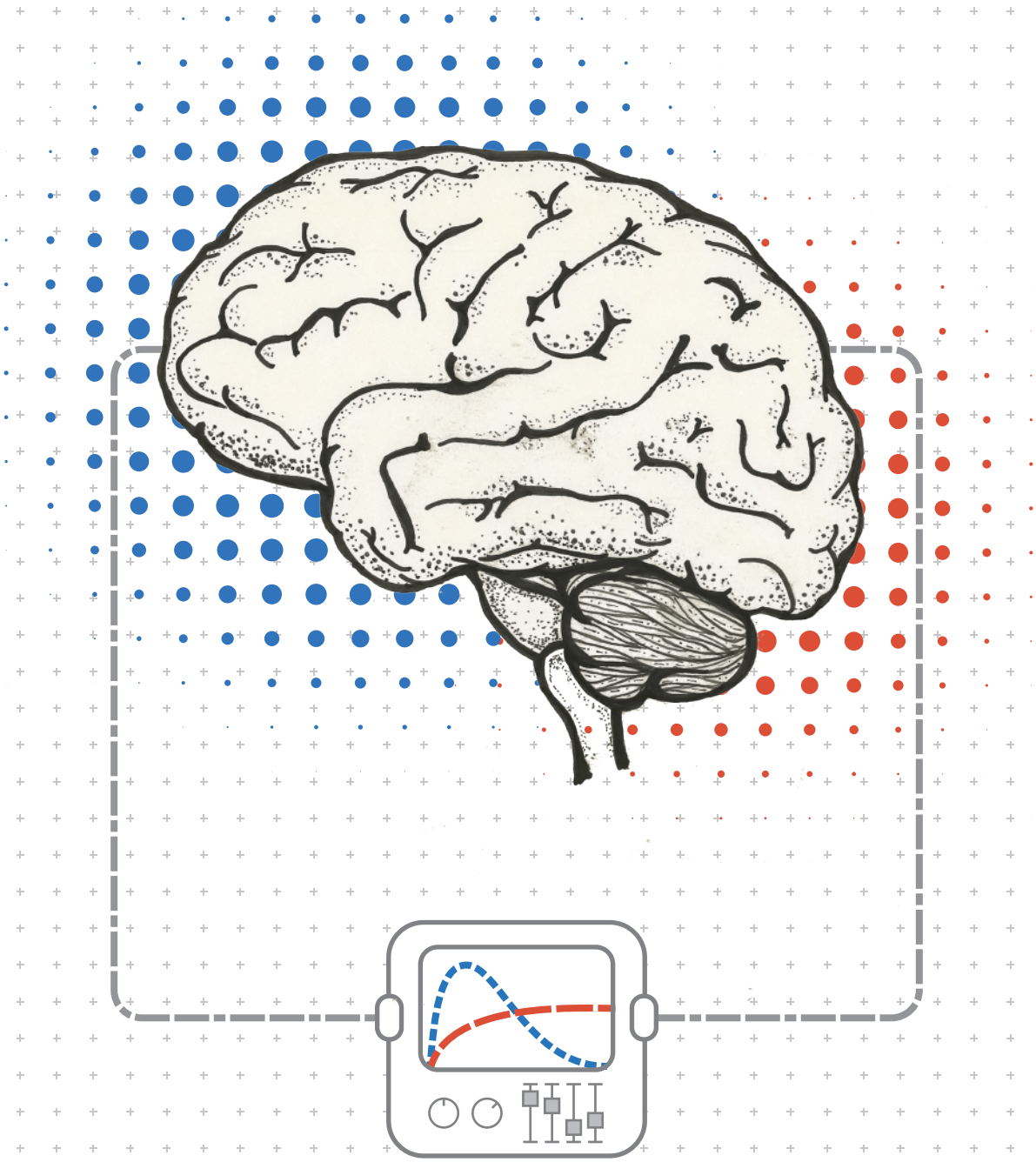

Optimal Tracking of the Fast and Slow States of Sensorimotor Adaptation for Rehabilitation Robotics

Ashwin George

Master of Science Thesis

Master of Science Thesis

Optimal Tracking of the Fast and Slow States of Sensorimotor Adaptation for Rehabilitation Robotics

by

Ashwin George

to obtain the degree of Master of Science
at the Delft University of Technology,

Student number:	4738640	
Project duration:	January 1, 2019 – July 28, 2020	
Thesis committee:	Prof. Dr. -Ing. Heike Vallery,	TU Delft, Supervisor
	Prof. Dr. Maarten Frens,	Erasmus MC, Supervisor
	Ir. Andrew Berry,	TU Delft, Supervisor
	Dr. Luka Peternel,	TU Delft

This report is confidential and cannot be made public until July 31, 2023.

TU Delft

Abstract

Robotic assistance for rehabilitation has benefited from the use of models for motor adaptation. The assist-as-needed paradigm for rehabilitation robotics was based on a single-state model of human adaptation to a neurological handicap. Recent studies have shown that human motor adaptation consists of two or more parallel adaptation processes. A two-state model of adaptation based on the presence of a fast process and a slow process has been widely adopted. The fast process adapts faster than the slow process but has a lower retention than the slow process. Designing training methods that can influence the individual adaptation processes could help make sure that patients retain what is desired (how to adapt to a neurological injury) and forget what is detrimental to rehabilitation (dynamics of the robotic assistance for example). The goal of this work is to design an optimal control paradigm for selectively influencing the slow and fast processes.

A feedforward discrete-time linear-quadratic tracking controller was designed for a 2-state linear time-invariant model of sensorimotor adaptation to increase the contribution of the slow process to the net adaptation at the end of training. This control signal was implemented as the sequence of visuomotor rotations in an upper-limb reaching task. This sequence of visuomotor rotations were dubbed the Adaptation-State-Tracking (AST) perturbation. The retention behaviour after this AST perturbation was compared with that after a non-adaptive (constant-level) perturbation. A between-subject comparison of the retention behaviour showed that the AST perturbation exhibited better retention than the constant-level perturbation ($p = 0.0415$). As far as the author is aware, this is first time the 2-state Linear Time-Invariant (LTI) model has been used to design a perturbation and to predict the subsequent behaviour of the participants. The sufficiency of the control based on the 2-state LTI model and the possibility of improving retention with optimal control could positively impact the domain of robot-assisted rehabilitation.

Contents

List of Figures

List of Tables

List of Abbreviations and Indices

∞ ..... Steady State (at Infinite Time)
$\mathbf{T}$ ..... terminal

AAN ..... Assist-As-Needed
ANOVA ..... Analysis of Variance
AST ..... Adaptation-State-Tracking

CL ..... Constant-Level

DMA ..... Difference in Movement Angles
DOF ..... Degrees of Freedom

EM ..... Expectation Maximisation

f ..... Fast

H ..... Human

ITI ..... Inter-Trial Interval

LQT ..... Linear-Quadratic Tracking
LTI ..... Linear Time-Invariant

MA ..... Movement Angle
MPC ..... Model Predictive Control
MSE ..... Mean Squared Error
MSMA ..... Mean Scaled Movement Angle

PDP ..... Process-Dissociation Procedure

R ..... Robot
r ..... Reference

s ..... Slow

1 Introduction

1.1. Motivation

1.1.1. Robot-Assisted Rehabilitation

The human nervous system with all its complex circuits and feedback loops plays a crucial role in controlling the movement of the human body. A neurological injury (like cerebrovascular accident or incomplete spinal cord injury) can lead to abnormalities in the motor function. Rehabilitation efforts to aid recovery from such neurological injuries involves providing assistance to patients for performing movements. Conventionally, therapists provide the necessary forces and support for the patients. In many cases, like gait training, this involves the application of large and repetitive forces often from uncomfortable poses. These can lead to strain and injuries for the therapists themselves. This is where robotic assisted rehabilitation becomes relevant. Robots can be designed to give consistent forces and movement patterns.

As the patients progressively learn, the level of assistance must be modulated so that eventually the patient can perform the actions without any assistance. Experienced therapists can intuitively modulate the level of assistance based on feedback from the patient. Robotic devices, on the other hand, lack this intuition. Hence, there is a need for designing the mechanisms by which robotic assistance changes as the patient learns.

Reinkensmeyer [2003] proposed that neurological injuries affect the sensorimotor mapping between sensory inputs and muscular activations. Reinkensmeyer et al. [2004] modelled the recovery process from a neurological injury as the adaptation to a new sensorimotor mapping. Based on these assumptions, Reinkensmeyer et al. [2004] designed the Assist-As-Needed (AAN) paradigm for rehabilitation robotics. According to the AAN paradigm the level of robotic assistance is slowly decreased as movement errors decrease. At the start of adaptation, the movement errors will be large. As rehabilitation progresses, the patient will slowly adapt and the movement errors will decrease. If the robotic assistance is not modulated, the patient will stop adapting and let the robot do most of the work. AAN forces the patient to adapt more and in the end, the share of the robot will be minimal.

Reinkensmeyer et al. [2004] modelled the rehabilitation behaviour by considering that the muscle force applied on a given trial ($x(k+1)$) is based on the muscle forces applied on the previous trial ($x(k)$) and the movement error on the previous trial ($e(k)$). The retention rate (a_{H}) dictates how much of the muscle forces on the previous trial influence those on the next trial. The learning rate (b_{H}) captures how the error in each trial influences the muscle forces. Thus the forces applied by the patient on each trial is governed by the equation

$$x(k+1) \quad = \quad a_{\mathrm{H}} \cdot x(k) + b_{\mathrm{H}} \cdot e(k). \tag{1.1}$$

In AAN, the robotic assistance at each trial ($\rho(k)$) is updated based on the movement error (e) as

$$\rho(k+1) \quad = \quad a_{\mathrm{R}} \cdot \rho(k) + b_{\mathrm{R}} \cdot e(k), \tag{1.2}$$

for the retention rate (a_{R}) and learning rate (b_{R}) chosen for the robot. With this control law it was shown that the human learns progressively if $a_{\mathrm{R}} < a_{\mathrm{H}}$[1].

[1] More details regarding the AAN rehabilitation is provided in Appendix A.

The adaptation model in Eq. (1.1) has only one state of adaptation (x_H). Recent advances in the field of neuroscience have hinted at the existence of multiple processes of adaptation (Smith et al. [2006]). This has led to models with more than one state of adaptation.

1.1.2. Single Process Vs Multiple Processes

Sensorimotor adaptation is the process of making adjustments in learned motor behaviour in response to changes in the dynamics of the body or the environment. These updates occur in a feedforward fashion as past experience of movement errors is used to update the motor commands for subsequent movements. Motor adaptation is a subset of the broader field of motor function (which includes other topics like motor skill learning and motor control). Motor adaptation is considered to be driven by sensorimotor error ($e(k)$) which can be caused by errors in sensing, planning or movement execution. As a response to this sensorimotor errors the nervous system make adjustments in order to minimise the error. The actual adjustments made are distributed over different aspects of the motor control loop. In order to save the trouble of keeping track of all these intricate changes, adaptation is usually studied in terms of an adaptation index. The adaptation index is a metric that encapsulates all the intricate changes associated with an adaptation task. Examples of adaptation indices are mean force applied per trial for a force-field adaptation and mean movement angle per trial for adaptation to a visuomotor adaptation. In Eq. (1.1), the adaptation index is the muscle force applied per trial ($x_H(k)$).

The single-state model of adaptation as shown in Eq. (1.1) cannot account for a range of behavioural findings in motor adaptation experiments. According to the one-state model, only the previous adaptation state ($x(k)$) and the sensorimotor error ($e(k)$) influence the next adaptation state ($x(k+1)$). As per this model, irrespective of the number of times participants have experienced a perturbation, as long they start from the same baseline adaptation level, they should exhibit identical behaviour. Experiments have shown that this is not the case and that the history of perturbations experienced by the participant have an effect on adaptation behaviour. Some of the behavioural effects[2] that are not explained by the single-state model of adaptation (as per Smith et al. [2006]) are:

- *Savings* — Faster re-adaptation from baseline behaviour to a perturbation that was previously experienced.
- *Anterograde Interference* — Slower adaptation from baseline behaviour to a perturbation in the opposite direction to that of a previously adapted perturbation.
- *Rapid De-adaptation* to baseline behaviour when the perturbation is removed.
- *Accelerated Re-adaptation* to a downscaled version of a previously experienced perturbation.
- *Spontaneous Recovery* from baseline behaviour after Error-Clamp Trials (in which error feedback is set to zero) following de-adaptation.

In response to these behavioural effects, different dichotomies have been suggested for separating the net adaptation into component processes [3]. The prominent dichotomies are the fast-slow and the explicit-implicit dichotomies. Section 1.2 provides a detailed introduction of the fast-slow and explicit-implicit dichotomies.

1.1.3. Rehabilitation based on Multiple Processes

As per the AAN paradigm of robotic rehabilitation, the most important metric to be considered is the adaptation index at the end of training ($x(k_T)$, for the final adaptation trial k_T). However, the existence of behavioural effects mentioned in Section 1.1.2 means that in addition to the final adaptation state, the history of the perturbation also plays a role in deciding the outcome of a rehabilitation intervention.

The effect of rehabilitation interventions usually decay with time and hence multiple training sessions are required for complete rehabilitation. Designing a training paradigm which improves retention can potentially reduce the number of training sessions needed for complete rehabilitation. The current work explores how the multiple process models of adaptation can be used to design a training paradigm for improving retention. As an initial step in this direction the current work looks at how perturbation schedules can be optimised for improving retention in adaptation experiments for healthy participants.

[2] A brief summary of the different adaptation tasks and the behavioural effects can be found in Appendices B.1 and B.2.
[3] More information from a literature survey on the multiple component processes of adaptation is included in Appendix C.

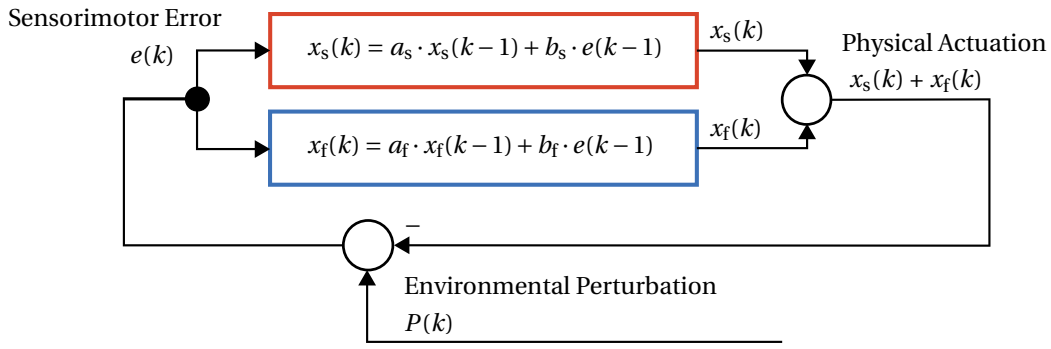

Figure 1.1: Block diagram showing the fast and slow processes arranged in parallel. Both processes are driven by the same sensorimotor error. The fast process has a higher learning rate ($b_f > b_s$). The slow process has more retention ($a_s > a_f$).

1.2. Multiple-Process Models of Adaptation

1.2.1. Fast-Slow Dichotomy

To account for the behavioural effects like savings, Smith et al. [2006] suggested that there are multiple interacting adaptive processes which together contribute to sensorimotor adaptation. Smith et al. [2006] proposes that motor adaption within a timescale of minutes has two distinct components - a *fast process* (x_f) and a *slow process*(x_s). The fast process has a faster learning rate(b_f) but a lower retention(a_f) and the slow process has a lower learning rate(b_s) but a higher retention(a_s). Both these process are adapted based on the sensorimotor error($e(k)$) experienced during each trial. The net motor output is a the result of the superposition of both the slow and fast processes (Fig. 1.1). Smith et al. [2006] has mathematically modelled these processes as follows:

$$\begin{aligned} x_s(k+1) &= a_s \cdot x_s + b_s \cdot e(k) \\ x_f(k+1) &= a_f \cdot x_f + b_f \cdot e(k) \\ x(k) &= x_s(k) + x_f(k) \\ 0 < b_s < b_f < 1 \,,\, 0 < a_f < a_s < 1 \end{aligned} \tag{1.3}$$

The fast process is crucial for the quick adaptation to transient perturbations like change in the weight of an object being lifted or in the slope of a hill being climbed. The slow process helps retain the adaptations in response to more steady perturbations like growth of the limbs[4]. Thus together they help the body adapt to a whole range of perturbations over different timescales.

This model (Eq. (1.3)) was fit onto experimental data from adaptation experiments. It could explain those characteristics mentioned earlier that the single state model cannot explain and is the most widely used model in literature (Smith et al. [2006], Kording et al. [2007], C-Hemminger and Shadmehr [2008], Ethier et al. [2008], Joiner and Smith [2008], Zarahn et al. [2008], Huang and Shadmehr [2009], Lee and Schweighofer [2009], Keisler and Shadmehr [2010], Sing and Smith [2010], Turnham et al. [2012], Trewartha et al. [2014], Colagiorgio et al. [2015], Inoue et al. [2015], Kim et al. [2015], McDougle et al. [2015], McDougle et al. [2017], Albert and Shadmehr [2018], Charalambous et al. [2018], Coltman et al. [2019], van Es and Knapen [2019]). More complex variants of fast-slow model have been suggested in literature [5].

The fast and slow processes have distinctive characteristics like generalisation (how adapting to one perturbation can benefit adaptation to other perturbations) and effector-dependence (e.g., how adapting with the right hand differs from adapting with the left hand). These characteristics are summarized in Table 1.1.

1.2.2. Explicit-Implicit Dichotomy

Mazzoni and Krakauer [2006] and Taylor et al. [2014] have observed another dichotomy in the contributing processes to sensorimotor adaptation - an *explicit process* and an *implicit process*. The explicit process is an aiming strategy (like, aiming 10 cm above the bullseye while throwing darts) of which the adapting organism

[4] It is possible that an ultra-slow process is responsible for the adaptation to limb growth that persists over very long timescales (Inoue et al. [2015]).

[5] Refer to Table C.5 on Appendix C for a summary of the different mathematical models of sensorimotor adaptation.

Table 1.1: Characteristics of the Fast and Slow Processes of Adaptation which were introduced by Smith et al. [2006].

Characteristics of Fast and Slow Processes	
Fast Process	**Slow Process**
More *learning rate* (Smith et al. [2006]).	Lower *learning rate* (Smith et al. [2006]).
Lower *retention rate* (Smith et al. [2006]).	More *retention rate* (Smith et al. [2006]).
Does not contribute much towards long-term *retention* (Joiner and Smith [2008],Charalambous et al. [2018]). But, is crucial for adaptations to sudden perturbations (Smith et al. [2006]).	Contributes more towards long-term *retention* (Joiner and Smith [2008],Charalambous et al. [2018]).
The fast process is *disrupted* by a secondary *declarative task* (Keisler and Shadmehr [2010]).	The slow process is *enhanced* when a task disrupts the fast process (Keisler and Shadmehr [2010]).
Dominates in cases of *rapid perturbation changes* (Pelisson et al. [2010]).	Dominates in cases of *gradual perturbation changes* (Pelisson et al. [2010]).
The fast process shows greater *generalisation* and is *effector-independent* (Keisler and Shadmehr [2010], Mandelblat-Cerf et al. [2011]).	The slow process shows lesser *generalisation* and is driven by *intrinsic coordinates* (Keisler and Shadmehr [2010], Mandelblat-Cerf et al. [2011]).

has conscious control and awareness. The implicit process results in a change in the internal model of which the organism is not consciously aware.

Taylor et al. [2014] isolated the explicit component of adaptation by seeing where the participants were aiming in a visuomotor rotation task. Subtracting the explicit component from the total adaptation gave an indication of the implicit adaptation component (Fig. 1.2).

Since aiming strategies can be adapted quickly and consciously, the explicit process of adaptation is usually faster than the implicit process of adaptation which is adapted without much conscious awareness. Taylor and Ivry [2011] suggested that the explicit process is driven by the target error and that the implicit process is driven by the sensory-prediction error. The properties of the explicit and implicit processes have been studied extensively (Keisler and Shadmehr [2010], Taylor et al. [2014], Trewartha et al. [2014], Kim et al. [2015], Leukel et al. [2015], McDougle et al. [2015], Morehead et al. [2015], Werner et al. [2015], Poh et al. [2016], Thurer et al. [2016], Butcher et al. [2017], McDougle et al. [2017], de Brouwer et al. [2018], French et al. [2018], Leow et al. [2018], Liew et al. [2018], Schween et al. [2018], van Es and Knapen [2019], Mazzoni and Krakauer [2006], Werner et al. [2019]). Table 1.2 provides the key features of the explicit and implicit components of sensorimotor adaptation.

1.2.3. Fast-Slow as Explicit-Implicit

McDougle et al. [2015] hypothesised that the explicit component of adaptation is the fast process and the implicit process is the slow process of adaptation. This idea has since gained popularity as can be seen from the increase in the number of studies relating the fast-slow processes with the explicit-implicit processes (Fig. C.3). It was observed that the explicit process adapts fast and the slow process adapts slowly. Both the fast process and the explicit process are disrupted by secondary cognitive tasks (Keisler and Shadmehr [2010], van Es and Knapen [2019]). The fast process and the explicit process also show better generalisation (Keisler and Shadmehr [2010], Mandelblat-Cerf et al. [2011], McDougle et al. [2017], Schween et al. [2018]). On the other hand, the slow process and the implicit process are both correlated with greater retention (Joiner and Smith [2008], Charalambous et al. [2018], Kim et al. [2015]).

Possible contradictions for this hypothesis was provided by Morehead et al. [2015]. Morehead et al. [2015] showed that savings (faster adaptation in successive sessions) was correlated with the size of the perturbation, which would not be explained by a linear model. Another discrepancy between the dichotomies is regarding the error that drives adaptation. The fast and slow process have been found to adapt based on the same error signal (Smith et al. [2006]). The explicit and implicit process on the other hand are adapted by different errors. The explicit process is thought to be adapted by the target error and the implicit process by the sensory-prediction error (Taylor et al. [2014]).

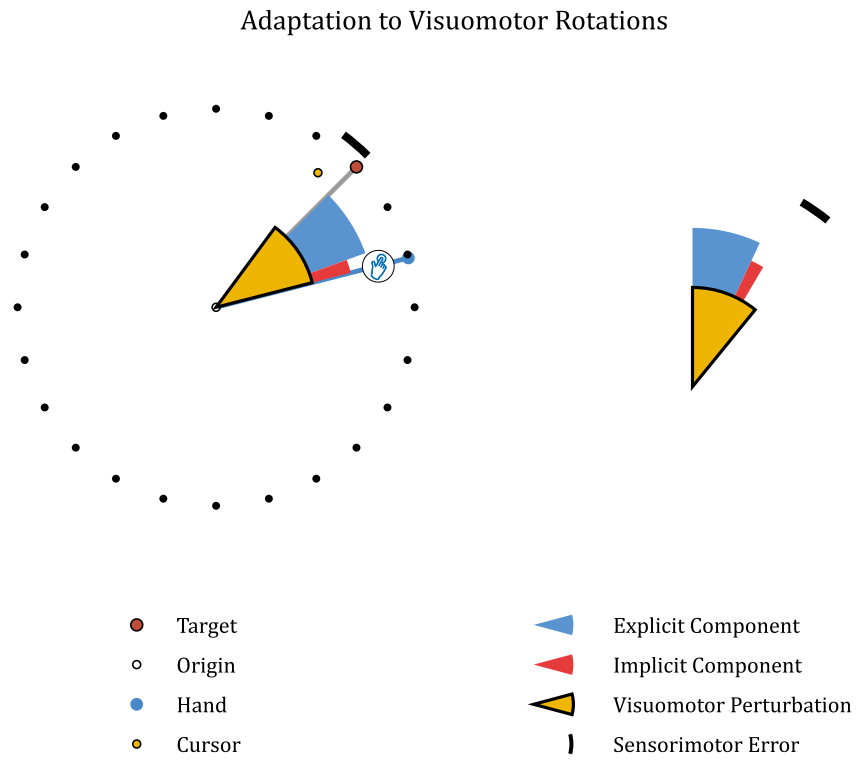

Figure 1.2: Explicit and Implicit Components of Adaptation for a visuomotor rotation task.
The net adaptation is the sum of the implicit and explicit components. Only the explicit component is accessible to conscious awareness. The explicit component is estimated from the reported aiming directions. The side panel illustrates how subtracting the explicit contribution from the net adaptation can be used to estimate the contribution of the implicit component.

The explicit-implicit dichotomy has important impact on rehabilitation studies as patients with different pathologies might have altered cognitive resources which might affect the adaptation behaviour. Accounting for the possibility of the fast and slow processes being identical to the explicit and implicit processes will thus have relevance to rehabilitation.

1.3. Project Structure

1.3.1. Research Goals

The main objective of this work are:

- Objective 1: Design a means of influencing the adaptation processes independently.
- Objective 2: Use this to maximize the contribution of the slow process with the aim of improving retention after adaptation.

As an example, visual perturbations (visuomotor rotations) during an upper-extremity reaching task are considered. An optimal perturbation schedule is to be designed based on the mathematical models of the fast and slow processes. Parameter estimation would be conducted to estimate the learning and retention rates of each participant. These estimated parameters would then be used to predict the adaptation behaviour of the participants in the subsequent adaptation blocks and to tailor the optimal perturbation schedule to each participant. As far as the author is aware, this is first time the fast-slow model has been used to design a perturbation and to predict the subsequent behaviour of the participants. Since there is a likely overlap between the fast-slow and the explicit-implicit dichotomies, the trajectories of the fast and slow processes that result from the optimisation should be coherent from the perspective of the explicit and implicit processes (i.e., the trajectories of the fast and slow processes should have the qualitative properties of the explicit and implicit processes respectively).

The designed perturbation will be compared against a constant perturbation to see if the optimal perturbation can improve retention after adaptation in healthy human participants. It was hypothesised that the

Table 1.2: Characteristics for the Explicit and Implicit Processes of Adaptation first proposed by (Mazzoni and Krakauer [2006]).

Characteristics of Explicit and Implicit Processes	
Explicit Process	**Implicit Process**
Learning component of which the participant is *aware* and is more under the control of conscious effort (Mazzoni and Krakauer [2006], Taylor et al. [2014]).	Learning component of which the participant is *unaware* and is more automated (Mazzoni and Krakauer [2006], Taylor et al. [2014]).
The explicit process adapts *fast.* (McDougle et al. [2015]).	The implicit process adapts *slowly* (McDougle et al. [2015]).
End-point Feedback and *instructions* promote the use of the explicit process (Liew et al. [2018], Taylor et al. [2014]).	*Online feedback* promotes the use of the implicit process (Liew et al. [2018], Taylor et al. [2014]).
The variance of the explicit process evolves in a *non-monotonic* fashion as adaptation progresses (Taylor et al. [2014]).	The variance of the implicit process evolves in a *monotonic* fashion as adaptation progresses (Taylor et al. [2014]).
Explicit visual feedback did not lead to an increase of *retention* Kim et al. [2015].	Implicit visual feedback is associated with greater *retention* Kim et al. [2015].
Explicit processes show greater and more complete *transfer* of learning (Werner et al. [2015], Poh et al. [2016], Werner et al. [2019]).	*Transfer* of implicit learning is generally not complete and is dependent on the degree of compatibility in intrinsic coordinates (Poh et al. [2016]).
Generalisation pattern of the explicit component to untrained regions of the workspace is flat (McDougle et al. [2017], Schween et al. [2018]).	*Generalisation* pattern of the implicit component to untrained regions of the workspace is not flat and shows peaks in the positions which were trained (McDougle et al. [2017], Schween et al. [2018]).
Enforcing or removing task errors both reduce the contribution of the explicit process (Leow et al. [2018]).	*Removing task errors* reduces the contribution of the implicit process. *Enforcing task errors* seem to have negligible effect on the implicit process (Leow et al. [2018]).
Increasing *cognitive load* reduces the capacity for applying the explicit process (van Es and Knapen [2019]).	When *cognitive load* is high the implicit process will dominate and hence the adaptation will be slower (van Es and Knapen [2019]).

movement angles in the retention block after the optimal perturbation would be greater than the movement angles in the retention block after the constant perturbation. The initial idea was to compare the retention after the two types of perturbations within subjects. This comparison did not show significant effects due to deficiencies in the washout between perturbations. An incomplete washout would mean that the second perturbation experienced by each participant would be tainted. This led to the second between-subject hypothesis which considers only the first perturbation experienced by each participant. In addition to the hypothesis tests, the completeness of the washouts and the accuracy of the model predictions will also be analysed.

1.3.2. Approach

The research approach is summarised in the following steps :

1. The 2-rate LTI model of adaptation (Eq. (1.3)) was chosen to design an optimal feedforward perturbation.

2. A discrete time Linear-Quadratic Tracking (LQT) perturbation was formulated for a desired terminal

state with zero contribution from the fast process and unit contribution from the slow process [6]. This perturbation will be referred to as the Adaptation-State-Tracking (AST) perturbation.

3. The formulated AST perturbation was tailored to each participant after conducting parameter estimation which fits the 2-rate LTI model of adaptation on the experimental data of each participant.

4. For the purpose of comparison, a Constant-Level (CL) perturbation which would produce the same terminal net adaptation as the AST perturbation was calculated based on the simulation of the AST perturbation and identified human model.

5. The AST and CL perturbations were presented to each participant in a random order and the retention after each adaptation block was studied.

6. The experimental results were analysed to check the hypothesis whether the average movement angles in the retention trials for the AST block was greater than those for the CL block.

1.3.3. Scope

The current work explores how an optimal perturbation schedule can be designed to improve retention after adaptation. Even though the long term motivation behind this work pertains to robotic rehabilitation, the current work does not involve any robotic assistance or recovery from a neurological injury. Only healthy participants were included for the experimental study. Motor adaptation (which is the modulation of learned behaviour) is distinct from motor-skill learning (which deals with how a new skill is acquired in the first place) and the latter is not the subject of the current work. The trial-based model of adaptation used in the model is only valid for short time intervals spanning only a couple of hours and does not account for decay of adaptation with time. Consolidation of the learned adaptations is also beyond the scope of this work.

1.3.4. Report Structure

Chapter 2 contains an account of the control design for the fast and slow processes of adaptation based on the two-state LTI model of adaptation (Eq. (1.3)). Chapter 3 deals with design of the visuomotor rotation experiments, how the perturbations were tailored for each participant, the hypotheses and details regarding the analysis of experimental observations. The results of the experiment are collected in Chapter 4. Chapter 5 discusses the results. The conclusions and recommendations for control engineers and therapists are included in Chapter 6.

[6] The value of unity for the slow process was an arbitrary choice. Since the model is LTI, the calculated input can be scaled to achieve any value of the slow state.

2

Controlling Adaptation Processes

2.1. Two-State Model of Adaptation

2.1.1. 2-State Linear Time-Invariant (LTI) Model

Many mathematical models have been proposed for modelling adaptation behaviour. For the present study, the 2-state LTI model was chosen. The motivation behind this choice is explained in this section.

Smith et al. [2006] proposed that sensorimotor adaptation can be modelled as the combination of fast and slow adaptive processes. The fast adaptive process (x_f) learns fast(b_f) but has lower retention(a_f) between trials. The slow process (x_f) on the other hand has a lower learning rate(b_s) but has higher retention(a_s) between trials. The net adaptation ($x(k)$) on each trial (k) is the sum of the fast adaptive process and the slow adaptive process. Both the fast and the slow processes are updated based on the net sensorimotor error ($e(k)$):

$$\begin{aligned} x_s(k+1) &= a_s \cdot x_s(k) + b_s \cdot e(k), \\ x_f(k+1) &= a_f \cdot x_f(k) + b_f \cdot e(k), \\ x(k) &= x_s(k) + x_f(k), \\ 0 < b_s < b_f < 1\,,\ 0 < a_f < a_s < 1. & \end{aligned} \tag{2.1}$$

For a given perturbation ($P(k)$), the sensorimotor error is calculated as

$$e(k) = P(k) - x(k) = P(k) - (x_s(k) + x_f(k))\,. \tag{2.2}$$

The parameters — a_s, b_s, a_f and b_f — are selected for each participant to fit the prediction of model Eq. (2.1) to experimental observations. In this models, these parameters are assumed to be invariant to perturbation blocks.

The decay of the adaptation processes are trial-based in the above model. There have been some models that look at the time-based decay of adaptive processes where the time-constants were used as the metric (Ethier et al. [2008], Kim et al. [2015]) . McDougle et al. [2015] studied the effect of changing the time between trials — inter-trial interval (ITI) — on the progress of adaptation. It was observed that the adaptation behaviour was virtually invariant for ITIs of up to 30 s. This has motivated the current study to favour trial-based models of adaptation over time-based models.

The fast and slow processes of adaptation proposed by Smith et al. [2006] provides a simple model to explain a range of behavioural findings related to sensorimotor adaptation. This model has since been used to model behavioural findings in a wide variety of adaptation tasks and is gaining popularity [1]. Many other papers have suggested more complex models of adaptive processes (Table C.5). The majority of these models are generalisations of the linear time-invariant model suggested by Smith et al. [2006]. "Varying-parameter" models (which have different learning and retention rates for each adaptation block, but, is LTI within each block) (Zarahn et al. [2008]) and three-rate model (Inoue et al. [2015]) were proposed to explain savings that were observed even after long washout periods.

[1] Refer Figs. C.2 and C.3 in Appendix C for more information on the popularity of the 2-state LTI model.

All the models in Table C.5 are abstract and over-simplified models used to study the complex interactions in the brain. Modelling all the complex interactions of the brain might lead to cumbersome models that are not very useful for real-time interventions during adaptation or rehabilitation. A simple model on the other hand gives us a good approximation of adaptive behaviour. Simple models have the added benefit that they have better interpretability. Thus, simple and interpretable models which provide good approximations of adaptation can be very useful in guiding rehabilitative efforts. The 2-state LTI model suggested by Smith et al. [2006] provides a nice trade-off between complexity and accuracy. It can sufficiently model adaptation behaviour within the timespan of a day. The fact that it is a linear time-invariant model means that controller design for such a model is relatively easy. Since the focus of the project is on the models of adaptation in a single day, the 2-state LTI model was selected to be adequate (Inoue et al. [2015] had showed that the 2-state LTI model was sufficient for predicting retention for experiments with up to 250 trials and that a 3-rate models were only needed to explain retention after 500 or more trials).

2.1.2. Model Parameters from Literature

The 2-state model introduced by Smith et al. [2006] is a simple model that can predict many of the experimental observations in sensorimotor adaptation experiments. This model has been widely used in literature on many sensorimotor adaptation tasks. The learning and retention parameters for various adaptation tasks were extracted from theses studies to be used as an initial estimate for running simulations and tuning the control gains. Also, it should be noted that all the parameters extracted here are for trial-based models.

The parameters for the slow and fast processes are plotted in Figs. 2.1 and 2.2. The values can also be found in Tables 2.1 and 2.2.

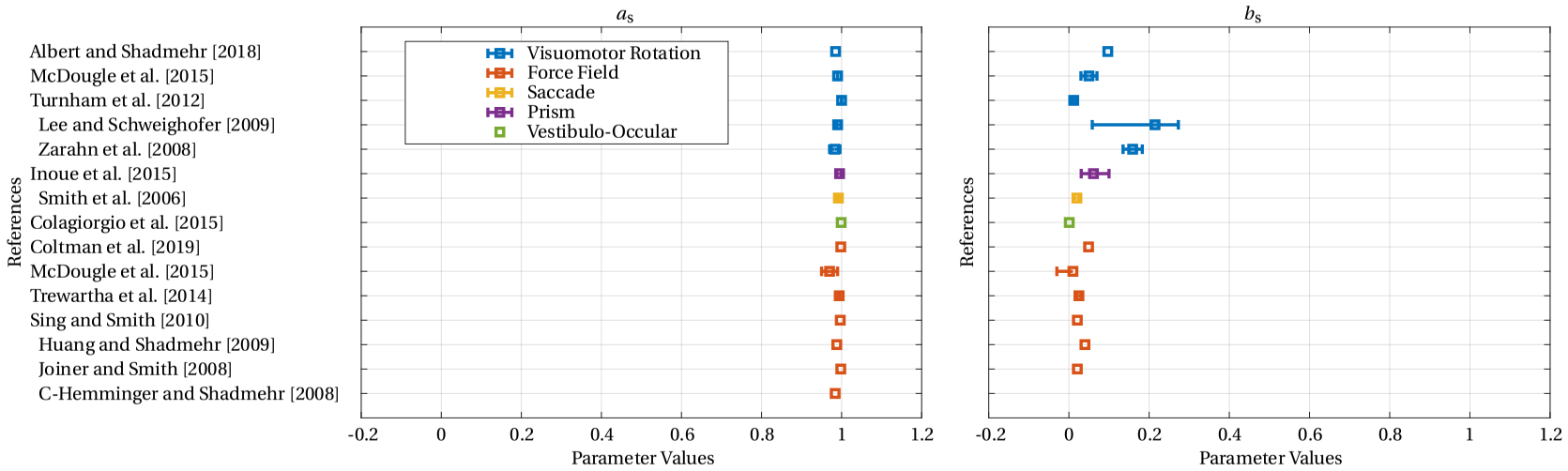

Figure 2.1: Parameters of the Slow Process of the two-rate adaptation models from literature for different adaptation tasks. The different types of adaptation tasks are described in Appendix B.1.

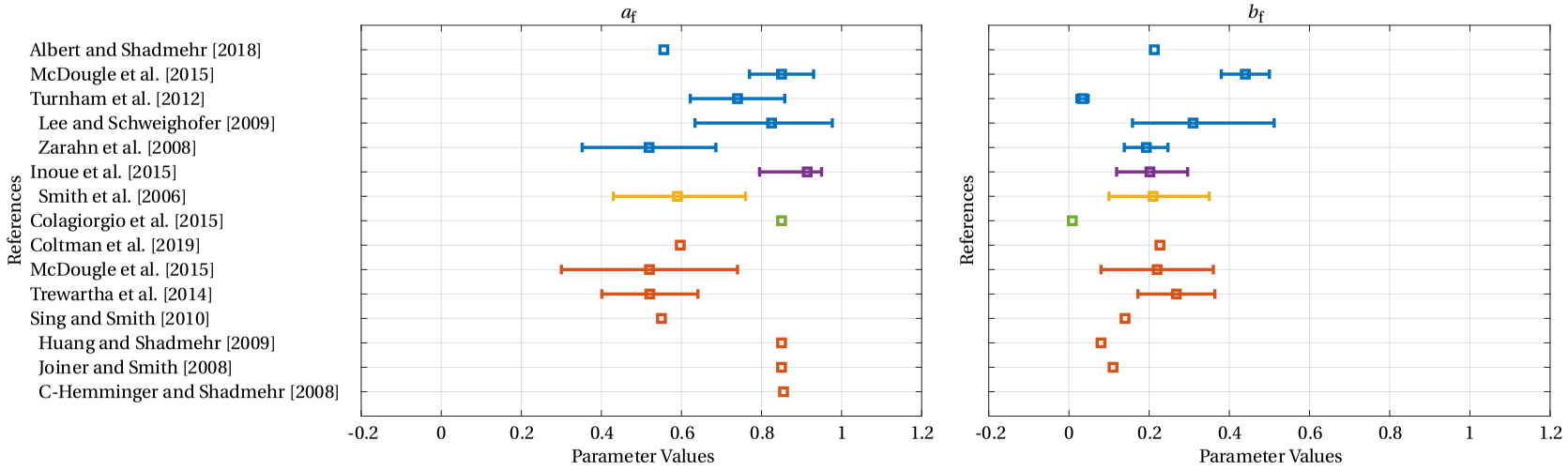

Figure 2.2: Parameters of the Fast Process of the two-rate adaptation models from literature for different adaptation tasks. The different types of adaptation tasks are described in Appendix B.1.

Table 2.1: Parameters of the Slow Process of Adaptation extracted from Literature

Article	Adaptation Type	Number of Participants	As Mean	As 95%CI Lower	As 95%CI Upper	Bs Mean	Bs 95%CI Lower	Bs 95%CI Upper
C-Hemminger and Shadmehr [2008]	Force Field	107	0.984					
Joiner and Smith [2008]	Force Field	48	0.998			0.021		
Huang and Shadmehr [2009]	Force Field	53	0.988			0.04		
Sing and Smith [2010]	Force Field	58	0.9967			0.021		
Trewartha et al. [2014]	Force Field	21	0.994	0.992	0.996	0.025	0.02	0.03
McDougle et al. [2015]	Force Field	10	0.97	0.95	0.99	0.01	0.05	
Coltman et al. [2019]	Force Field	53	0.998			0.049		
Smith et al. [2006]	Saccade	14	0.992	0.99	0.994	0.02	0.013	0.025
Colagiorgio et al. [2015]	Vestibulo-Occular	8	0.999			0.0009		
Inoue et al. [2015]	Visuomotor Prism	7	0.995	0.987	0.999	0.0612	0.0307	0.1
Zarahn et al. [2008]	Visuomotor Rotation	14	0.983	0.97	0.996	0.159	0.135	0.183
Lee and Schweighofer [2009]	Visuomotor Rotation	12	0.9901	0.9876	0.9986	0.2147	0.0582	0.2729
Turnham et al. [2012]	Visuomotor Rotation	27	1	1	1	0.012	0.008	0.016
McDougle et al. [2015]	Visuomotor Rotation	9	0.99	0.99	0.99	0.05	0.03	0.07
Albert and Shadmehr [2018]	Visuomotor Rotation	20	0.985			0.097		

Table 2.2: Parameters of the Fast Process of Adaptation extracted from Literature

Article	Adaptation Type	Number of Participants	Af Mean	Af 95%CI Lower	Af 95%CI Upper	Bf Mean	Bf 95%CI Lower	Bf 95%CI Upper
C-Hemminger and Shadmehr [2008]	Force Field	107	0.855					
Joiner and Smith [2008]	Force Field	48	0.85			0.11		
Huang and Shadmehr [2009]	Force Field	53	0.85			0.08		
Sing and Smith [2010]	Force Field	58	0.55			0.14		
Trewartha et al. [2014]	Force Field	21	0.521	0.401	0.641	0.268	0.172	0.364
McDougle et al. [2015]	Force Field	10	0.52	0.3	0.74	0.22	0.08	0.36
Coltman et al. [2019]	Force Field	53	0.597			0.227		
Smith et al. [2006]	Saccade	14	0.59	0.43	0.76	0.21	0.1	0.35
Colagiorgio et al. [2015]	Vestibulo-Occular	8	0.85			0.0085		
Inoue et al. [2015]	Visuomotor Prism	7	0.914	0.795	0.95	0.202	0.119	0.296
Zarahn et al. [2008]	Visuomotor Rotation	14	0.519	0.352	0.686	0.193	0.138	0.247
Lee and Schweighofer [2009]	Visuomotor Rotation	12	0.8251	0.6338	0.9767	0.3096	0.1585	0.5118
Turnham et al. [2012]	Visuomotor Rotation	27	0.74	0.622	0.858	0.034	0.02	0.048
McDougle et al. [2015]	Visuomotor Rotation	9	0.85	0.77	0.93	0.44	0.38	0.5
Albert and Shadmehr [2018]	Visuomotor Rotation	20	0.556			0.213		

2.2. Slow and Steady Training

2.2.1. Influencing the Fast and Slow Processes

The fast and the slow process help the body to adapt to perturbations acting over different timescales. Dichotomies with more component processes have been suggested, but for the current work, the 2-state model with a fast and a slow process was chosen. The fast process enables quick adaptation to rapid perturbations but also forgets them fast (Smith et al. [2006], Pelisson et al. [2010]). The slow process on the other hand helps the body adapt to more gradual and permanent perturbations (Smith et al. [2006], Pelisson et al. [2010]). The fast process forgets what it learns fast and thus does not contribute much towards long-term retention. The slow process on the other hand retains what it learns for longer and thus significantly contributes toward long-term retention (Joiner and Smith [2008], Charalambous et al. [2018]).

The contrasting characteristics of the fast and slow processes if harnessed could be useful in designing training/rehabilitation paradigms that cater to different goals. If maximising the retention of learned behaviour is the goal, it could be achieved by teaching it to the slow process. The LTI model described in Eq. (2.1) lends itself to optimal control design to selectively influence the fast and slow processes. As far as the author is aware, this is first time optimal control is applied to selectively influence the slow and fast states of adaptation. Previous studies have looked at how the fast and slow states evolve in response to perturbations. Here, the perturbation is designed to generate specific trajectories for the fast and slow states.

Retention is strongly related to the slow process. Based on this observation, it was hypothesised that increasing the contribution of the slow process will improve retention after adaptation. This was the goal of the optimal control design.

2.2.2. Implication of overlap with Explicit and Implicit Processes

We could use the mathematical model of the fast-slow processes to design controllers. But since these are over-simplified abstractions of complex neural processes, it would be important to check whether the trajectories suggested by the control make sense when considering the qualitative properties of the explicit and implicit processes.

The convergence of the fast-slow and explicit-implicit dichotomies could have profound impact on adaptation studies. The Fast-Slow dichotomy has yielded mathematical models for adaptation but rely on hidden states which cannot be directly measured. The Explicit-Implicit dichotomy on the other hand provides clear characteristics which can be used to directly estimate the adaptive components. A marriage of these dichotomies would yield a mathematical model for adaptive processes with distinctive properties. The relevance of the explicit-implicit dichotomy to rehabilitation warrants this qualitative regularisation.

The explicit process usually exhibits overshooting behaviour and is generally non-monotonic. The implicit process evolves more gradually and shows a monotonic nature. To qualitatively regularise the optimal trajectories, they will be visually examined to ensure that the optimal fast state and slow state have trajectories that obey the characteristics of the explicit process and the implicit process respectively.

2.2.3. Control Objective

The main goal of this work is to increase the retention after an adaptation session. Since the slow process is correlated with more retention, it was posited that increasing the contribution of the slow process will increase the retention. Since the net adaptation is the combination of the slow and fast processes, increasing the contribution of the slow process is equivalent to decreasing the contribution of the fast process (for the case where the net adaptation is to be kept constant). Considering the overlap of the fast-slow and explicit-implicit dichotomies, the trajectories of the fast and slow states from the optimal control should be consistent with the nature of the explicit and implicit processes. All these factors boil down to the following requirements:

1. Increase the contribution of the slow process.
2. Decrease the contribution of the fast process (for the case where net adaptation has to be kept the same).
3. Ensure that the slow state trajectory is consistent with the properties of the implicit process (i.e., monotonicity)
4. Ensure that the fast state trajectory is consistent with the properties of the explicit process (i.e., overshooting and non-monotonicity)

To achieve these goals we have to find the optimal input ($u(k)$) which has to be applied as the perturbation ($P(k)$). This input will thus result in a sensorimotor error ($e(k)$) as

$$e(k) = P(k) - (x_s(k) + x_f(k)) = u(k) - (x_s(k) + x_f(k)). \tag{2.3}$$

2.3. Infinite-Time Control for the Slow Process

2.3.1. Analytical Solution for Infinite-Time Control

Infinite-time control is providing a steady input ($u(k)$) which drives the state of a system asymptotically to some desired state at infinite time. For the problem at hand, this offers less flexibility over the final states because two states (x_s,x_f) have to be controlled with one input (u). So, for the infinite-time control, only the final slow state will be considered. Our goal is to find the steady input (u) for maintaining the slow process at desired value (lets take, $x_{s,r} = 1$). The value of the fast process($x_{f,\infty}$) , in this case, is unimportant for us.

At steady state,

$$x_s(k+1) = x_s(k) = x_{s,r} = 1. \tag{2.4}$$

Looking at equations 2.1 and steady-state condition 2.4 for the slow process, we get the steady-state value of the error (e_∞) as

$$e_\infty = \frac{(1-a_s)\cdot x_{s,r}}{b_s}. \tag{2.5}$$

Substituting this steady-state error back into the model equation, we can see that the steady-state value for the fast process is given as

$$\boxed{x_{f,\infty} = \frac{b_f}{1-a_f}\cdot\frac{(1-a_s)\cdot x_{s,r}}{b_s}}. \tag{2.6}$$

The error (e_∞) is the difference between the perturbation (which is the control input u in our case) and the sum of the states x_s and x_f. Thus the expression for the steady input u is given by the relation

$$u = x_{s,r} + x_{f,\infty} + e_\infty = x_{s,r} + \frac{b_f}{1-a_f}\cdot\frac{(1-a_s)\cdot x_{s,r}}{b_s} + \frac{(1-a_s)\cdot x_{s,r}}{b_s}. \tag{2.7}$$

We can see that the required input u varies linearly with the desired level of the slow process. This is expected since this is a linear system. Simplifying the relation we get

$$\boxed{u = \left(1 + \frac{b_f}{1-a_f}\cdot\frac{1-a_s}{b_s} + \frac{1-a_s}{b_s}\right)\cdot x_{s,r}}. \tag{2.8}$$

If this input u is applied continuously for infinite time, the state of adaptation asymptotically approaches the desired state starting from any initial state. This is an instance of infinite-time control.

2.3.2. Example of Infinite-Time Control

Assuming that the system parameters are [2]

$$\begin{aligned} a_s &= 0.996 \quad b_s = 0.003 \\ a_f &= 0.92 \quad\;\; b_f = 0.03, \end{aligned} \tag{2.9}$$

solving equations 2.6 and 2.8, for $x_{s,r} = 1$ we get,

$$\begin{aligned} x_{f,\infty} &= 0.5 \quad \text{and} \\ u &= 2.8333. \end{aligned} \tag{2.10}$$

The dynamics of this system for the above constant input u and initial conditions $[x_{s,0}; x_{f,0}] = [0;0]$ is plotted in Fig. 2.3.

[2] This is an arbitrary choice which is consistent with the requirements for the learning and retention parameters

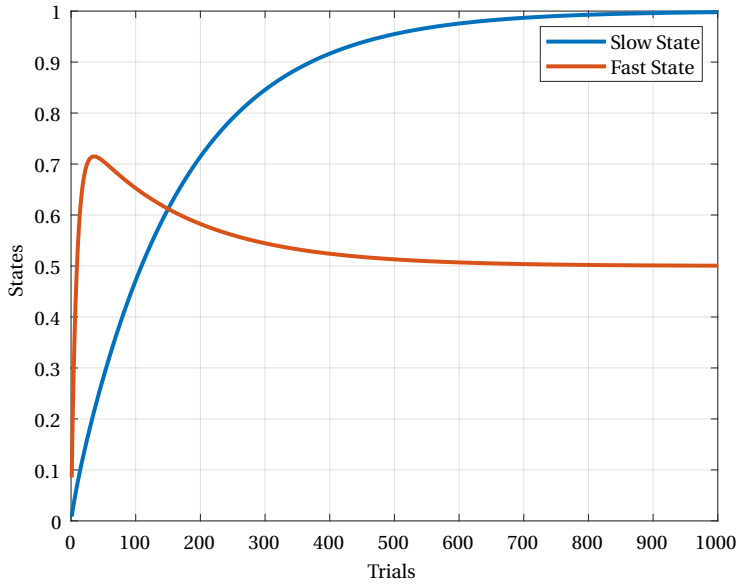

Figure 2.3: Infinite-time control of the slow and fast processes. The values have been normalised to so that the desired value of the slow process is unity.

2.3.3. Inferences regarding Infinite-Time Control

We can see that for the example shown above, the steady-state error e_∞ is non-zero. This implies that the adaptation can never fully reach the level of the perturbation.

The states decay if left unperturbed, since a_s and a_f are less than 1. To maintain the states at a steady value, the degradation of the states must be compensated by an error. This error acts on the states through the parameters b_s and b_f. Since we are interested in the slow state, we can focus on the values of a_s and b_s. In the example above, the value of b_s is very small and hence the steady-state error required to maintain the slow process at $x_{s,r}$ is large.

2.4. Adaptation-State-Tracking (AST) Perturbation

2.4.1. Linear-Quadratic Tracking (LQT) Problem Formulation for Slow and Fast Processes

Optimal control is a subdomain of control theory where the objective is the find the optimal input which minimises some cost function. The cost function usually has terms related to the magnitude of the input and deviations of states from some desired values. For such a cost function, the optimal input is based on a trade-off between the input and state deviations. Linear-Quadratic Tracking (LQT) is a common case of optimal control where a quadratic cost function is defined for a linear system in order to track some desired trajectory of the state/output.

A Linear-Quadratic Tracking (LQT) problem was formulated to find the optimal perturbation ($P(k)$) which would make the slow and fast states (x_s and x_f) of adaptation track some desired trajectory (rather than a fixed steady-state value). Thus the input $u(k)$ is the perturbation $P(k)$ and the output $\boldsymbol{y}(k)$ is a vector containing the slow and fast states ($[x_s \;\; x_f]^\intercal$). Using Eq. (2.1) and Eq. (2.2), we can rewrite the model equations in terms of the perturbations ($u(k)$) as

$$\begin{aligned} x_s(k+1) &= a_s \cdot x_s(k) + b_s \cdot [u(k) - (x_s(k) + x_f(k))] = (a_s - b_s) \cdot x_s(k) + (-b_s) \cdot x_f(k) + b_s \cdot u(k), \\ x_f(k+1) &= a_f \cdot x_f(k) + b_f \cdot [u(k) - (x_s(k) + x_f(k))] = (-b_f) \cdot x_s(k) + (a_f - b_f) \cdot x_f(k) + b_f \cdot u(k), \\ \boldsymbol{y}(k) &= \begin{bmatrix} x_s(k) & x_f(k) \end{bmatrix}^\intercal. \end{aligned} \tag{2.11}$$

This system of equations can be written as

$$
\begin{aligned}
\boldsymbol{x}(k+1) &= \mathbf{A}\cdot\boldsymbol{x}(k) + \mathbf{B}\cdot\boldsymbol{u}(k), \\
\boldsymbol{y}(k) &= \mathbf{C}\cdot\boldsymbol{x}(k), \\
\text{where,} \qquad \boldsymbol{x}(k) &= \begin{bmatrix} x_\mathrm{s}(k) & x_\mathrm{f}(k) \end{bmatrix}^\mathsf{T}, \quad \boldsymbol{u}(k) = \begin{bmatrix} u(k) \end{bmatrix} \\
\mathbf{A} = \begin{bmatrix} a_\mathrm{s} - b_\mathrm{s} & -b_\mathrm{s} \\ -b_\mathrm{f} & a_\mathrm{f} - b_\mathrm{f} \end{bmatrix}, &\quad \mathbf{B} = \begin{bmatrix} b_\mathrm{s} & b_\mathrm{f} \end{bmatrix}^\mathsf{T}, \quad \text{and} \quad \mathbf{C} = \begin{bmatrix} 1 & 0 \\ 0 & 1 \end{bmatrix}.
\end{aligned}
\tag{2.12}
$$

This linear system is observable if $a_\mathrm{s} \neq a_\mathrm{f}$. The conditions for controllability are — $a_\mathrm{s} \neq a_\mathrm{f}$, $b_\mathrm{s} \neq 0$ and $b_\mathrm{f} \neq 0$.

As described in Section 2.2.3, the goal was to increase the contribution of the slow state and decrease the contribution of the fast state. This can be achieved by making the fast state zero ($x_\mathrm{f} = 0$). If the fast state is zero, all the adaptation will be from the slow process ($x = x_\mathrm{s}$). Since the system as described in Eq. (2.12) is linear, if an optimal input to achieve a nominal desired state is known, then the optimal input to achieve any other state which is a scaled version of the nominal state is obtained by scaling the optimal input for the nominal case. Considering this, the reference for the slow process was set as one and the reference for the fast state was set as zero ($[x_\mathrm{s}\ ,\ x_\mathrm{f}] = [1\ ,\ 0]$). Based on this requirement a quadratic cost function was defined as the deviation from a reference trajectory $\boldsymbol{z}(k)$:

$$
\begin{aligned}
J(\boldsymbol{x}(k_0), \boldsymbol{u}, k_0) = &\frac{1}{2}\left[\boldsymbol{z}(k_\mathrm{T}) - \mathbf{C}\boldsymbol{x}(k_\mathrm{T})\right]^\mathsf{T}\mathbf{F}\left[\boldsymbol{z}(k_\mathrm{T}) - \mathbf{C}\boldsymbol{x}(k_\mathrm{T})\right] \\
&+ \frac{1}{2}\sum_{k=k_0}^{k_\mathrm{T}-1}\Big[\left[\boldsymbol{z}(k) - \mathbf{C}\boldsymbol{x}(k)\right]^\mathsf{T}\mathbf{Q}\left[\boldsymbol{z}(k) - \mathbf{C}\boldsymbol{x}(k)\right] + \boldsymbol{u}^\mathsf{T}(k)\mathbf{R}\boldsymbol{u}(k)\Big]
\end{aligned}
\tag{2.13}
$$

where,
k_0 - is the initial trial number,
k_T - is the terminal trial number,
$\boldsymbol{z}(k)$ - is the reference vector for $\boldsymbol{y}(k)$ for the k^{th} instant,
$\mathbf{Q}$ - is a 2×2 positive semi-definite weighting matrix for the deviation from the reference,
$\mathbf{R}$ - is a 1×1 positive definite weighting matrix for the input, and
$\mathbf{F}$ - is a 2×2 positive semi-definite weighting matrix for the terminal error from the reference.

The desired terminal state is $\boldsymbol{z}(k_\mathrm{T}) = [x_\mathrm{s}(k_\mathrm{T})\ ,\ x_\mathrm{f}(k_\mathrm{T})]^\mathsf{T} = [1\ ,\ 0]^\mathsf{T}$. Adaptation was assumed to start from the initial state $\boldsymbol{x}(k_0) = [x_\mathrm{s}(k_0)\ ,\ x_\mathrm{f}(k_0)]^\mathsf{T} = [0\ ,\ 0]^\mathsf{T}$. The Adaptation-State-Tracking (AST) perturbation was chosen to have a duration of 100 trials ($k_\mathrm{T} = 100$). Considering the possible overlap between the slow state and the implicit process, the ideal trajectory for the slow process would be monotonic. This motivated the selection of an exponential function that asymptotically approached unity for the reference trajectory of the slow state. The shape factor of the exponential function was hand tuned. An elegant choice for the fast state is a steady value of zero. Reducing the weight associated with the trajectory error for the fast process would result in overshooting and non-monotonic optimal trajectories for the fast state. Thus the following reference trajectory was chosen :

$$
\boldsymbol{z}(k) = \begin{bmatrix} 1 - \exp\left(\frac{-k}{10}\right) \\ 0 \end{bmatrix}. \tag{2.14}
$$

2.4.2. Unconstrained Discrete-Time Linear-Quadratic Tracking Solution

The solution for the optimal control problem from Section 2.4.1 can be obtained using Pontryagin's Minimum Principle (see, e.g., Naidu [2002]). The detailed derivation of the Linear-Quadratic Tracking (LQT) solution from Pontryagin's Principle is provided in Appendix D. The main steps necessary to solve the linear-quadratic tracking with unconstrained input for a discrete-time model are listed in Table 2.3. This gives the optimal input trajectory $\boldsymbol{u}(k)$ and the optimal state trajectories $\boldsymbol{y}(k)$.

The unconstrained discrete-time LQT solution was implemented in MATLAB. The system described in Eq. (2.12) depends on the learning and retention parameters. To tune the weights ($\mathbf{Q}$, $\mathbf{R}$ and $\mathbf{F}$) of the cost function (Eq. (2.13)), learning and retention parameters obtained from literature (Tables 2.1 and 2.2 and Figs. 2.1 and 2.2) were used. The mean learning and retention parameters documented in papers which conducted visuomotor rotation experiments were used to generate virtual participants. The weights $\mathbf{Q}$, $\mathbf{R}$ and $\mathbf{F}$ were then

Table 2.3: Steps for Discrete-Time Linear-Quadratic Tracking with Unconstrained Input

Discrete-Time Linear-Quadratic Tracking with Unconstrained Input

Step 1:

Solve the matrix difference Riccati equation

$$\mathbf{P}(k) = \mathbf{A}^{\top}\left[\mathbf{P}^{-1}(k+1) + \mathbf{E}\right]^{-1}\mathbf{A} + \mathbf{V} \tag{2.15}$$

with final condition

$$\mathbf{P}(k_{\mathrm{T}}) = \mathbf{C}^{\top}\mathbf{F}\mathbf{C} \tag{2.16}$$

and the vector difference equation

$$\boldsymbol{g}(k) = \mathbf{A}^{\top}\left\{\mathbf{I} - \left[\mathbf{P}^{-1}(k+1) + \mathbf{E}\right]^{-1}\mathbf{E}\right\}\boldsymbol{g}(k+1) + \mathbf{W}\boldsymbol{z}(k) \tag{2.17}$$

with the boundary condition

$$\boldsymbol{g}(k_{\mathrm{T}}) = \mathbf{C}^{\top}\mathbf{F}\boldsymbol{z}(k_{\mathrm{T}}) \tag{2.18}$$

where,

$$\mathbf{E} = \mathbf{B}\mathbf{R}^{-1}\mathbf{B}^{\top}, \quad \mathbf{V} = \mathbf{C}^{\top}\mathbf{Q}\mathbf{C} \quad \text{and} \quad \mathbf{W} = \mathbf{C}^{\top}\mathbf{Q}. \tag{2.19}$$

Step 2:

Solve for the optimal state $\boldsymbol{x}^*(t)$ from the equation:

$$\boldsymbol{x}^*(k+1) = [\mathbf{A} - \mathbf{B}\mathbf{L}(k)]\,\boldsymbol{x}^*(k) + \mathbf{B}\mathbf{L}_g(k)\boldsymbol{g}(k+1) \tag{2.20}$$

with the initial condition

$$\boldsymbol{x}(t_0) = \boldsymbol{x}_0 \tag{2.21}$$

where,

$$\begin{aligned}\mathbf{L}(k) &= \left[\mathbf{R} + \mathbf{B}^{\top}\mathbf{P}(k+1)\mathbf{B}\right]^{-1}\mathbf{B}^{\top}\mathbf{P}(k+1)\mathbf{A}\\ \mathbf{L}_g(k) &= \left[\mathbf{R} + \mathbf{B}^{\top}\mathbf{P}(k+1)\mathbf{B}\right]^{-1}\mathbf{B}^{\top}.\end{aligned} \tag{2.22}$$

Step 3:

The optimal control $\boldsymbol{u}^*(k)$ is obtained as

$$\boldsymbol{u}^*(k) = -\mathbf{L}(k)\boldsymbol{x}^*(k) + \mathbf{L}_g(k)\boldsymbol{g}(k+1). \tag{2.23}$$

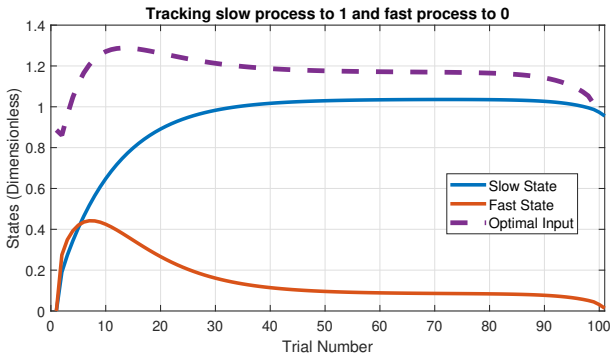

(a) Good Example where the trajectories of the fast and slow states agree with the properties of the explicit and implicit processes. Trajectories like these were favoured when tuning the weights of the cost function.

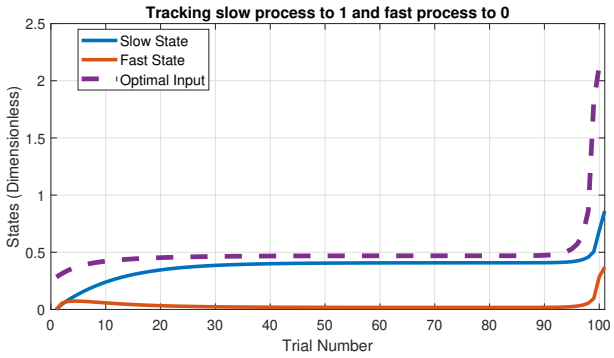

(b) Bad Example where the trajectories of the fast and slow states does not agree with the properties of the explicit and implicit processes. Trajectories like these were excluded when tuning the weights of the cost function. Here the slow state is moving to the final state with a jump; which is uncharacteristic of the slow/implicit process.

Figure 2.4: Qualitative Regression Examples.

tuned such that the optimal state trajectories for all the virtual participants were acceptable. One of the main considerations while judging the acceptability of the state trajectories was the overlap with the implicit and explicit processes — the slow process should evolve monotonously and the fast process shows overshooting and is non-monotonous. The input and state trajectories that resulted from the final selection of weights are plotted in Figs. 2.5a and 2.5b respectively. Note the high variability in behaviour depending on the human parameters. Also, not all are successful in finite time. The hand tuned values of the weights are

$$\mathbf{Q} = \begin{bmatrix} 100 & 0 \\ 0 & 1 \end{bmatrix}, \quad \mathbf{R} = \begin{bmatrix} 1 \end{bmatrix} \quad \text{and} \quad \mathbf{F} = \begin{bmatrix} 100 & 0 \\ 0 & 0.1 \end{bmatrix}. \tag{2.24}$$

The perturbation for the experiment is an angular offset expressed in degrees. All the weights are dimensionless and the cost function is in units of squared degrees. More generally, the perturbation and motor adaptation are quantified in the same domain and the cost function has the same units, but squared. The weights were tuned such that the deviations from the reference trajectory were more severely penalised for the slow state than the fast state. The relaxed penalisation of the deviations of the fast state allows for the non-monotonous overshooting behaviour which was one of the design criteria.

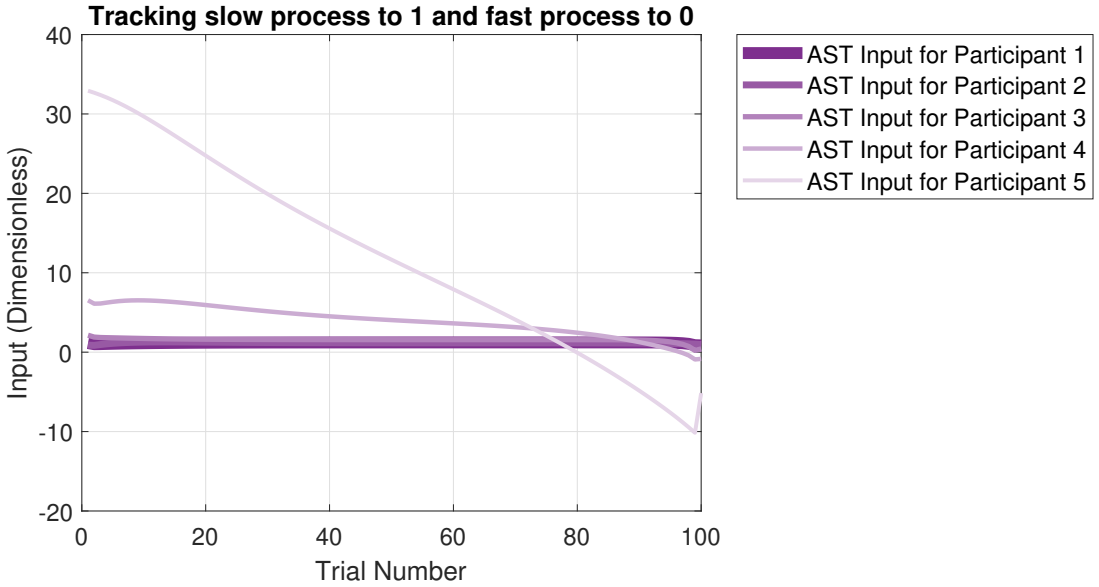

(a) AST inputs for virtual participants with parameters as seen in literature.

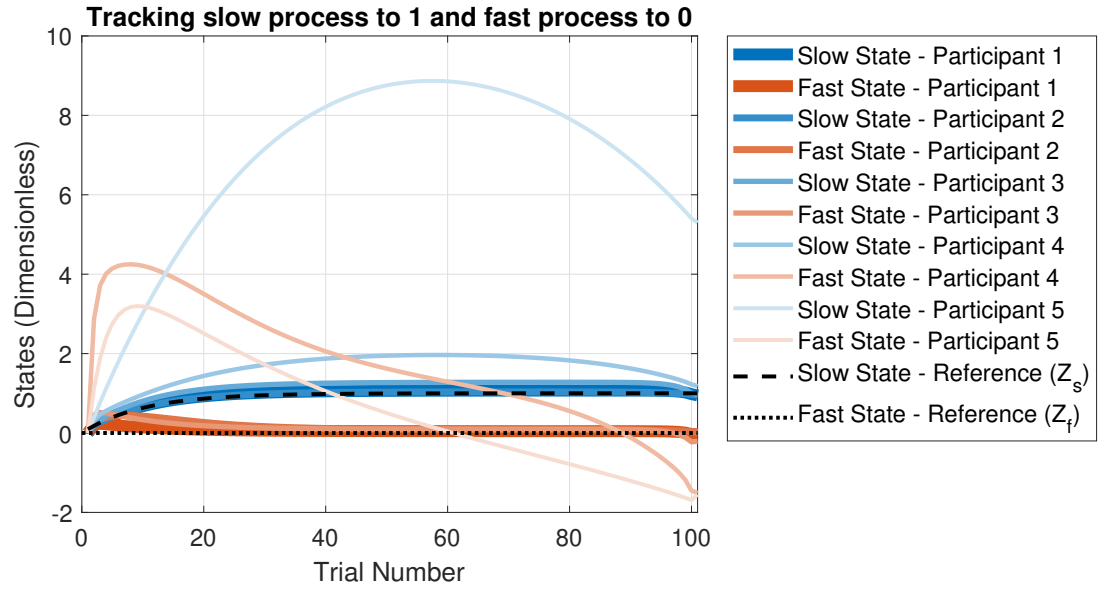

(b) Optimal state trajectories for the AST inputs for the virtual participants.

Figure 2.5: Optimal input and state trajectories from Adaptation-State-Tracking (AST) for virtual participants with learning and retention rates as seen in literature. The participants have been arranged in ascending order of the maximum value of the AST input. Refer to Table 2.4.

Table 2.4: Learning and retention of the virtual participants. The participants have been arranged in ascending order of the maximum value of the AST input. These values have been taken from Tables 2.1 and 2.2

Virtual Participants				
Participant Number	a_s	a_f	b_s	b_f
Participant 1	0.9830	0.5190	0.1590	0.1930
Participant 2	0.9901	0.8251	0.2147	0.3096
Participant 3	1.0000	0.7400	0.0120	0.0340
Participant 4	0.9900	0.8500	0.0500	0.4400
Participant 5	0.9850	0.5560	0.0970	0.2130

3

Experimental Methods

3.1. Constant-Level (CL) Perturbation

3.1.1. Selecting a Benchmark Perturbation

A benchmark perturbation was required against which the AST perturbation can be compared. Constant level perturbations are commonplace in sensorimotor adaptation studies and was selected as the benchmark perturbation. The level of the perturbation was to be chosen based on some criteria for a just comparison with the AST perturbation. The purpose of the AST perturbation was to improve retention after training. In rehabilitation interventions, the final state of adaptation of the patient is a major consideration for evaluating the patients progress. Thus the final state of adaptation after the training block can be used as the basis for relating the AST and CL perturbations of each participant. Showing that the AST perturbation can produce better retention than a CL perturbation which produces the same final state of adaptation can objectively prove the superiority of the AST perturbation. The CL perturbation will also have to be the same number of trials as the AST perturbation.

3.1.2. Calculation of the Contrast Perturbation Level

The value of CL perturbation is constant for all the 100 trials ($\boldsymbol{u}(k) = u_{\mathrm{CL}}$). Assuming that the initial state of adaptation is $\boldsymbol{x}(k_0) = [x_{\mathrm{s}}(k_0)\,,\, x_{\mathrm{f}}(k_0)]^{\mathsf{T}} = [0\,,\, 0]^{\mathsf{T}}$, Eq. (2.12) shows that the final net adaptation after the CL perturbation ($x_{\mathrm{CL}}(k_{\mathrm{T}})$) (which is the sum of the slow ($x_{\mathrm{s,CL}}(k_{\mathrm{T}})$) and fast states ($x_{\mathrm{f,CL}}(k_{\mathrm{T}})$) is a function of the initial state and the constant input u_{CL} :

$$x_{\mathrm{CL}}(k_{\mathrm{T}}) = x_{\mathrm{s,CL}}(k_{\mathrm{T}}) + x_{\mathrm{f,CL}}(k_{\mathrm{T}}) = f_{\mathrm{CL}}(\boldsymbol{x}(k_0), u_{\mathrm{CL}}). \tag{3.1}$$

The final net adaptation after the AST adaptation ($x_{\mathrm{AST}}(k_{\mathrm{T}})$) is the sum of the slow ($x_{\mathrm{s,AST}}(k_{\mathrm{T}})$) and fast ($x_{\mathrm{f,AST}}(k_{\mathrm{T}})$) states at the end of the AST perturbation can be obtained from the optimal state trajectories of the AST perturbation:

$$x_{\mathrm{AST}}(k_{\mathrm{T}}) = x_{\mathrm{s,AST}}(k_{\mathrm{T}}) + x_{\mathrm{f,AST}}(k_{\mathrm{T}}). \tag{3.2}$$

The condition of equal final net adaptation ($x_{\mathrm{CL}}(k_{\mathrm{T}}) = x_{\mathrm{AST}}(k_{\mathrm{T}})$) implies that

$$f_{\mathrm{CL}}(\boldsymbol{x}(k_0), u_{\mathrm{CL}}) = x_{\mathrm{s,AST}}(k_{\mathrm{T}}) + x_{\mathrm{f,AST}}(k_{\mathrm{T}}). \tag{3.3}$$

Solving Eq. (3.3) for u_{CL} gives the level of the required CL perturbation. This was solved using the symbolic toolbox of MATLAB for the optimal trajectories resulting from the AST algorithm.

3.2. Experiment Design

3.2.1. Task

The experiments were conducted in the neuroscience department of Erasmus MC, Rotterdam. The AST and CL perturbations were implemented for adaptations to visuomotor rotations. In a visuomotor rotation experiment, the participants are asked to move a cursor on a screen with the help of a manipulandum or a stylus

(Figs. 3.1a, 3.1b and 3.2). For unperturbed conditions, the cursor would move just as the manipulandum or stylus is moved. When visuomotor rotations are applied, the cursor movements will be rotated by a certain angle about the origin of the movement. In each movement trial, the participants are asked to hit targets shown on the screen. When visuomotor rotations are applied, the hand movements have to compensate for the visuomotor rotation for the cursor to hit the target. This compensation of the hand movement is the adaptation and the angle of the rotational offset of the hand movement is taken as the adaptation index.

For the current study a 2DOF robotic manipulandum was used. The manipulandum was placed under a table and participants would use their right hand to hold the manipulandum below the table (Fig. 3.2). The table obstructed direct vision of the hand and the visual scene with the cursor and the targets were projected onto the table. Moving the manipulandum made the cursor move on the screen. A black cloth worn around the neck of the participant and attached to the table ensured that participants could not get any visual feedback on the position of the arm. On each trial, the cursor starts at the origin and one target appears pseudorandomly in one of three positions arranged 10 cm from the origin. The three targets were arranged along a circular arc at -30°, 0° and 30° from the origin as shown in Fig. 3.2. The participants were instructed to make shooting movements to make the cursor shoot through the target. The robotic manipulandum was designed to apply forces on the hand. As soon as the cursor crosses an imaginary circle on which the targets are arranged the cursor disappears and a simulated force field captures the hand and slows it down. After each trial the robotic manipulandum provides small forces to guide the hand back to the origin for the next trial. After the participant brings the hand back to the origin, the cursor becomes visible again and the next trial starts with a new target. The experiment was conducted in blocks of perturbations perturbation each with either 200, 130 or 60 trials. There were four types of perturbation blocks — Parameter Estimation (Block - A), Washout (Block - B), AST Perturbation (Block - C) and CL Perturbation (Block D) (Fig. 3.3). The schedule of the perturbation blocks for the participants is described in Fig. 3.4. More details regarding the perturbation blocks are included in the Section 3.3.

The perturbation blocks shown in Fig. 3.4 were presented after a familiarisation block of 60 trials. Initially some experiments were conducted with a shorter familiarisation block. This led to learning effects that seeped into the parameter estimation block. To stabilize the learning effects a longer familiarisation block of 60 trials was chosen and the earlier participants with smaller familiarisation blocks were excluded. Based on initial experiments some changes were made to the settings of the parameter estimation to rectify for some technical issues. The 16 participants discussed in the Section 3.3.2 were all tested under similar conditions.

3.2.2. Participants

The details of the participants are included in Table 3.1. All the participants were right handed individuals who were invited from among the students of TU Delft and Erasmus MC, Rotterdam. There were 16 participants (13 males and 3 females) from an age range of 19-29 years with a median age of 25 years. Pilot experiments on four participants showed an effect size of 2.2087 for the Difference in Movement Angles (DMA) metric (defined in Section 3.4.2). G*Power was used to calculate the number of participants required to have an $\alpha = 0.05$ and power $(1-\beta) = 0.95$ for a one-tailed one-sample t-test. The required number of participants was found to be 5 which is much lower than the 16 chosen for the main experiment.The participants were split into two equal groups (of 8) based on the order of presentation of the perturbation blocks.

3.2.3. Data Acquisition and Processing

The hand position was measured recorded using the encoders on the manipulandum at a sample rate of 200 Hz with the analog inputs from a motor controller card (DMC-1826; Galil Motion Control). Hand velocity was calculated by differentiating the hand position and smoothing using Savitzky-Golay filtering with a filtering width of 25 ms and order of 4. The Inter-Trial Interval (ITI) was 1000 ms. The maximum time per trial is 1500 ms after which the target disappears and the hand the guided back to the origin for the next trial. The hand movement on each trial is analysed from movement onset (defined as the time point when movement velocity exceeds 0.04 m/s) to movement end (defined as the time point when the distance from the origin is equal to or larger than 10 cm). The movement angle of the hand with respect to the target is metric the used to assess adaptation. The movement angle was calculated as the angle between the vector connecting the origin and the target and the vector connecting the hand positions at movement onset and movement end. The perturbations were signed such that counter-clockwise perturbations are positive. The hand movement angles on the other hand were signed so that clockwise rotations are positive. This convention was chosen for ease in interpretation of movement angles with respect to perturbation angles. With this convention, for a perturbation of +30°, a hand movement angle of +30° would be a complete adaptation where the cursor

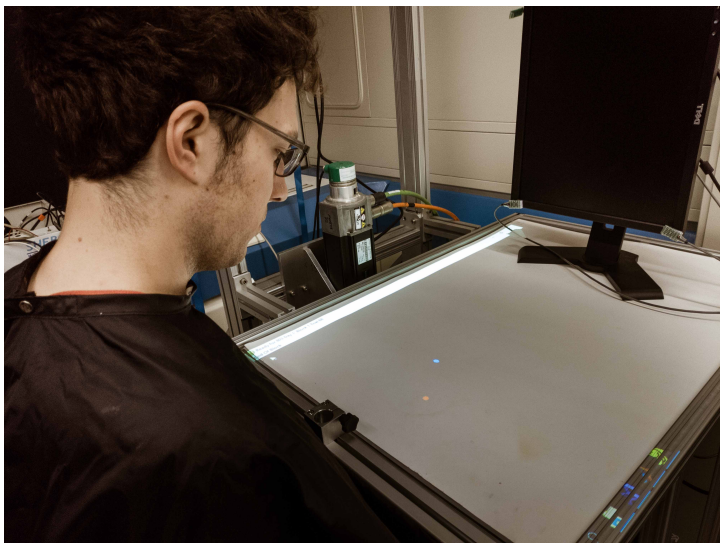

(a) The target and the cursor are projected on to the table.

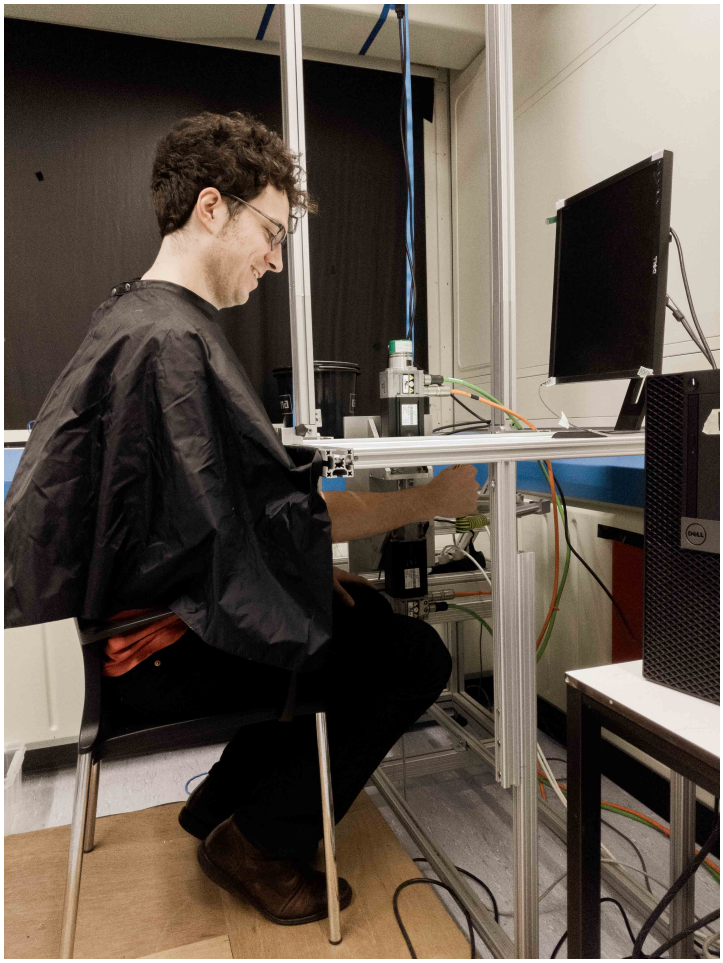

(b) The participant moves the manipulandum under the table to control the cursor.

Figure 3.1: Photos of the Experiment Setup

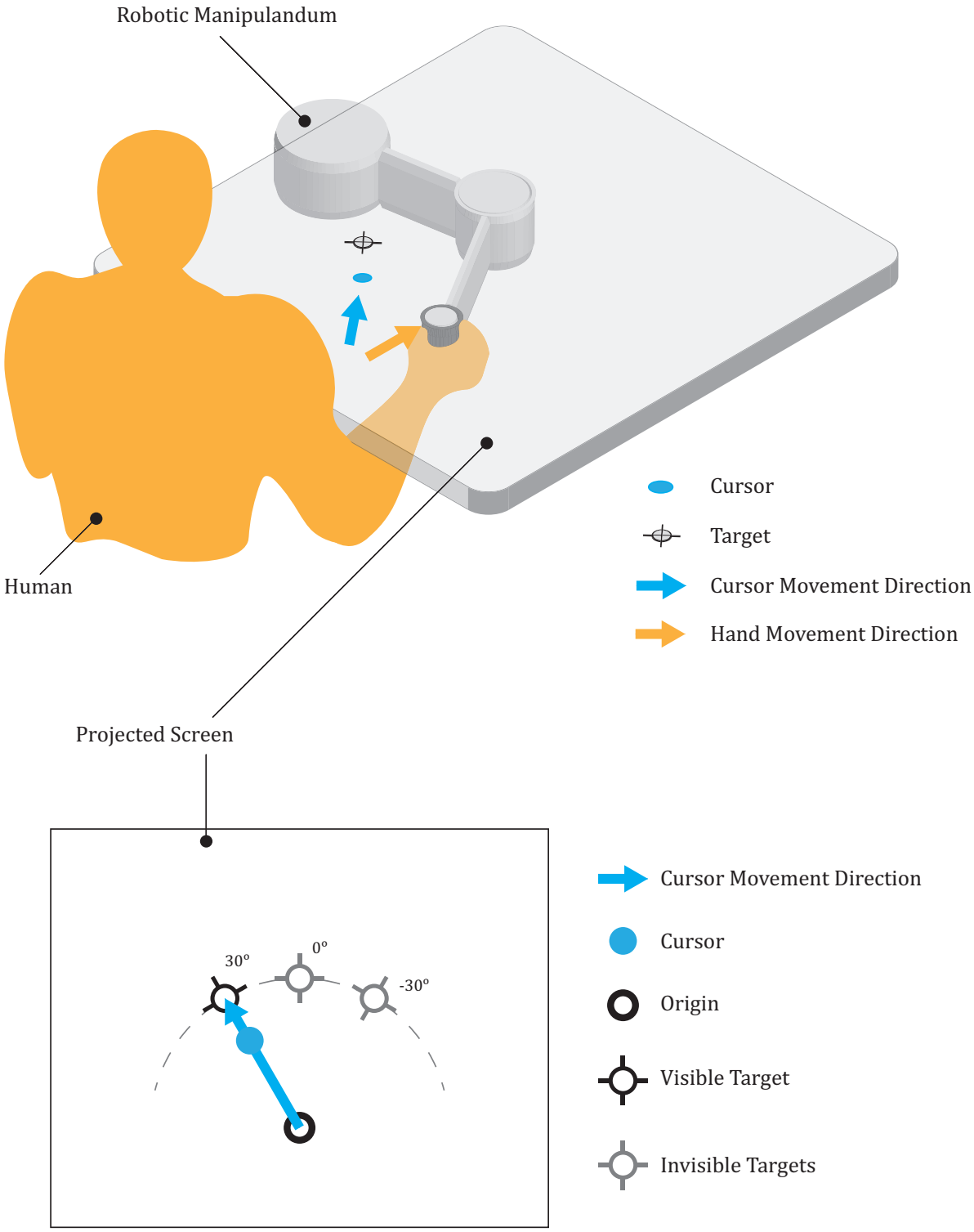

Figure 3.2: Experimental setup. The participants grasps a manipulandum placed beneath a table to control the motion of a cursor on screen projected on top of the table. A black cloth was worn around the neck of the participants and attached to the table to occlude direct vision of the arm. This is not shown in figure. In perturbation trials, the direction of cursor movement is rotated from the direction of arm movement about the origin. On each trial the participants are asked to hit targets randomly chosen from one of three positions.

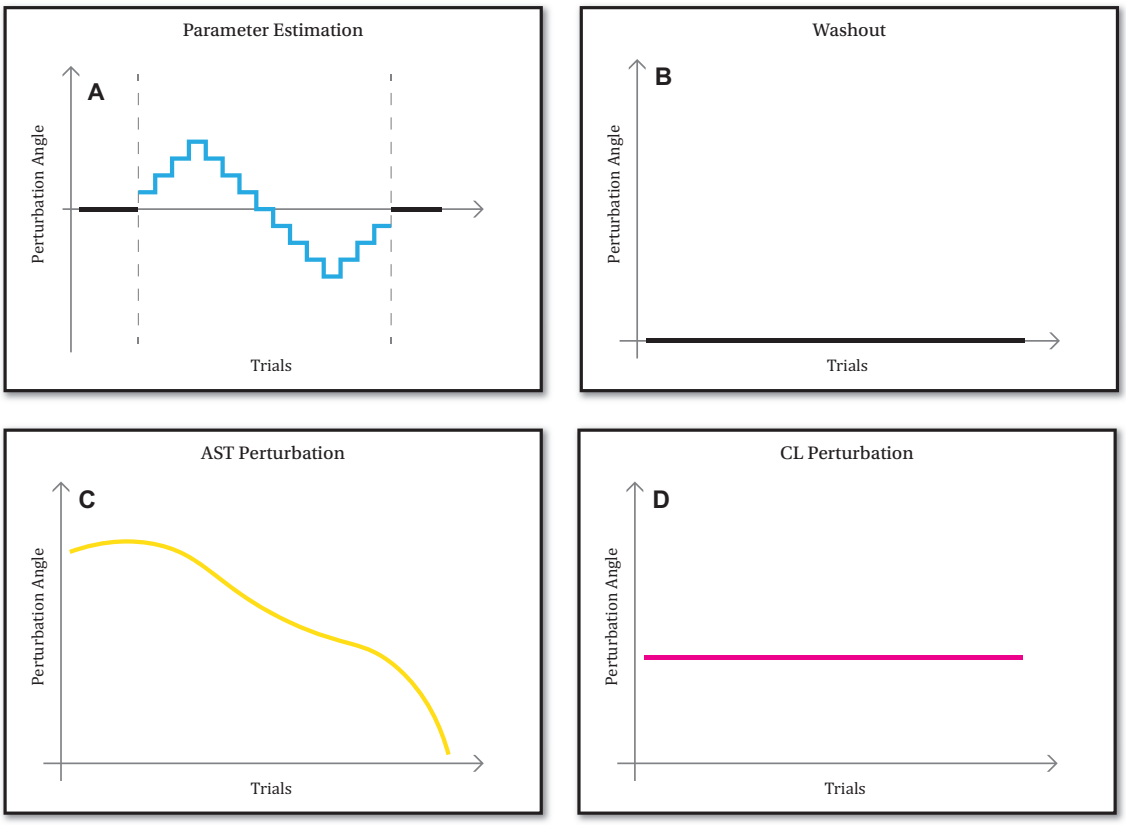

Figure 3.3: Perturbation Blocks

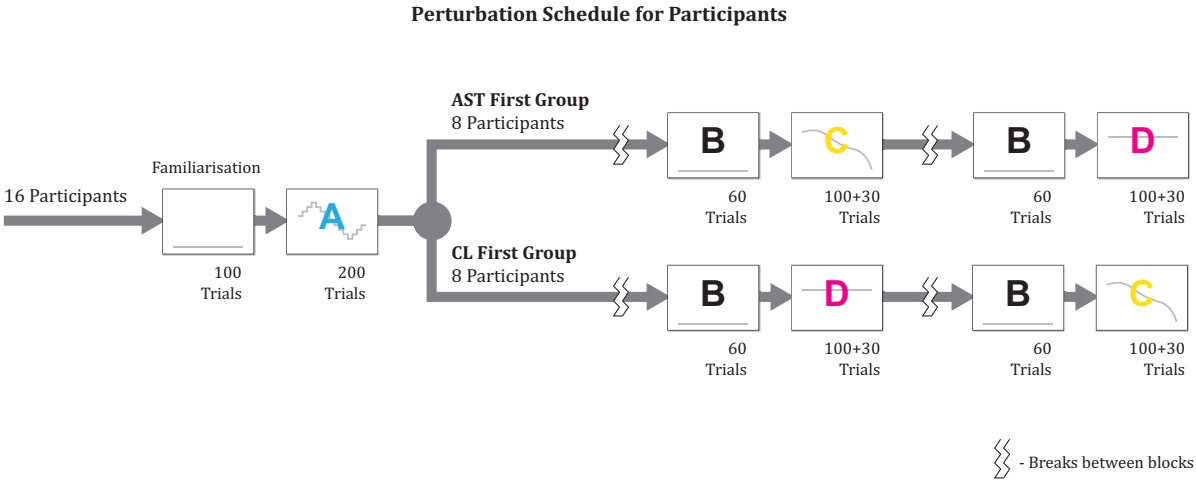

Figure 3.4: The schedule of presentation of perturbation blocks for groups of participants. The order of the AST and CL perturbations are randomized between participants. The C-block has 100 trials of the AST perturbation followed by 30 retention trials. The D-block has 100 trials of the CL perturbation followed by 30 retention trials.

Table 3.1: Details of the participants.

Participant Details			
Participant ID	**Gender**	**Age**	**Perturbation Order**
P1	Male	25	AST First
P2	Male	27	CL First
P3	Male	22	AST First
P4	Male	26	CL First
P5	Male	28	CL First
P6	Male	24	AST First
P7	Male	24	AST First
P8	Male	19	AST First
P9	Male	29	CL First
P10	Male	28	AST First
P11	Male	25	CL First
P12	Female	26	AST First
P13	Male	27	CL First
P14	Male	24	CL First
P15	Female	25	AST First
P16	Female	23	CL First

perfectly hits the target.

3.3. Personalised Perturbations

3.3.1. Parameter Estimation

A staircase perturbation similar to the one used by van der Vliet et al. [2018] was used to estimate the learning and retention parameters of each participant. The magnitude of the perturbation signal changes in increments of $+2^\circ$ or -2° every 6-9 trials. The number of trials between increments were randomly chosen to prevent the participant from guessing when the perturbation signal will change (Fig. 3.5). The perturbation magnitude increased from 0° to a maximum of $+8^\circ$ and then decreased back to 0° in 60 trials. In the following 60 trials, the perturbations moved towards a minimum of -8° and then to 0°. The third set of 60 trials was similar to the first set and moved to $+8^\circ$ and back to 0°. The last 20 trials of the perturbation block were at 0° intended at bringing the participants closer to baseline behaviour. The increments were limited to a magnitude of 2° to minimise the chances of participants getting explicit awareness about the perturbations. When creating the perturbation block A for the experiment, the targets were also randomised within the 3 candidate locations.

The learning and retention parameters were estimated from the observed adaptation behaviour of the participants to the parameter estimation perturbation using the toolbox from Albert and Shadmehr [2018] which uses Expectation Maximisation (EM). Albert and Shadmehr [2018] had showed that expectation maximisation provided a better estimate of the fast and slow states of adaptation than least mean square error minimisation. The hyperparameters used for running the estimation are listed in Table 3.2[1]. These were tuned and finalized after some initial experiments. The minimum difference between the retention rates of the fast and slow states and the minimum difference between the learning rates of the fast and slow states

[1] The upper and lower bounds for a_s, a_f, b_s and b_f were set at the same levels as the paper which introduced the toolbox (Albert and Shadmehr [2018]).

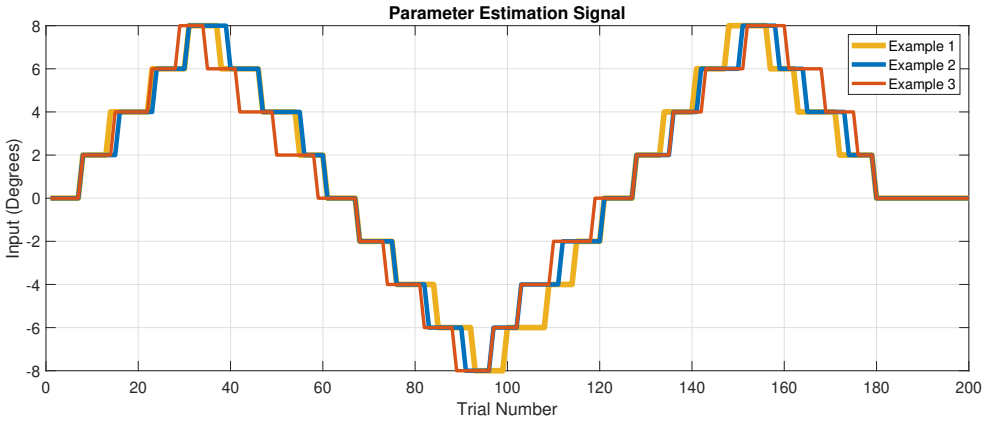

Figure 3.5: Parameter Estimation Signal. Three examples have been shown to illustrate how the randomisation of increments was used to make the signal unpredictable.

were set as 0.05 to ensure that the slow and fast states have appreciable differences in learning and retention rates. If this is not ensured, it was observed that in some cases some parameters had a value of zero while two other parameters have nearly identical values. This is akin to fitting a single rate model. To enforce the fitting of a proper two rate model the constraint was set at 0.05. This ensures that the system described by the estimated parameters are observable and controllable. The toolbox fits a 2-state model onto the adaptation behaviour of the participants and outputs estimates of the learning rates, the retention rates and the initial state of adaptation.

Table 3.2: Hyperparameters for the Expectation Maximisation Toolbox used to estimate the learning and retention rates.

Hyperparameters for Parameter Estimation		
Parameter	**Search Space**	**Initial Estimate**
Slow state retention factor (a_s)	(0,1.1)	0.95
Fast state retention factor (a_f)	(0,1.1)	0.9
Slow state learning rate (b_s)	(0,1)	0.05
Fast state learning rate (b_f)	(0,1)	0.30
Initial slow state ($x_s(k_0)$)	(-5,5)	0
Initial fast state ($x_f(k_0)$)	(-5,5)	0
State noise variance	(1e-7,10)	0.5
Motor noise variance	(1e-7,10)	0.5
Initial state variance	(1e-7,10)	0.5
Settings	**Value**	
Number of Iterations	100	
Minimum difference between (a_s) and (a_f)	0.05	
Minimum difference between (b_s) and (b_f)	0.05	

3.3.2. Scaled Inputs

The learning and retention parameters of each participant estimated from the behavioural results of Block A is used to tailor the AST and CL perturbations. The perturbations are calculated as described in Sections 2.4 and 3.1. At this stage, the perturbations might have different peak magnitudes for each participant as is seen

in Fig. 2.5a. The perturbation magnitude should be limited for the purposes of the experiment. For the experiment 30° was selected as the maximum limit for the perturbation magnitude. The AST perturbation was scaled to have a maximum magnitude of 30° (Fig. 3.6a) which would result in optimal state trajectories which are also scaled up (Fig. 3.6b). The CL perturbation is also scaled by the same factor as the AST perturbation so that the net adaptation at the end of 100 trials is same for both perturbations.

3.3.3. Perturbation Blocks

The Familiarisation Block had 100 trials of 0° perturbation in which the participants can get accustomed to the experimental setup. Perturbation Block A is comprised of 200 trials of the staircase perturbation for parameter estimation. Block B was a washout block with 60 trials of 0° perturbation.

The AST and CL perturbations were embedded in Blocks C and D respectively. The 100 trials of the AST/CL perturbations were followed by 30 retention trials. The retention trials were included to study how the adaptation decays after the perturbations. In the retention trials, the participants experienced zero sensorimotor error ($e(n) = 0°$). This was achieved by making the cursor hit the target perfectly on all trials. The cursor would move along the line connecting the origin and the target as the hand moved away from the origin. At any given instant, the distance between the cursor and the origin would be equal to the distance between the hand and the origin. The number of retention trials were limited to 30 so as to avoid the participants from becoming aware of the retention trials.

In all the perturbation blocks, the target were randomly selected from one of 3 locations are described in Fig. 3.2. Online feedback about the cursor position was provided during each trial as it moved from the origin towards the target. The cursor would disappear at the end of each trial (i.e., when the distance from the origin surpasses 10 cm) and only reappear at the start of the next trial.

3.4. Analysis

3.4.1. Model Predictions

The experiments were based on the assumption that the parameter estimation from Block A was sufficiently accurate to predict the adaptation behaviour of the participants in the perturbations blocks that followed. To check the aptness of the parameter estimation from Block A, the Expectation Maximisation (EM) toolbox was used to fit the 2-state model onto the adaptation behaviour for the AST and CL perturbations. This provided the learning and retention parameters for the model that best fit the behavioural findings of the corresponding blocks. The initial state of adaptation was a free parameter that was tuned to get the best fit. To make sure that arbitrary initial values were not selected for the start of the actual perturbation of interest (Blocks C and D), the washout blocks that preceded Blocks C and D were also considered while fitting the model. Thus for the AST and CL blocks, the models were fit for 190 trials (60 trials of Block B + 130 trials of Block C/D). It must also be noted that the perturbation signals in Blocks C and D were not the ideal perturbations for use in system identification. Since the goal of conducting the parameter estimation for Blocks C and D were only to verify that the parameters estimated from Block A were representative of the adaptation behaviour of the participant, the parameter estimates from Block A were given as the initial estimates while running the EM toolbox for the AST and CL blocks. The search space was the same for all cases.

The parameters estimated were then used to simulate the mean adaptation trajectories - including trajectories for the fast, slow and net adaptation. The predicted Movement Angle (MA), observed MA and the mean-fit MA were plotted for each participant. The mean-fit fast and slow states were also plotted against their predicted trajectories. The difference between the predicted trajectories and the mean-fit ones were quantified in terms of MSEs. For the current project, all the analysis was done in MATLAB except for the Analysis of Variance (ANOVA) for which IBM SPSS Statistics was used.

3.4.2. Within-Subject Analysis

The Difference in Movement Angles (DMA) averaged over the 30 retention trials at the end of Blocks C and D was used as the metric to test if retention after AST perturbation was better than that after the CL perturbation. The DMA was calculated in terms of the MAs in the i^{th} trial of Block C $\left(\theta_{\text{C}}(i)\right)$ and the MAs in the i^{th} trial of Block D $\left(\theta_{\text{D}}(i)\right)$ as [2]

[2] In some cases where participants did not complete some trials, the corresponding trials for both Block C and Block D were disregarded in the summation. In these cases, the sum was divided by the actual number of trials considered (instead of the default value of 30).

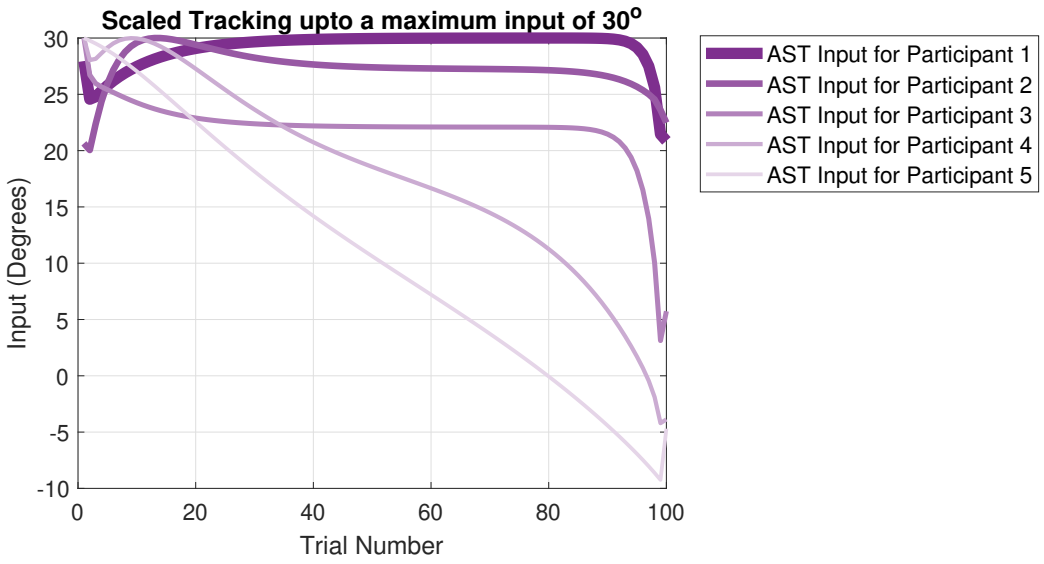

(a) Scaled inputs

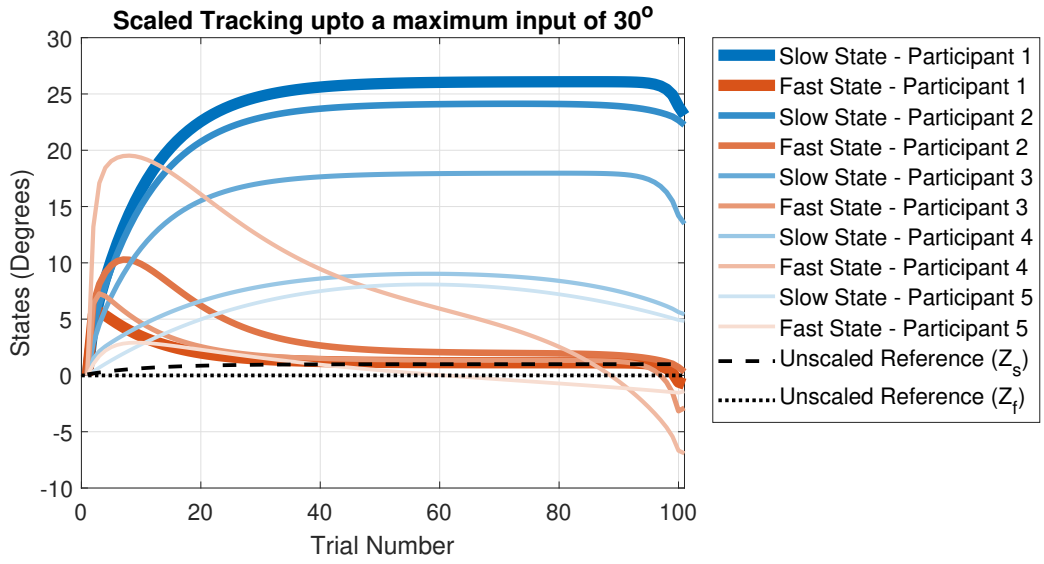

(b) Optimal state trajectories for scaled inputs

Figure 3.6: Scaled optimal input and state trajectories from Adaptation-State-Tracking (AST) for virtual participants with learning and retention rates as seen in literature.

$$DMA = \frac{1}{30} \cdot \sum_{i=101}^{130} \Big[\theta_{\mathrm{C}}(i) - \theta_{\mathrm{D}}(i)\Big]. \tag{3.4}$$

Based on this metric the following within-subject hypothesis was formulated:

H1: Within-Subject Hypothesis

It was hypothesised that the AST perturbation would result in more retention than the CL perturbation and that this would be reflected in the value of DMA having a value greater than zero for each participant.

$$DMA > 0. \tag{3.5}$$

A one-sample Kolmogorov-Smirnov test (with $\alpha = 0.05$) was used to check if the DMAs were non-normal. Since the test showed that the DMAs were significantly non-normal, a one-tailed one-sample Wilcoxon signed-rank test (with $\alpha = 0.05$) was used to check hypothesis H1.

3.4.3. Washout Effects

During initial analysis, it was observed that in most of the participants that violated hypothesis H1 belonged to the AST-First group. This warranted a closer look into the completeness of the washout between the perturbation blocks. An incomplete washout would mean that there might be residual adaptation from the previous perturbation block which might result in distorted results when doing a within-subject analysis. The presence of residual adaptation would be reflected in the parameter estimates for the first and second perturbation blocks. One sample Kolmogorov-Smirnov tests where used to test the normality of the distributions of parameter estimates. They showed that the null hypothesis of normality can be rejected for all the parameters. To uncover any possible effects of perturbation order on the parameters, the participants were divide according to the order of presentation of perturbations. And, two-tailed paired-sample Wilcoxon signed-rank tests (with $\alpha = 0.05$) were used to compare each of the learning and retention parameters of the first and second perturbation blocks.

The DMA metric considers both the perturbation blocks experienced by a participant. If the washout is incomplete, the second perturbation block experienced by the participants might be tainted. To separately quantify the adaptation behaviour of each participant on both the perturbation blocks, a new metric (Mean Scaled Movement Angle (MSMA)) was formulated after tests of hypothesis H1 returned non-significant results. As explained in Section 3.2.2, the inputs for each participant was scaled up so that the maximum perturbation angle was $+30^\circ$. This means that different participants are trained to different terminal states. To conduct an consistent analysis, the MAs should be scaled back by the same factor (γ) as the input for each participant. Thus Mean Scaled Movement Angles (MSMAs) for the perturbation blocks was formulated as [3]

$$\begin{aligned} MSMA_{\mathrm{AST}} &= \frac{1}{\gamma} \cdot \frac{1}{30} \cdot \sum_{i=101}^{130} \Big[\theta_{\mathrm{C}}(i)\Big], \\ MSMA_{\mathrm{CL}} &= \frac{1}{\gamma} \cdot \frac{1}{30} \cdot \sum_{i=101}^{130} \Big[\theta_{\mathrm{D}}(i)\Big]. \end{aligned} \tag{3.6}$$

A mixed ANOVA was conducted to explore any interactions between the MSMAs of the perturbation blocks (within-subject factor) and the perturbation order (between-subject factor). The mixed ANOVA was conducted using IBM SPSS Statistics 25. The analysis of the completeness of the washout was explorative in nature.

[3] In some cases where participants did not complete some trials, the corresponding trials were disregarded in the summation. In these cases, the sum was divided by the actual number of trials considered (instead of the default value of 30).

3.4.4. Between-Subject Analysis

After recognising that the washout between perturbations might have been incomplete and that there might be residual adaptations that leak into the perturbation block that is experienced last, a second between-subject hypothesis was formulated to compare the retention after AST and CL perturbations. In this hypothesis, only the first perturbation block experienced by each participant is considered. To compare the AST-first and CL-first groups, the MSMA metric was used. The between-subject hypothesis was formulated as:

H2: Between-Subject Hypothesis

It was hypothesised that the AST perturbation would result in more retention than the CL perturbation and that this would be reflected in the value of MSMAs for the AST-first group having a value greater than the MSMAs for the CL-first group.

$$MSMA_{\text{AST}} > MSMA_{\text{CL}}. \tag{3.7}$$

It should be noted that this hypothesis H2 was formulated after the experiments were conducted. This was formulated after observing that incomplete washout might have caused the hypothesis H1 to have non-significant effects.

A one-sample Kolmogorov-Smirnov test (with $\alpha = 0.05$) was used to check if the MSMAs were non-normal. Since the test showed that the MSMAs were significantly non-normal, a one-tailed Mann-Whitney U-test (with $\alpha = 0.05$) was used to compare the two groups of MSMAs.

4

Results

4.1. Model Predictions

The estimates of the learning and retention parameters of each participant for each adaptation block is plotted in Fig. 4.1, grouped by perturbation order [1]. A red upward pointing triangle denotes the participants belonging to the AST-first group and the participants from the CL-first group are denoted by a yellow downward pointing triangle. Based on these parameters, the mean-fit MAs were simulated for each adaptation block. These mean-fit MAs were plotted along with the predicted MAs and the observed MAs. The predicted, observed and mean-fit net adaptation for the AST Block is plotted in Fig. 4.2. The predicted, observed and mean-fit net adaptation for the CL Block is plotted in Fig. 4.3. Since the fast and slow states cannot directly be measured, model simulations based on the estimated learning and retention rates were used to find the mean-fit fast and slow states of adaptation. The predicted and mean-fit trajectories of the fast and slow states for the AST block is plotted in Fig. 4.4. The predicted and mean-fit trajectories of the fast and slow states for the CL block is plotted in Fig. 4.5. The MSEs between the predicted and mean-fit trajectories for each participant are summarised in Fig. 4.6. It can be seen that the predicted and mean-fit trajectories for the net adaptation line up well. This is also reflected in the relatively low MSEs for the net adaptation (Fig. 4.6). Thus the 2-state LTI model was able to predict the adaptation behaviour. The fast and slow states on the other hand, show more deviations from the predicted values.

4.2. Within-Subject Results

The initial hypothesis (H1) was based on a within-subject analysis. For this the retention after the AST and CL blocks of each participant was compared with each other using the DMA metric. The DMAs of all the participants are plotted in Fig. 4.7. A one-sample Kolmogorov-Smirnov test on the DMAs (with $\alpha = 0.05$) showed that the null hypothesis of assuming a normal distribution can be rejected ($p < 0.001$). One-tailed one-sample Wilcoxon signed-rank test (with $\alpha = 0.05$) used to check hypothesis H1 did not show a significant effect ($p = 0.1567$).

4.3. Washout Effects

The comparisons of the learning and retention parameters of the first and second perturbations is plotted in Fig. 4.8. While carrying out the comparisons, the AST-first and CL-first groups were treated separately. One-sample Kolmogorov-Smirnov tests showed that all the parameter distributions deviated from a normal distribution ($p < 0.001$ for all). The results of the two-tailed paired-sample Wilcoxon signed-rank tests are mentioned in the corresponding plots. Even though none of the effect sizes are significant, there is a weak effect for the AST-first group on the retention rate of the slow process a_s ($p = 0.1094$) and the learning rate of the fast process b_f ($p = 0.1094$).

The mixed ANOVA of all the MSMAs showed no significant effect of the perturbation block , $F(1,12) = 0.92$, $p = 0.767$. The perturbation order had more effect on the MSMAs albeit non-significant, $F(1,12) = 3.98$, $p = 0.069$. There was a weak non-significant interaction between the perturbation order and the perturbation block on the MSMAs, $F(1,12) = 2.82$, $p = 0.119$.

[1] Refer to Appendix E for some additional results regarding parameter estimation, input scaling and terminal MAs.

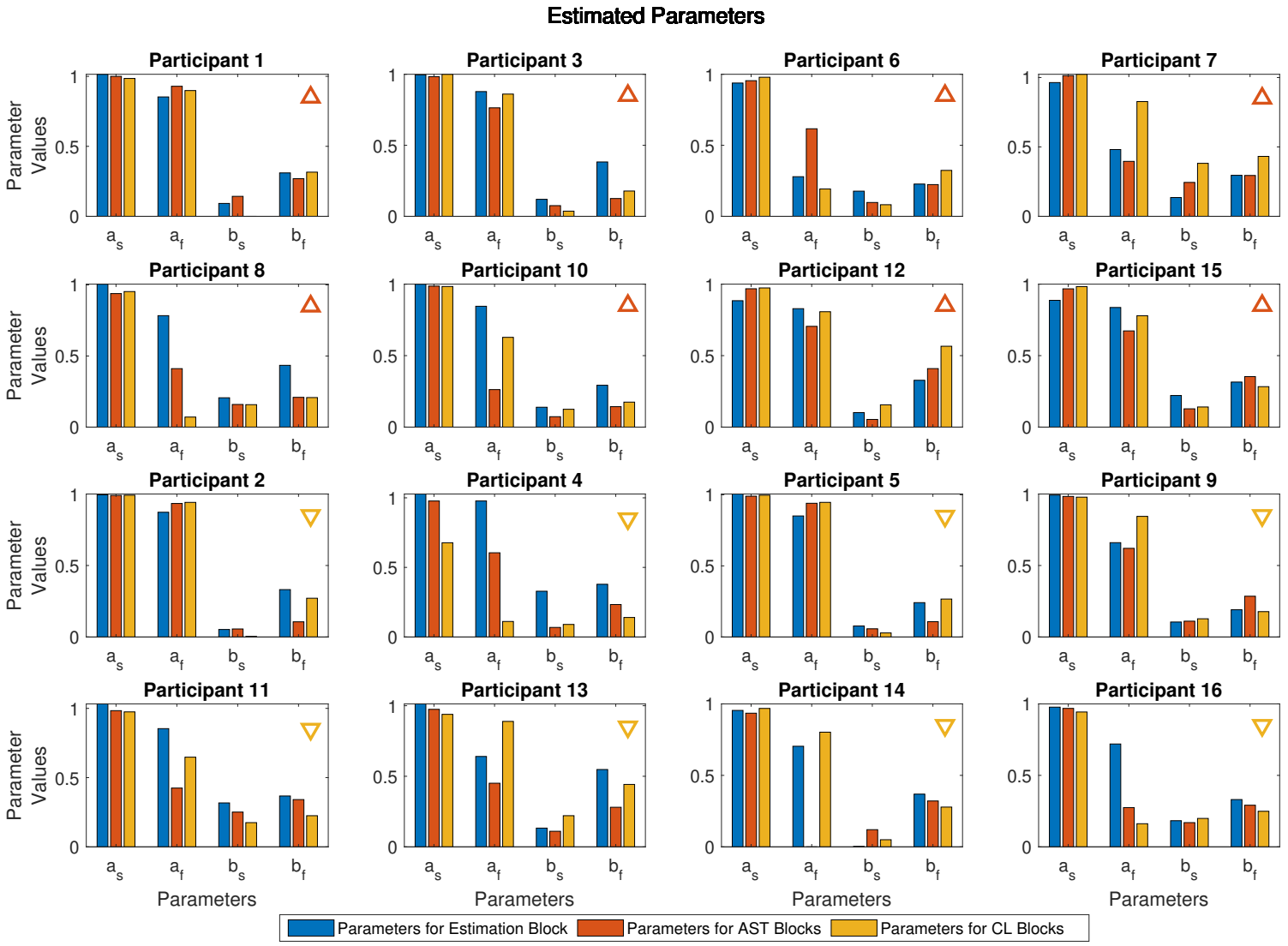

Figure 4.1: Estimated Learning and Retention Rates. The participants from the AST-First group is indicated by the red upward-pointing triangle and those from the CL-First group are denoted by the yellow downward-pointing triangle. The learning and retention rates estimated for the parameter estimation block (shown in blue) were the ones used to predict adaptation behaviour and to design the AST perturbation. The parameter estimates for the other two blocks (shown in red and yellow) were just used to study how the parameters might vary from the initial estimates.It must be noted that the AST and CL perturbations might not be perfect for conducting parameter estimation and that the values shown in red and yellow might be less reliable than the ones shown in blue.

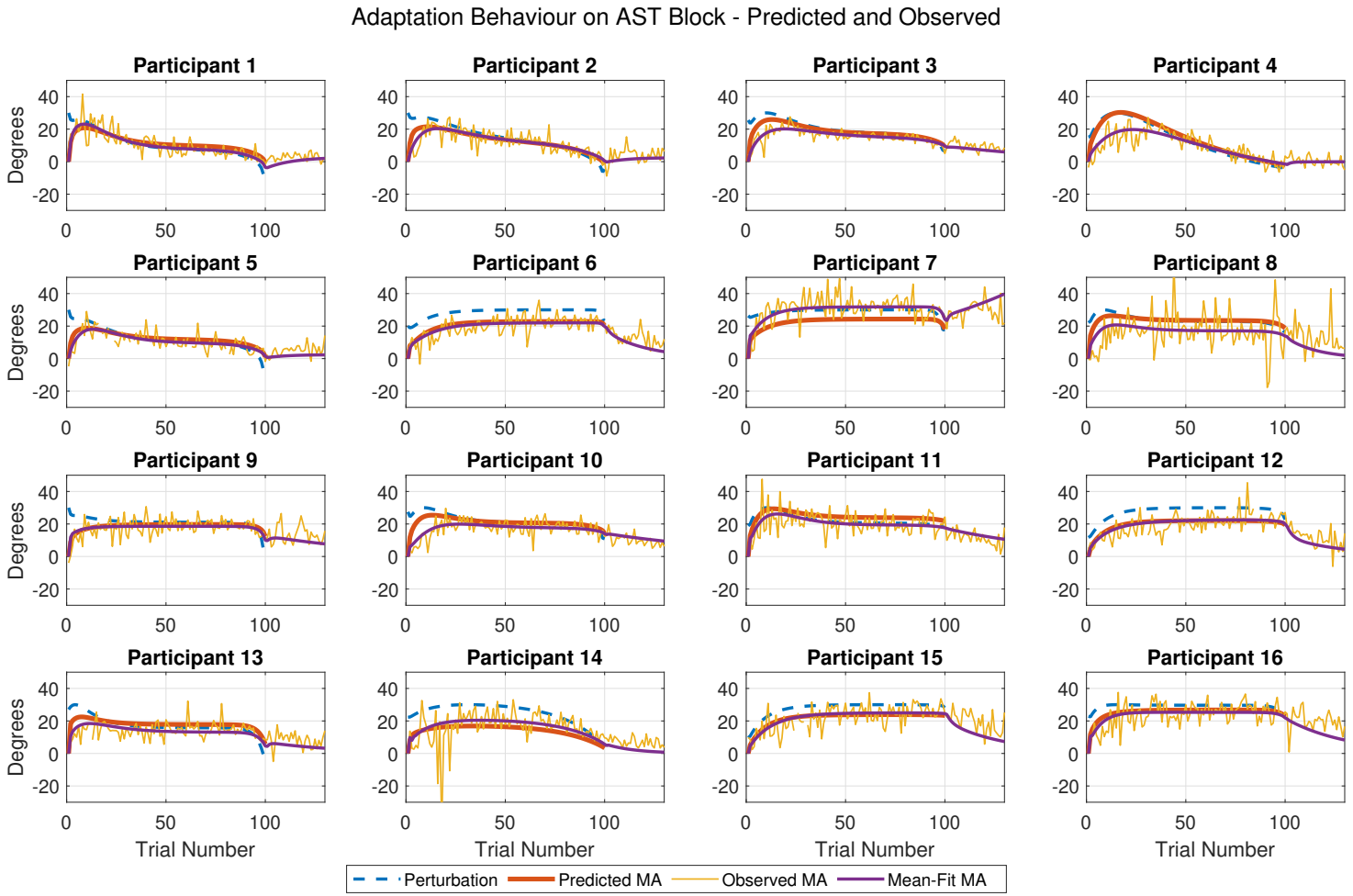

Figure 4.2: Movement Angle (MA) for AST Block. The parameters for the parameter estimation block (shown in blue in Fig. 4.1) were used to calculate the predicted behaviour.

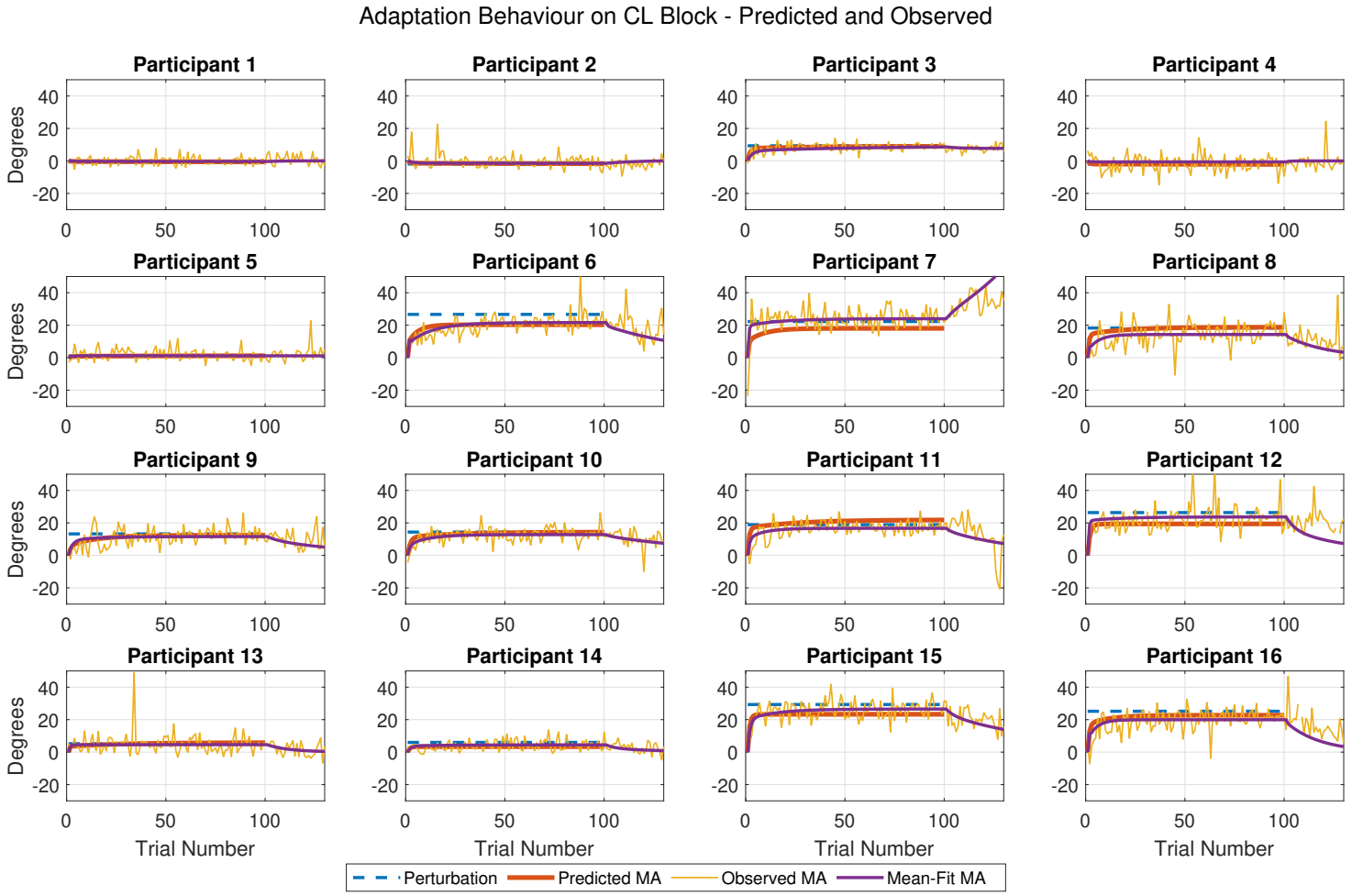

Figure 4.3: Movement Angle (MA) for CL Block. The parameters for the parameter estimation block (shown in blue in Fig. 4.1) were used to calculate the predicted behaviour.

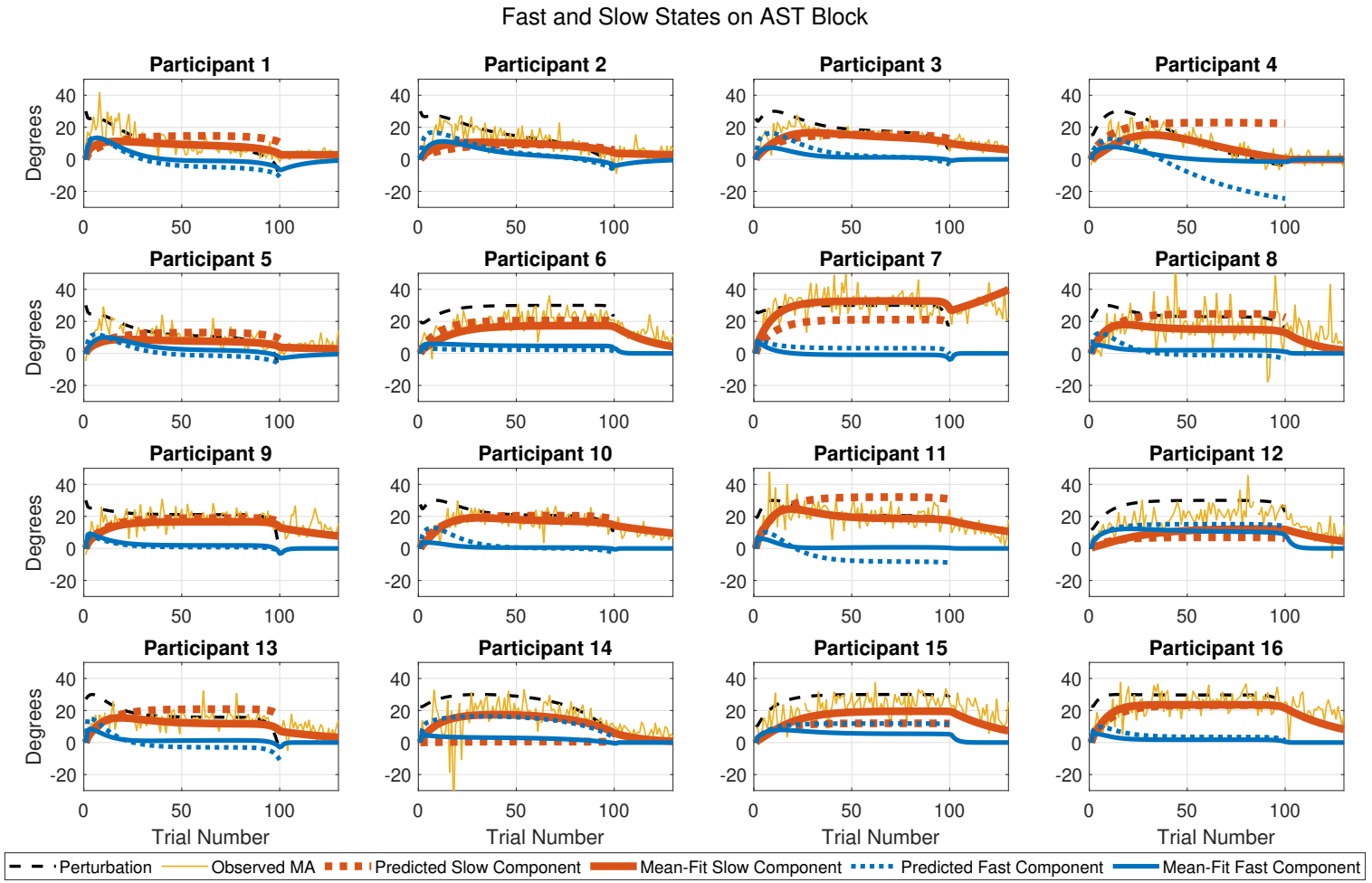

Figure 4.4: Fast and Slow States for AST Block. The parameters for the parameter estimation block (shown in blue in Fig. 4.1) were used to calculate the predicted behaviour.

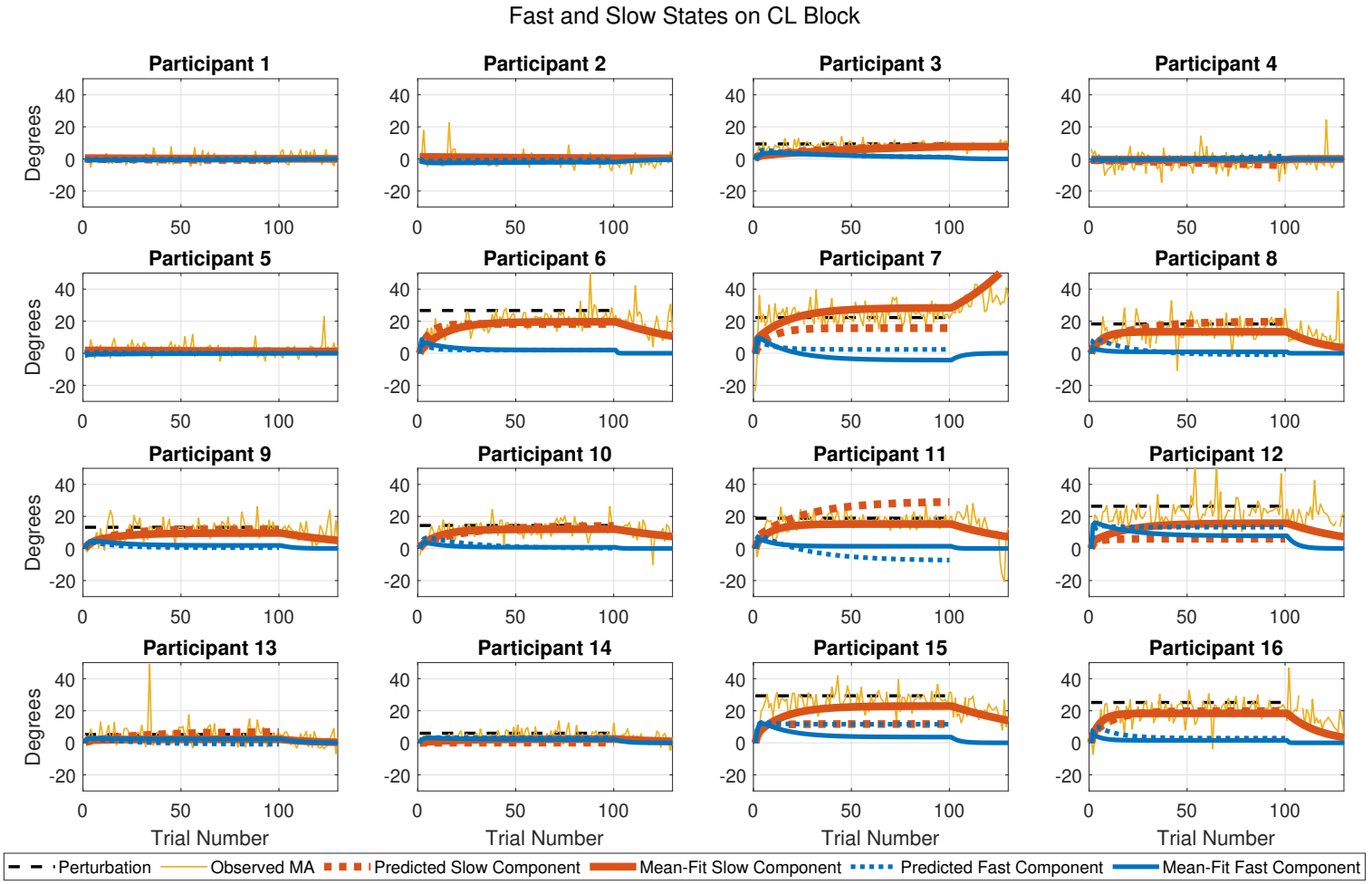

Figure 4.5: Fast and Slow States for CL Block. The parameters for the parameter estimation block (shown in blue in Fig. 4.1) were used to calculate the predicted behaviour.

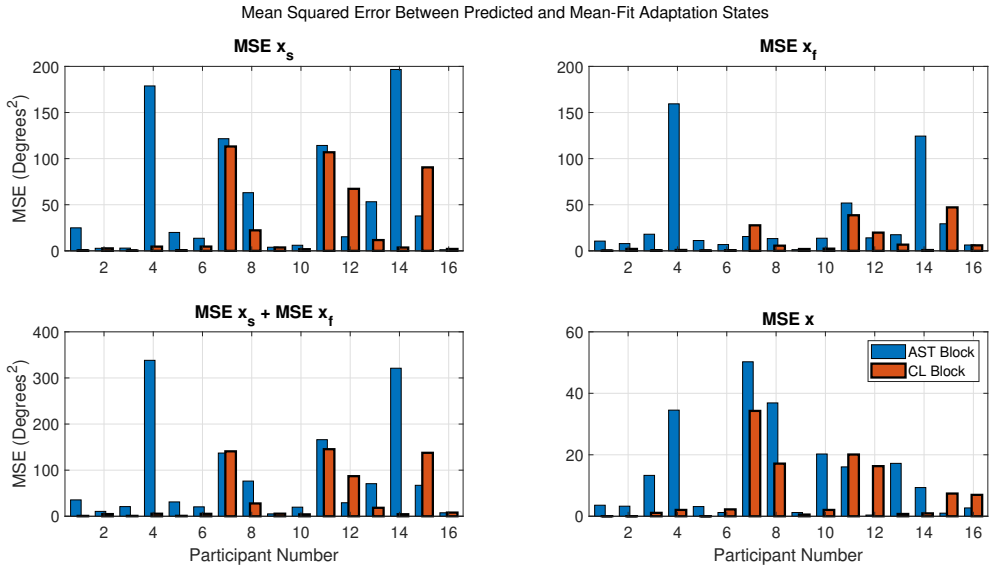

Figure 4.6: MSE between predicted and mean-fit adaptation behaviour. Since the comparison is between the predicted and mean-fit values, the effect of randomness in the adaptation behaviour does not affect this metric.

4.4. Between-Subject Results

Since the incompleteness of the washout blocks might have tainted the second perturbation block experienced by the participants, a second hypothesis (H2) was formulated after the experiment which only considers the first perturbation block experienced by the participants. In order to conduct the between-subject analysis the metric MSMA of the first adaptation block experienced by the participants were used. Fig. 4.9 plots the scaled MAs of the first adaptation blocks and illustrates how the MSMAs were calculated. The MSMAs of the two groups of participants are shown in Fig. 4.10. One-sample Kolmogorov-Smirnov tests (with $\alpha = 0.05$) showed that for $MSMA_{\text{AST}}$ the null hypothesis of assuming a normal distribution could be rejected ($p = 0.0013$) and that the null hypothesis of normality for $MSMA_{\text{CL}}$ cannot be rejected ($p = 0.0513$). A one-tailed Mann-Whitney U-test (with $\alpha = 0.05$) used to compare the two groups of MSMAs showed significant difference between the MSMAs of the two groups ($p = 0.0415$). Thus $MSMA_{\text{AST}}$ is significantly greater than $MSMA_{\text{CL}}$ which shows that retention is improved by the use of the AST perturbation.

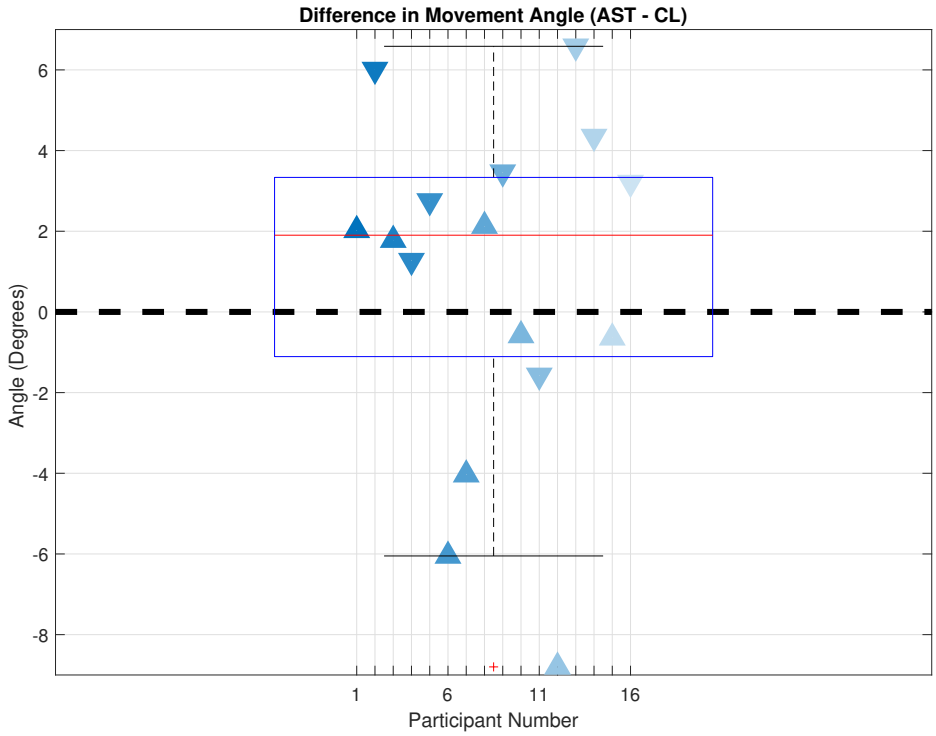

Figure 4.7: DMA. Upward arrows indicate participants who were presented with AST perturbation first. The downward arrow represents participants who experienced the CL perturbation first.

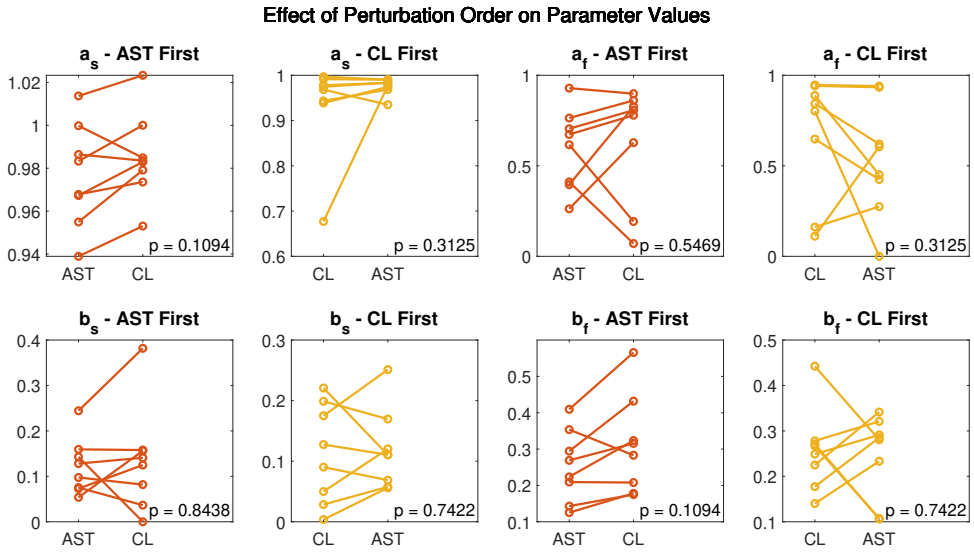

Figure 4.8: Effect of perturbation order on learning and retention parameters. The p-values obtained from conducting two-tailed paired-sample Wilcoxon signed-rank tests to compare the learning rates for the first and second perturbation blocks is mentioned at the right bottom corner of the corresponding plots. The perturbations are plotted such that the first perturbation is always on the left.

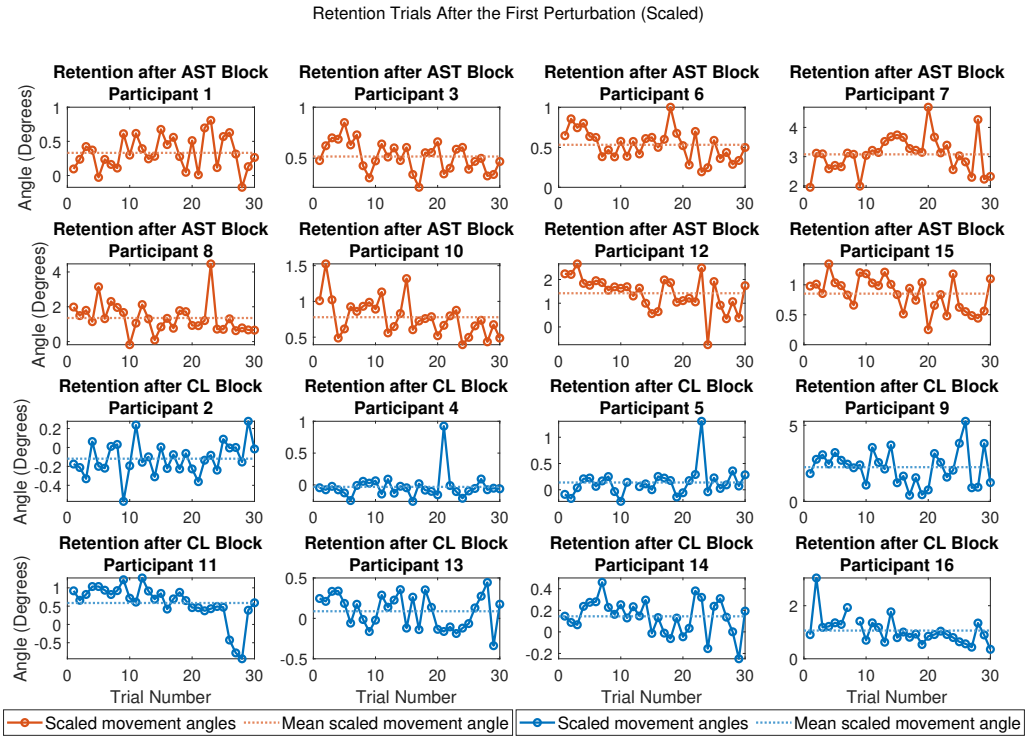

Figure 4.9: Scaled Movement Angles in the retention trials after the first perturbation block.

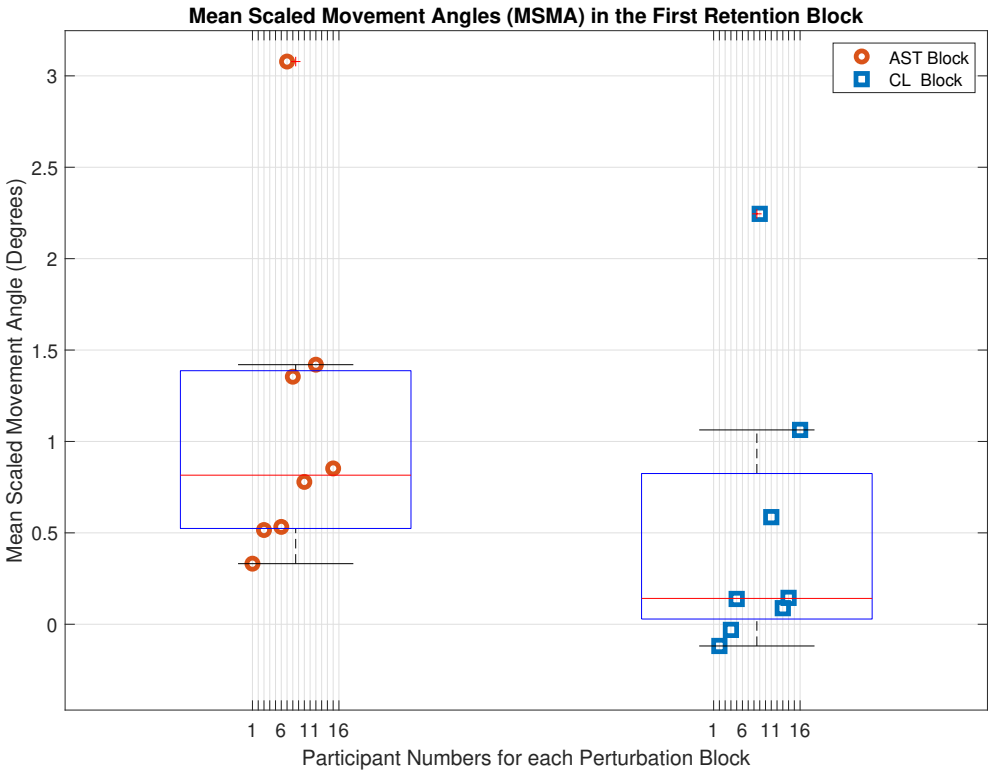

Figure 4.10: MSMA

5

Discussion

5.1. Does AST improve adaptation?

The between-subject analysis (for hypothesis H2) showed that the AST perturbation generated significantly better retention than the CL perturbation ($p = 0.0415$). The original within-subject analysis (for hypothesis H1) on the other hand only showed a weak effect of the AST in improving retention ($p = 0.1567$). 6 out of the 16 participants violated hypothesis H1. Of these 6, 5 were from the AST-first group. This hints that the retention caused by the AST block outlasting the washout block and leaking into the CL block that followed. This prompted the analysis into the completeness of the washout block. The discussion on washout is detailed in Section 5.3.

The natures of the component processes of adaptation exhibit dichotomies. The present work focuses on the difference in retention between the fast and slow processes. The slow process was found be the major contributor towards long-term retention (Joiner and Smith [2008],Charalambous et al. [2018]). It was hypothesised that increasing the contribution of the slow process would improve retention. This hypothesis was proven in the between-subject analysis. Beyond this particular hypothesis, the results prove that the component processes of adaptation can be influenced by manipulating the perturbation schedule. This opens up possibilities for enhancing not only retention, but also other aspects of adaptation like generalisation, transferability, cognitive load and reaction times. The slow/implicit process has lower cognitive requirements and is thus less affected by secondary tasks (Keisler and Shadmehr [2010], van Es and Knapen [2019]). Therefore, the AST perturbation designed here will likely reduce the effect of secondary tasks on the adaptation. Generalisation and transfer are associated with the fast/explicit component of adaptation (Keisler and Shadmehr [2010], Mandelblat-Cerf et al. [2011], McDougle et al. [2017], Schween et al. [2018], Werner et al. [2015], Poh et al. [2016], Werner et al. [2019]). Thus to improve generalisation and transfer, the AST perturbation should be designed to increase the contribution of the fast state and reduce the contribution of the slow state ($[x_s\ ,\ x_f] = [0\ ,\ 1]$).

Combining explicit aiming instructions with AST perturbations might provide better control over adaptation. This idea hinges on the explicit-implicit nature of the fast-slow processes of adaptation. Instructions can be used to control the trajectory of the explicit process. The schedule of instructions must parallel the optimal trajectory of the fast process from AST calculation. Mazzoni and Krakauer [2006] had explored the effects of giving instructions to counteract a visuomotor rotation. It was observed that instruction was able to produce rapid compensation of rotational perturbations. But, as time went by, the growth of the implicit process led to increase in errors. This problem of increasing error due to growth of the implicit adaptation might be rectified by the varying the instructions with each trial based on the optimal trajectory for the fast process. Thus by intelligently manipulating the instruction and perturbation, we can improve learning and retention. Leukel et al. [2015] had shown that the experts as opposed to novices have a stronger (more precise) explicit process and that they have longer retention. It might be possible that experts modulate their explicit process to improve the contribution of the implicit process which is more stable. AST perturbations might enable the application of this strategy to rehabilitation.

Context-based adaptation has not been explored in this work. Lee and Schweighofer [2009] showed that context based adaptation can be modelled with a 1-fast N-slow model. A single fast process is shared by all the contexts and each context has a slow process associated with it (N slow states for N contexts). AST

perturbations designed for multiple contexts could be used to verify the validity of the 1-fast N-slow model.

One of the main contributions of this thesis is the thinking of adaptation as a standard linear control problem. This enables many new options for influencing adaptation with existing linear control theory, including optimal control. Adaptation-State-Tracking (AST) in the current work was based on a feedforward control design. This is a basic control design. The open-loop aspect is a useful first step in that it enables the evaluation of how accurate the underlying model is. The effectiveness of the AST perturbation illustrated in the current work warrants the use of more involved control designs. Feedback with state estimators can be used to ensure that the actual adaptation states follow the predicted trajectories. Model Predictive Control (MPC) could be used to generate optimal trajectories for the input and states while obeying constraints.

5.2. Is the 2-state LTI model sufficient?

The predicted MAs from 2-state LTI model suggested by Smith et al. [2006] were similar to the observed MAs (Figs. 4.2 and 4.3). The EM toolbox for estimating the learning and retention parameters from Albert and Shadmehr [2018] was instrumental in tuning the model parameters to fit each individual participant. The similarity of the predicted and observed MAs validate the 2-state LTI model where adaptation is composed of two error-driven processes acting at different timescales and the use of EM for fitting the model to each individual. The AST and CL perturbations were designed based on the 2-state LTI model and the AST perturbation exhibited more retention as hypothesised. This proves that the 2-state LTI model can be used to design perturbations to influence the characteristics of adaptation. As far as the author is aware, this is first time the 2-state LTI model has been used to design a perturbation and to predict the subsequent behaviour of the participants.

The fast and slow states have larger MSEs between predicted and observed values than the predicted and observed MAs for the net adaptation (Fig. 4.6). There is no direct method of probing the slow and fast states. They can only be estimated based on model fits as seen in the following articles — C-Hemminger and Shadmehr [2008], Joiner and Smith [2008], Huang and Shadmehr [2009], Sing and Smith [2010], Trewartha et al. [2014], McDougle et al. [2015], Coltman et al. [2019], Smith et al. [2006], Colagiorgio et al. [2015], Inoue et al. [2015], Zarahn et al. [2008], Lee and Schweighofer [2009], Turnham et al. [2012], McDougle et al. [2015] and Albert and Shadmehr [2018]. The perturbation signal in Block A (parameter estimation block) was designed with the objective of getting the best estimate of the learning and retention parameters. The staircase shape of the perturbation ensures maximum frequency content. The AST and CL perturbations on the other hand, are not the perfect signals for conducting parameter estimations (since some frequencies might be missing in the signal). This might be the reason why the estimates of the fast and slow states show large deviations from the predicted values (Figs. 4.4 and 4.5). Contrary to the fast and slow processes, there are many methods for measuring the explicit and implicit processes of adaptation — Process Dissociation Procedure (PDP) (Werner et al. [2015]), self-reported aim (Taylor et al. [2014]), and gaze-based estimation (de Brouwer et al. [2018]). These methods could be used to check the effects of the AST perturbation on the explicit and implicit components and verify the overlap between the fast-slow and explicit-implicit dichotomies proposed by McDougle et al. [2015]. If there is an overlap between the dichotomies, real-time estimates of the explicit and implicit components can be useful in designing online feedback controllers for the fast and slow states of adaptation.

Piecewise-linear perturbations have been widely used in studies that try to fit the fast and slow process models of adaptation: C-Hemminger and Shadmehr [2008], Joiner and Smith [2008], Sing and Smith [2010], Trewartha et al. [2014], McDougle et al. [2015], Coltman et al. [2019], Smith et al. [2006], Inoue et al. [2015], Zarahn et al. [2008], Lee and Schweighofer [2009] and McDougle et al. [2015] uses combinations of step signals alone whereas Huang and Shadmehr [2009], Turnham et al. [2012], Colagiorgio et al. [2015] and Albert and Shadmehr [2018] incorporates trapezoidal/triangular perturbation signals along with step signals. Turnham et al. [2012] uses an additional random signal also. None of the papers use smooth nonlinear perturbations like the AST perturbation. The MSEs for the AST perturbation blocks observed from the current experiment were likely to have larger values than the CL perturbation. This lack of fit hints at system dynamics associated with nonlinear perturbations that are not modelled by the 2-state LTI model by Smith et al. [2006].

Contradictions for the linear model in relation to the explicit and implicit processes have been observed by Morehead et al. [2015]. Morehead et al. [2015] found that the contribution of the explicit process is more prominent for larger perturbations while the contribution of the implicit process is not dependent on the size of the perturbation. This cannot be explained by a linear model of adaptation. Berniker and Kording [2011] suggested a model of adaptation where large perturbations are attributed to world rotation and smaller per-

turbations are attributed to body rotation. The magnitude of the error determines which component undergoes adaptation. Incorporating a similar nonlinear relation between the sensorimotor error and the fast process might be able to capture the explicit character of the fast process. The nonlinearity could be in the form of a minimum error threshold below which the fast process is not adapted. With this condition, for small perturbations, only the slow process will be adapted. As the magnitude of the error increases, the contribution of the fast process increases. This is in agreement with the observations of Morehead et al. [2015]. This nonlinear response to error might have originated from the presence of execution noise. van der Vliet et al. [2018] found that the net adaptation rate was positively correlated with planning noise and negatively correlated with the execution noise. Larger execution noise would mean that participants would be less likely to properly attribute the error on a particular trial to motor noise or external perturbations. This lack of awareness might hinder the fast/explicit process. Going by this logic, a lower planning noise would result in a lower error threshold which in turn would lead a greater contribution of the fast process. The larger contribution of the fast process will increase the overall adaptation rate as observed by van der Vliet et al. [2018]. Werner et al. [2015] suggested the use of Process-Dissociation Procedure (PDP) to estimate the contributions of the explicit and implicit components. Experiments with AST and CL perturbations followed by PDP can be useful in verifying whether the fast and slow process are the explicit and implicit processes.

Scaling of the inputs was done based on the assumption of linearity. In the light of nonlinear characteristics, it might be better to avoid scaling the input signals. Also, scaling of the inputs to make sure that all the participants have the same maximum perturbation magnitude means that the final level of the slow process is different for each participant. This is not ideal for conducting a between-subject analysis. Future work might benefit from not having scaled inputs. Instead, have all the participants train to the same level of adaptation.

The retention parameters of the slow process (a_s) found in the prior literature were very close to 1, which is the usual upper bound in studies (Fig. 2.1 and Table 2.1). The search space for a_s for the current study was set as $(0, 1.1)$ to prevent the saturation of a_s at 1. A value of a_s slightly greater than 1 would mean than for a steady perturbation, the adaptation would overshoot and stop at a value higher than what is required to just cancel out the effect of the perturbation (refer Section 2.3 and Fig. 2.3). The sensorimotor error ($e(k)$) through the term $b_s \cdot e(k)$ would limit the adaptation from indefinitely increasing. But in the case of error-clamp trials like those of the retention trials, the absence of sensorimotor error can prevent the adaptation from stopping. In real-life, this type of escalating adaptation might be limited by other neural dynamics which are not captured by the 2-state LTI model. It is interesting to note that participant 7 showed this kind of behaviour for both perturbation blocks and is reflected in a_s values slightly greater than 1. Some other participants also have estimates of a_s slightly greater than 1 — all of which is closer to 1 than 1.1. Thus the issue of saturation of the estimates of a_s at the upper bound is precluded with the current selection of the search space.

5.3. Washout vs Non-stationarity

The parameter estimates for the perturbation blocks were used to probe the effectiveness of the washout block between Blocks C and D. It was observed that the retention rate of the slow process (a_s) and the learning rate of the fast process (b_f) increased slightly from the first to the second perturbation for the AST-first group (Fig. 4.8). The slow process contributes more towards net retention ($a_s > a_f$) and the fast process contributes more towards the net learning rate of adaptation ($b_f > b_s$). Larger values of a_s and b_f means that net adaptation has more retention and is faster, which is indicative of savings when moving from the AST perturbation to the CL perturbation. Thus the washout does not completely bring the adaptation back to baseline behaviour. The weak effects of the perturbation order ($F(1,12) = 3.98,\ p = 0.069$) and the interaction between the perturbation order and the perturbation block ($F(1,12) = 2.82,\ p = 0.119$) on the MSMAs also hint at the incompleteness of washout.

The length of the washout blocks was set at 60 trials as a trade-off between a long washout and a short experiment duration. Zarahn et al. [2008] noted that savings-like behaviour was still evident with washouts of 40 trials. Inoue et al. [2015] suggested a 3-state LTI model of adaptation with an additional "ultra-slow" process. Inoue et al. [2015] stated that the 2-state LTI model was sufficient for predicting retention for experiments with upto 250 trials. For adaptation experiments with more than 500 trials, the 3-state LTI model was needed to predict retention. Huang and Shadmehr [2009] and Turnham et al. [2012] had suggested that the learning and retention rates may vary in response to statistics of the perturbations. To minimise the impact of such non-stationarities, the experiment duration should be limited. Interestingly, 60 trials were sufficient to washout the effects of the CL perturbation. This is evident in the lack of significant difference between

the estimated parameters for the CL-first group. This might also hint that the AST perturbation is training an ultra-slow process that is not modelled.

Future experiments might benefit from longer washouts between the AST and CL perturbation blocks. Or the washout block can be bypassed in favour of a between-subject design. For a between-subject experiment design, it would be better to avoid the scaling of the inputs to ensure that all the participants adapt to the same final state of adaptation. In this case, the desired terminal state should be a small angle (for visuomotor rotation experiments) for the slow state, like $[x_s\ ,\ x_f] = [0^\circ\ ,\ 5^\circ]$.

5.4. Augmenting Rehabilitation

Assist-As-Needed (AAN) is a paradigm in robot-assisted rehabilitation where the level of robotic assistance is reduced in response to a reduction in trajectory errors (Reinkensmeyer et al. [2004], Liu and Reinkensmeyer [2004] and Emken and Reinkensmeyer [2004]). AAN assumes that rehabilitation from a neurological injury can be modelled as a adaptation process (Reinkensmeyer [2003]). AAN is based on a single-state model of adaptation. Adaptation-State-Tracking (AST) on the other hand, is based on a 2-state LTI model and can thus leverage the presence of savings-like effects. AAN considers the perturbation on each trial to be the sum of the effect of the neurological injury and the effect of the robotic assistance. To utilise AST for rehabilitation, the level of robotic assistance should be controlled to make the net perturbation (robot + neurological injury) follow the trajectory of the AST perturbation. One of the main benefits of AAN is that task-errors are minimised throughout rehabilitation. Applying the feedforward AST from the start of rehabilitation can lead to high task-errors which might be harmful for patients (especially in the case of walking and balance). To prevent the problem of high task errors, AAN can be employed in the initial stages of rehabilitation and the AST can be used in the final stages to push the adaptation to the required state. This hybrid approach would also solve the problem of incomplete rehabilitation (Emken et al. [2007]) associated with AAN. While AAN updates are based on task error, parameter estimation using EM enables AST to predict adaptation behaviour.

AST-based AAN might also be achieved by defining a cost function that weighs off robot control effort and human error for the 2-state LTI model. This could be implemented as an MPC problem with feedback and state estimators. The MPC formulation allows for applying constraints on task errors too.

Human-assisted rehabilitation might also benefit from the AST perturbations. AST produces an overshooting trajectory for the fast/explicit process. An understanding of the structure of AST and the overshooting trajectory of the fast process might be useful for rehabilitation practitioners to control the level of assistance and perturbation. Estimates of the slow and fast states of adaptation could be used as indicators of adaptation in addition to the level of net adaptation. In this work, the parameter estimates from the EM toolbox was used to tune the AST perturbation. Rehabilitation practitioners with practice might be able to fit AST-style perturbations to each patient based on feedback from the patients.

Shadmehr and Krakauer [2008] suggests that different regions of the brain are responsible for the different elements of optimal control associated with motor control. The cerebellum was believed to be responsible for internal model formation. State estimation was thought to rely on the parietal cortex. The basal-ganglia is assumed to take care of the cost functions and rewarding mechanisms. The best actions are then converted into motor commands and implemented by the primary motor cortex and the premotor cortex. This hypothesis suggests that neural injuries to different regions of the brain will lead to different types of movement pathologies. This is indeed what is seen in patients with neurological deficits.

Adaptations on the whole is based on cerebellar-thalamic-cortical and cerebellar-basal ganglia networks (Mawase et al. [2017],Kim et al. [2015]). Experimental evidence paints a picture where the prefrontal cortex and the parietal lobes contribute to the fast process and the explicit process (Kim et al. [2015], Thurer et al. [2016] and Liew et al. [2018]). The cerebellum contributes to both the fast the slow processes as well as both explicit and implicit processes (Kim et al. [2015] and Butcher et al. [2017]). Posterior cerebellum is supposed to be responsible for a fast component while anterior-medial cerebellum is the basis for a slow component (Kim et al. [2015]). A vast body of literature exists on the neural activations during sensorimotor adaptation apart from the ones mentioned here. A more detailed account is available in Appendix C.5.

Deficits to particular regions of the brain can thus lead to deficiencies in the fast and slow processes. These should be accounted for when designing AST based rehabilitation interventions. For example, an injury to the prefrontal cortex will impair the fast process and thus the AST design should reflect the deficiency. Stimulating the neural regions was also found to influence the components of adaptation. Transcranial Direct Current Stimulations (tDCMs) is one such stimulation method which was used to increase or decrease the activation of different neural regions (Herzfeld et al. [2014], Liew et al. [2018]). Stimulations such as these

could be used to augment AST perturbations. Since the fast/explicit and slow/implicit processes are believed to originate from different neural regions, AST could possibly be used to selectively activate the adaptation processes for the purpose of studying the neural regions associated with each adaptation process.

6

Conclusion and Recommendations

6.1. Conclusion

An Adaptation-State-Tracking (AST) perturbation was designed to increase the share of the slow process of adaptation. It was believed that increasing the contribution of the slow process would improve retention. The AST perturbation is based on the 2-state LTI model of adaptation suggested by Smith et al. [2006]. For the experiments, the learning and retention parameters of the participants were estimated with the help of staircase perturbations and the EM toolbox from Albert and Shadmehr [2018]. Personalised AST perturbations were calculated for each participant based on these estimated parameters. Comparison of the AST and CL perturbations revealed superior retention for the AST perturbation. The within-subject comparison did not show significant effects ($p = 0.1567$). An incomplete washout block is believed to have let the effects of the AST block leak into the CL block for the AST-first group. A between-subject analysis conducted with only the first perturbation blocks revealed a significantly greater retention for the AST perturbation ($p = 0.0415$). The incompleteness of washout after the AST perturbation hints at the possibility of AST training an ultra-slow process that was not modelled — which is good for improving retention. The effectiveness of the AST perturbation opens up the possibility of designing rehabilitation paradigms which can selectively target different aspects of human sensorimotor adaptation.

6.2. Recommendations

- **Experiment Design**: A between-subject experiment design can be used to preclude the effects of incomplete washouts. All the participants should be trained to the same level of adaptation (say 5° for the slow state and 0° for the fast state). The input signals should not be scaled differently for different participants.

- **Deeper into Adaptation Processes**: Overlap with explicit-implicit could be explored by using the same perturbations (AST and CL) but followed by a PDP instead of the retention block. PDP can be used to find the contributions of the explicit and implicit components of adaptation. This can be used to verify the connection between the fast-slow components and the explicit-implicit components of adaptation. Explicit processes have been shown to be sensitive to large and abrupt errors. The 2-state LTI model captures no such effect. Since there is a likely overlap between the fast-slow and explicit-implicit dichotomies, it might be wise to introduce error-based non-linearities into the models of adaptation. An error threshold could be incorporated into the dynamics of the fast/explicit process to capture the effects of the saliency of errors. AST could possibly be used to selectively activate the adaptation processes for the purpose of studying the neural regions associated with each adaptation process.

- **Better Control Schemes**: Feedback and state estimators could be used to ensure that the actual adaptation behaviour matches the optimal trajectories predicted by AST. An online MPC formulation would be able to optimally track the adaptation states and also satisfy constraints on the inputs or states.

- **Rehabilitation**: AST-based trajectories for assistance and instruction could be useful in improving retention in rehabilitation intervention. Qualitatively, these trajectories would engender an overshooting

trajectory for the fast/explicit process. Qualitative understanding of the structure of AST perturbations and the optimal state trajectories can be beneficial in human-assisted rehabilitation. Human practitioners might be able to intuitively tune the level of assistance to fit the learning and retention characteristics of each patient. It would be interesting to study whether an understanding of AST can be utilised by human practitioners to modulate the level of assistance given to participants. The benefits of using estimates of the slow and fast states of adaptation as additional markers for evaluating the progress of patients could also be studied.

Bibliography

[1] S. T. Albert and R. Shadmehr. Estimating properties of the fast and slow adaptive processes during sensorimotor adaptation. *Journal of Neurophysiology*, 119(4):1367–1393, 2018. ISSN 0022-3077. doi: 10.1152/jn.00197.2017.

[2] J. A. Anguera, P. A. Reuter-Lorenz, D. T. Willingham, and R. D. Seidler. Contributions of spatial working memory to visuomotor learning. *Journal of Cognitive Neuroscience*, 22(9):1917–1930, 2010. ISSN 0898-929X. doi: 10.1162/jocn.2009.21351.

[3] J. A. Anguera, P. A. Reuter-Lorenz, D. T. Willingham, and R. D. Seidler. Failure to engage spatial working memory contributes to age-related declines in visuomotor learning. *Journal of Cognitive Neuroscience*, 23(1):11–25, 2011. ISSN 0898-929X. doi: 10.1162/jocn.2010.21451.

[4] M. Berniker and K. P. Kording. Estimating the relevance of world disturbances to explain savings, interference and long-term motor adaptation effects. *PLoS Computational Biology*, 7(10):e1002210, 2011. ISSN 1553734X (ISSN). doi: 10.1371/journal.pcbi.1002210.

[5] P. A. Butcher, R. B. Ivry, S. H. Kuo, D. Rydz, J. W. Krakauer, and J. A. Taylor. The cerebellum does more than sensory prediction error-based learning in sensorimotor adaptation tasks. *Journal of Neurophysiology*, 118(3):1622–1636, 2017. ISSN 0022-3077. doi: 10.1152/jn.00451.2017.

[6] S. E. C-Hemminger and R. Shadmehr. Consolidation patterns of human motor memory. *Journal of Neuroscience*, 28(39):9610–9618, 2008. ISSN 0270-6474. doi: 10.1523/JNEUROSCI.3071-08.2008.

[7] C. C. Charalambous, C. C. Alcantara, M. A. French, X. Li, K. S. Matt, H. E. Kim, S. M. Morton, and D. S. Reisman. A single exercise bout and locomotor learning after stroke: physiological, behavioural, and computational outcomes. *Journal of Physiology-London*, 596(10):1999–2016, 2018. ISSN 0022-3751. doi: 10.1113/JP275881.

[8] P. Colagiorgio, G. Bertolini, C. J. Bockisch, D. Straumann, and S. Ramat. Multiple timescales in the adaptation of the rotational vor. *Journal of Neurophysiology*, 113(9):3130–3142, 2015. ISSN 0022-3077. doi: 10.1152/jn.00688.2014.

[9] S. K. Coltman, J. G. Cashaback, and P. L. Gribble. Both fast and slow learning processes contribute to savings following sensorimotor adaptation. *J Neurophysiol*, 121(4):1575–1583, 2019. ISSN 0022-3077. doi: 10.1152/jn.00794.2018.

[10] A. J. de Brouwer, M. Albaghdadi, J. R. Flanagan, and J. I. Gallivan. Using gaze behavior to parcellate the explicit and implicit contributions to visuomotor learning. *Journal of Neurophysiology*, 120(4):1602–1615, 2018. ISSN 0022-3077.

[11] J. L. Emken and D. J. Reinkensmeyer. Accelerating motor adaptation by influencing neural computations. *Conf Proc IEEE Eng Med Biol Soc*, 6:4033–6, 2004. ISSN 1557-170X (Print) 1557-170X (Linking). doi: 10.1109/IEMBS.2004.1404126.

[12] J. L. Emken, J. E. Bobrow, and D. J. Reinkensmeyer. Robotic movement training as an optimization problem: Designing a controller that assists only as needed. *2005 Ieee 9th International Conference on Rehabilitation Robotics*, pages 307–312, 2005. ISSN 1945-7898. doi: 10.1109/ICORR.2005.1501108.

[13] J. L. Emken, R. Benitez, and D. J. Reinkensmeyer. Human-robot cooperative movement training: learning a novel sensory motor transformation during walking with robotic assistance-as-needed. *J Neuroeng Rehabil*, 4:8, 2007. ISSN 1743-0003 (Electronic) 1743-0003 (Linking). doi: 10.1186/1743-0003-4-8.

[14] V. Ethier, D. S. Zee, and R. Shadmehr. Spontaneous recovery of motor memory during saccade adaptation. *Journal of Neurophysiology*, 99(5):2577–2583, 2008. ISSN 0022-3077. doi: 10.1152/jn.00015.2008.

[15] M. A. French, S. M. Morto, C. C. Charalambous, and D. S. Reisman. A locomotor learning paradigm using distorted visual feedback elicits strategic learning. *Journal of Neurophysiology*, 120(4):1923–1931, 2018. ISSN 0022-3077. doi: 10.1152/jn.00252.2018.

[16] D. J. Herzfeld, D. Pastor, A. M. Haith, Y. Rossetti, R. Shadmehr, and J. O'Shea. Contributions of the cerebellum and the motor cortex to acquisition and retention of motor memories. *Neuroimage*, 98:147–58, 2014. ISSN 1053-8119. doi: 10.1016/j.neuroimage.2014.04.076.

[17] V. S. Huang and R. Shadmehr. Persistence of motor memories reflects statistics of the learning event. *Journal of Neurophysiology*, 102(2):931–940, 2009. ISSN 0022-3077. doi: 10.1152/jn.00237.2009.

[18] M. Inoue, M. Uchimura, A. Karibe, J. O'Shea, Y. Rossetti, and S. Kitazawa. Three timescales in prism adaptation. *Journal of Neurophysiology*, 113(1):328–338, 2015. ISSN 0022-3077. doi: 10.1152/jn.00803.2013.

[19] W. M. Joiner and M. A. Smith. Long-term retention explained by a model of short-term learning in the adaptive control of reaching. *Journal of Neurophysiology*, 100(5):2948–2955, 2008. ISSN 0022-3077. doi: 10.1152/jn.90706.2008.

[20] A. Keisler and R. Shadmehr. A shared resource between declarative memory and motor memory. *Journal of Neuroscience*, 30(44):14817–14823, 2010. ISSN 0270-6474. doi: 10.1523/Jneurosci.4160-10.2010.

[21] S. Kim, K. Ogawa, J. C. Lv, N. Schweighofer, and H. Imamizu. Neural substrates related to motor memory with multiple timescales in sensorimotor adaptation. *Plos Biology*, 13(12):23, 2015. ISSN 1545-7885. doi: 10.1371/journal.pbio.1002312.

[22] S. Kim, Y. Oh, and N. Schweighofer. Between-trial forgetting due to interference and time in motor adaptation. *PLoS One*, 10(11):e0142963, 2015. ISSN 1932-6203. doi: 10.1371/journal.pone.0142963.

[23] S. J. Kim, M. Ogilvie, N. Shimabukuro, T. Stewart, and J. H. Shin. Effects of visual feedback distortion on gait adaptation: Comparison of implicit visual distortion versus conscious modulation on retention of motor learning. *IEEE Trans Biomed Eng*, 62(9):2244–50, 2015. ISSN 0018-9294. doi: 10.1109/TBME.2015.2420851.

[24] Y. Kojima, Y. Iwamoto, and K. Yoshida. Memory of learning facilitates saccadic adaptation in the monkey. *J Neurosci*, 24(34):7531–9, 2004. ISSN 0270-6474. doi: 10.1523/JNEUROSCI.1741-04.2004.

[25] K. P. Kording, J. B. Tenenbaum, and R. Shadmehr. The dynamics of memory as a consequence of optimal adaptation to a changing body. *Nature Neuroscience*, 10(6):779–786, 2007. ISSN 10976256 (ISSN). doi: 10.1038/nn1901.

[26] J. Y. Lee and N. Schweighofer. Dual adaptation supports a parallel architecture of motor memory. *Journal of Neuroscience*, 29(33):10396–10404, 2009. ISSN 0270-6474. doi: 10.1523/JNEUROSCI.1294-09.2009.

[27] L. A. Leow, W. Marinovic, A. de Rugy, and T. J. Carroll. Task errors contribute to implicit aftereffects in sensorimotor adaptation. *European Journal of Neuroscience*, 48(11):3397–3409, 2018. ISSN 0953-816X. doi: 10.1111/ejn.14213.

[28] C. Leukel, A. Gollhofer, and W. Taube. In experts, underlying processes that drive visuomotor adaptation are different than in novices. *Front Hum Neurosci*, 9:50, 2015. ISSN 1662-5161 (Print) 1662-5161. doi: 10.3389/fnhum.2015.00050.

[29] S. L. Liew, T. Thompson, J. Ramirez, P. A. Butcher, J. A. Taylor, and P. A. Celnik. Variable neural contributions to explicit and implicit learning during visuomotor adaptation. *Frontiers in Neuroscience*, 12:18, 2018. ISSN 1662-453X. doi: 10.3389/fnins.2018.00610.

[30] J. Liu and D. Reinkensmeyer. Motor adaptation as an optimal combination of computational strategies. *Conf Proc IEEE Eng Med Biol Soc*, 6:4025–8, 2004. ISSN 1557-170X (Print) 1557-170X (Linking). doi: 10.1109/IEMBS.2004.1404124.

[31] Y. Mandelblat-Cerf, I. Novick, and E. Vaadia. Expressions of multiple neuronal dynamics during sensorimotor learning in the motor cortex of behaving monkeys. *Plos One*, 6(7):14, 2011. ISSN 1932-6203.

[32] F. Mawase, S. Bar-Haim, and L. Shmuelof. Formation of long-term locomotor memories is associated with functional connectivity changes in the cerebellar-thalamic-cortical network. *Journal of Neuroscience*, 37(2):349–361, 2017. ISSN 0270-6474. doi: 10.1523/Jneurosci.2733-16.2017.

[33] P. Mazzoni and J. W. Krakauer. An implicit plan overrides an explicit strategy during visuomotor adaptation. *J Neurosci*, 26(14):3642–5, 2006. ISSN 1529-2401 (Electronic) 0270-6474 (Linking). doi: 10.1523/JNEUROSCI.5317-05.2006.

[34] S. D. McDougle, K. M. Bond, and J. A. Taylor. Explicit and implicit processes constitute the fast and slow processes of sensorimotor learning. *Journal of Neuroscience*, 35(26):9568–9579, 2015. ISSN 0270-6474. doi: 10.1523/JNEUROSCI.5061-14.2015.

[35] S. D. McDougle, K. M. Bond, and J. A. Taylor. Implications of plan-based generalization in sensorimotor adaptation. *Journal of Neurophysiology*, 118(1):383–393, 2017. ISSN 0022-3077. doi: 10.1152/jn.00974.2016.

[36] J. R. Morehead, S. E. Qasim, M. J. Crossley, and R. Ivry. Savings upon re-aiming in visuomotor adaptation. *J Neurosci*, 35(42):14386–96, 2015. ISSN 0270-6474. doi: 10.1523/JNEUROSCI.1046-15.2015.

[37] D. S. Naidu. *Optimal Control Systems.* CRC Press, Inc. ; Boca Raton, FL, USA, 2002. ISBN 0849308925.

[38] D. Pelisson, N. Alahyane, M. Panouilleres, and C. Tilikete. Sensorimotor adaptation of saccadic eye movements. *Neuroscience and Biobehavioral Reviews*, 34(8):1103–1120, 2010. ISSN 0149-7634. doi: 10.1016/j.neubiorev.2009.12.010.

[39] E. Poh, T. J. Carroll, and J. A. Taylor. Effect of coordinate frame compatibility on the transfer of implicit and explicit learning across limbs. *Journal of Neurophysiology*, 116(3):1239–1249, 2016. ISSN 0022-3077. doi: 10.1152/jn.00410.2016.

[40] D. Reinkensmeyer, D. Aoyagi, J. Emken, J. Galvez, W. Ichinose, G. Kerdanyan, J. Nessler, S. Maneekobkunwong, B. Timoszyk, K. Vallance, R. Weber, R. de Leon, J. Bobrow, S. Harkema, J. Wynne, and V. Edgerton. Robotic gait training: toward more natural movements and optimal training algorithms. *Conf Proc IEEE Eng Med Biol Soc*, 7:4818–21, 2004. ISSN 1557-170X (Print) 1557-170X (Linking). doi: 10.1109/IEMBS.2004.1404333.

[41] D. J. Reinkensmeyer. How to retrain movement after neurologic injury: a computational rationale for incorporating robot (or therapist) assistance. In *Proceedings of the 25th Annual International Conference of the IEEE Engineering in Medicine and Biology Society (IEEE Cat. No.03CH37439)*, volume 2, pages 1479–1482 Vol.2, 2003. ISBN 1094-687X. doi: 10.1109/IEMBS.2003.1279616.

[42] R. Schween, J. A. Taylor, and M. Hegele. Plan-based generalization shapes local implicit adaptation to opposing visuomotor transformations. *Journal of Neurophysiology*, 120(6):2775–2787, 2018. ISSN 0022-3077. doi: 10.1152/jn.00451.2018.

[43] R. Shadmehr and J. W. Krakauer. A computational neuroanatomy for motor control. *Exp Brain Res*, 185 (3):359–81, 2008. ISSN 1432-1106 (Electronic) 0014-4819 (Linking). doi: 10.1007/s00221-008-1280-5.

[44] G. C. Sing and M. A. Smith. Reduction in learning rates associated with anterograde interference results from interactions between different timescales in motor adaptation. *Plos Computational Biology*, 6(8): 14, 2010. ISSN 1553-734X. doi: ARTNe100089310.1371/journal.pcbi.1000893.

[45] M. A. Smith, A. Ghazizadeh, and R. Shadmehr. Interacting adaptive processes with different timescales underlie short-term motor learning. *Plos Biology*, 4(6):1035–1043, 2006. ISSN 1545-7885. doi: 10.1371/journal.pbio.0040179.

[46] J. A. Taylor, J. W. Krakauer, and R. B. Ivry. Explicit and implicit contributions to learning in a sensorimotor adaptation task. *Journal of Neuroscience*, 34(8):3023–3032, 2014. ISSN 0270-6474. doi: 10.1523/JNEUROSCI.3619-13.2014.

[47] Jordan A. Taylor and Richard B. Ivry. Flexible cognitive strategies during motor learning. *PLOS Computational Biology*, 7(3):1–13, 03 2011. doi: 10.1371/journal.pcbi.1001096.

[48] B. Thurer, C. Stockinger, A. Focke, F. Putze, T. Schultz, and T. Stein. Increased gamma band power during movement planning coincides with motor memory retrieval. *Neuroimage*, 125:172–181, 2016. ISSN 1053-8119. doi: 10.1016/j.neuroimage.2015.10.008.

[49] K. M. Trewartha, A. Garcia, D. M. Wolpert, and J. R. Flanagan. Fast but fleeting: Adaptive motor learning processes associated with aging and cognitive decline. *Journal of Neuroscience*, 34(40):13411–13421, 2014. ISSN 0270-6474. doi: 10.1523/JNEUROSCI.1489-14.2014.

[50] E. J. A. Turnham, D. A. Braun, and D. M. Wolpert. Facilitation of learning induced by both random and gradual visuomotor task variation. *Journal of Neurophysiology*, 107(4):1111–1122, 2012. ISSN 0022-3077. doi: 10.1152/jn.00635.2011.

[51] R. van der Vliet, M. A. Frens, L. de Vreede, Z. D. Jonker, G. M. Ribbers, R. W. Selles, J. N. van der Geest, and O. Donchin. Individual differences in motor noise and adaptation rate are optimally related. *eNeuro*, 5 (4), 2018. ISSN 2373-2822. doi: 10.1523/eneuro.0170-18.2018.

[52] D. M. van Es and T. Knapen. Implicit and explicit learning in reactive and voluntary saccade adaptation. *Plos One*, 14(1):20, 2019. ISSN 1932-6203. doi: 10.1371/journal.pone.0203248.

[53] S. Werner, B. C. van Aken, T. Hulst, M. A. Frens, J. N. van der Geest, H. K. Struder, and O. Donchin. Awareness of sensorimotor adaptation to visual rotations of different size. *Plos One*, 10(4):18, 2015. ISSN 1932-6203. doi: 10.1371/journal.pone.0123321.

[54] S. Werner, H. K. Struder, and O. Donchin. Intermanual transfer of visuomotor adaptation is related to awareness. *PLoS One*, 14(9):e0220748, 2019. ISSN 1932-6203 (Electronic) 1932-6203 (Linking). doi: 10.1371/journal.pone.0220748.

[55] A. L. Wong and M. Shelhamer. A long-memory model of motor learning in the saccadic system: A regime-switching approach. *Annals of Biomedical Engineering*, 41(8):1613–1624, 2013. ISSN 00906964 (ISSN). doi: 10.1007/s10439-012-0669-2.

[56] E. Zarahn, G. D. Weston, J. Liang, P. Mazzoni, and J. W. Krakauer. Explaining savings for visuomotor adaptation: Linear time-invariant state-space models are not sufficient. *Journal of Neurophysiology*, 100(5):2537–2548, 2008. ISSN 0022-3077.

A

Assist-as-Needed Rehabilitation

The "Assist-as-Needed" paradigm for robotic rehabilitation was conceived based on a model for how people adapt to a neurological injury (Reinkensmeyer et al. [2004]). Rehabilitation was considered as an adaptation to an altered sensorimotor mapping which was a result of some neurological injury (Appendix A.1) and models of human adaptation were used to arrive at a slacking control for rehabilitation using robotic assistance (Appendix A.2).

A.1. Rehabilitation as Adaptation

Assist-as-needed control for robotic rehabilitation was designed based on the assumption that neurological injuries affect the sensorimotor mapping between sensory inputs and muscular activations (Reinkensmeyer [2003]), and that the recovery process from a neurological injury can be modelled as the adaptation to a new sensorimotor mapping (Reinkensmeyer et al. [2004]). Simulations using a Markov model of adaptation have shown the benefits of assist-as-needed rehabilitation for Hebbian-learning based adaptations (Reinkensmeyer [2003]). Reinkensmeyer et al. [2004] combines this with an understanding of adaptive strategies (Liu and Reinkensmeyer [2004]) and how motor learning can be enhanced by transiently increasing the trajectory error (Emken and Reinkensmeyer [2004]) to develop the slacking controller (detailed in Appendix A.2).

Liu and Reinkensmeyer [2004] tells us that motor adaptation can be modelled as an optimal combination of four major adaptive strategies:

1. *Internal Model Formation*: when the forces are small and predictable.
2. *Impedance Control*: when the forces are small and unpredictable.
3. *Force Minimisation*: when the forces are large.
4. *Trajectory Planning*: for both large and small forces.

The internal model formation is the change in the mapping between the sensory input and the muscular output. This is useful in the feedforward control of motion. Impedance control is useful when the effect of small external perturbations can be minimized by the stiffening of the body. Force minimization refers to the dynamic optimization strategy that tries to optimize the muscle activations with the goal of minimizing some cost function related to force, torque or energy consumption. Trajectory optimization refers to shifting the equilibrium trajectory in the opposite direction to that of the mean of the environmental perturbations.

Liu and Reinkensmeyer [2004] has formulated a mathematical model of adaptation based on the following learning law in which the muscle forces on a given trial depend on the muscles forces on the previous trial and the trajectory error on the current trial :

$$u_{i+1} = f_{\mathrm{H}} \cdot u_i - g_{\mathrm{H}} \cdot |x_i - x_d| \tag{A.1}$$

where[1]

[1]The nomenclature used in the Appendix is different from the nomenclature in the main text. The nomenclature in Section 1.1.1 is chosen to be consistent with the nomenclature used throughout the main text. The nomenclature in Appendix A is chosen to be consistent with the original papers for ease of reference.

u_i = the average force generated by the body muscles on the ith trial
x_i = the average deviation in the ith trial
x_d = the desired deviation
g_H = the learning gain of the nervous system (H for Human)
f_H = forgetting(retention) factor of the nervous system, $f_H < 1$

Additionally, considering that the human body acts like a spring of constant stiffness K when an external force F_i is acts on it, we get,

$$x_i - x_d = -\frac{1}{K}(F_i + u_i) \tag{A.2}$$

Combining Eqs. (A.1) and (A.2) we get:

$$x_{i+1} = \left(f_H - \frac{g_H}{K}\right)x_i - \frac{f_H}{K}F_i + \frac{1}{K}F_{i+1} + \left(1 - \left(f_H - \frac{g_H}{K}\right)\right)x_d \tag{A.3}$$

which can be written as:

$$x_{i+1} = a_0 x_i + b_1 F_i + b_0 F_{i+1} + c_0 \tag{A.4}$$

where,

$$a_0 = f_H - \frac{g_H}{K} \qquad b_1 = -\frac{f_H}{K} \qquad b_0 = \frac{1}{K} \qquad c_0 = \left(1 - \left(f_H - \frac{g_H}{K}\right)\right)x_d$$

Liu and Reinkensmeyer [2004] has applied the above model to the adaptation of a reaching task in a force field (upper-body task). The adaptation behaviour has been explained on the basis of an optimal control paradigm where the nervous system tries to minimize a cost function based on the kinematic error (e), the resultant muscle force (u) and the muscle stiffness (K):

$$J = f_1(e) + f_2(u) + f_3(K) \tag{A.5}$$

The internal model formation strategy is useful for predictive or feedforward control and is dominant when the learning gain g_H and forgetting(retention) factor f_H are large. As the internal model becomes more accurate the values of f_H and g_H are increased. The impedance control strategy is dominant when the perturbations are small and predictable. In these cases the muscle stiffness K is increased to minimise the effect of random perturbations. When the external forces are large, the cost function is dominated by the muscle force term and thus force minimization strategies are applied. Trajectory planning shifts the equilibrium point x_d opposite to the the average perturbation field to minimize the kinematic error. Thus the various characteristics of the reaching adaptation was explained in Liu and Reinkensmeyer [2004] with the help of the adaptation model (Eq. (A.3)). Emken and Reinkensmeyer [2004] showed that the same model is applicable for a stepping adaptation (lower-body task).

This model was later used to model the recovery from neurological injury in Reinkensmeyer et al. [2004] and was subsequently used to formalize the Assist-as-Needed rehabilitation as an optimization problem (Emken et al. [2005]).

A.2. Slacking Assistance

Reinkensmeyer et al. [2004] developed the "Assist-as-Needed" paradigm of robotic rehabilitation which was based on a computational model of rehabilitation. This model was based on the idea that recovery from a neurological injury can be considered as the relearning of a mapping between input senses and output muscle forces. The adaptation model (Eq. (A.4)) which was applied to reaching (Liu and Reinkensmeyer [2004]) and stepping (Emken and Reinkensmeyer [2004]) adaptations was used as the model for recovery from a neurological injury.

Reinkensmeyer et al. [2004] noted that the model of adaptation showed that the nervous system "slacks" while adapting; ie, at each trial, the nervous system has a tendency to rely on the previous trials too, so that the resulting adaptation lags behind the perturbation signal. It was shown that an assistive robotic device that "out-slacked" the nervous system was able to force the human to learn the adaptation while at the same time

limiting the kinematic error. This requirement for minimizing the trajectory error is crucial for applications like walking where large errors are harmful to the patient.

Reinkensmeyer et al. [2004] modelled the robotic assistance as a position-controlled device that acted like a spring and produced a force proportional to the trajectory error:

$$R_i = -G(x_i - x_d) \tag{A.6}$$

The stiffness of the assistance G was adapted based on the trajectory error on previous trials. Assuming that the human body behaves like a spring as described in Eq. (A.2), we get the equation for the coupled human-robot system as:

$$x_i = -\frac{1}{K+G}(F_i + u_i) + x_d \tag{A.7}$$

The learning law associated with the nervous system is as described earlier in Eq. (A.1). To "out-slack" this nervous system the stiffness of the robotic assistance R was adapted on based on the trajectory error in the previous trials as:

$$R_{i+1} = f_R \cdot R_i + g_R \cdot |x_i - x_d| \tag{A.8}$$

where,

f_R = forgetting(retention) factor of the robot , $f_R < 1$

g_R = learning gain of the robot

Thus the stiffness of the robotic assistance increases if the trajectory error on the previous trial was large and decreases if the trajectory error on the previous trial was small. With this control law, it was shown that the human learns progressively if the slacking of the assistance is more than the slacking of the human, which forces the human to adapt.

This "Assist-as-Needed" paradigm was further formalized as an optimization problem in Emken et al. [2005]. Emken et al. [2005] considered the following cost function based on trajectory error and robotic assistance force for the minimization problem:

$$J = \frac{1}{2}(x_{i+1} - x_d)^2 + \frac{\lambda_R}{2}(R_{i+1})^2 \tag{A.9}$$

where, λ_R is a constant that weighs the relative cost of the error and force terms.

The total perturbation F_i was assumed to be the sum of the effect of the neurological impairment I_i and the robotic assistance R_i:

$$F_i = R_i + I_i \tag{A.10}$$

Substituting equation A.10 into equation A.4 gives:

$$x_{i+1} = a_0 x_i + b_1 R_i + b_0 R_{i+1} + b_1 I_i + b_0 I_{i+1} + c_0 \tag{A.11}$$

Now the minimum of the cost function (equation A.9) occurs when

$$\frac{\partial J}{\partial R_{i+1}} = (x_{i+1} - x_d)\frac{\partial x_{i+1}}{\partial R_{i+1}} + \lambda_R R_{i+1} = 0 \tag{A.12}$$

Taking the partial derivative of x_{i+1} with respect to R_{i+1} from equation A.11, we get the optimality condition as:

$$R_{i+1} = -\frac{b_0}{\lambda_R}(x_{i+1} - x_d) \tag{A.13}$$

Substituting for x_{i+1} from equation A.11, we get:

$$R_{i+1} = f_R R_i - g_R K(x_i - x_d) + c_R\left(f_H I_i - I_{i+1}\right) \tag{A.14}$$

where,

$$f_R = \frac{f_H}{\lambda_R K^2 + 1} \qquad g_R = \frac{f_H - \hat{g}_H}{\lambda_R K^2 + 1} \qquad c_R = \frac{1}{\lambda_R K^2 + 1} \qquad \hat{g}_H = \frac{g_H}{K} \tag{A.15}$$

The optimal robotic assistance as described in equations A.14 and A.15 is similar to that of the neural controller described by the learning law A.1 and has both a forgetting(retention) term f_R and a learning gain g_R. It is also evident that A.14 is a more rigorous definition of the slacking robotic assistance described earlier in A.8.

This "Assist-as-Needed" paradigm of robotic rehabilitation is based on the assumption that motor adaptation in humans can be satisfactorily modelled by the learning law described in equation A.1. However, recent advances in neuroscience has pointed to the existence of multiple learning processes in motor adaptation. Incorporating such models of adaptation with multiple processes into the robotic rehabilitation paradigm could open up new dimensions of control for robotic rehabilitation.

B

Sensorimotor Adaptation — Addendum

B.1. Sensorimotor Adaptation Tasks

This section gives an overview of the various sensorimotor adaptation tasks that have been studied in neuroscience.

Visuomotor Rotation

In these tasks, the participant moves a stylus or manipulandum to move a cursor on a screen. The goal is to make reaching movements to hit targets on the screen. The motion of the cursor on the screen is rotated such that the participant has to compensate for this rotation to hit the target.

Force Field

In force field adaptation, the participant has to move a manipulandum to make the cursor hit target shown on a screen. A viscous curl force field perturbs the motion of the hand in a direction perpendicular to that of the movement.

Prism Rotation

In these tasks, the participants are made to wear prism goggles that create a rotation of visual feedback. The objective is to hit target by throwing balls while having rotated visual feedback.

Saccade

There are two types of saccade adaptation — gain-up and gain-down. In gain-up saccade adaptation , the target location moves farther away from the origin as saccade progresses. During saccade no feedback can be obtained and to adapt to such a sudden shift in target, the adaptation has to rely on internal models. A gain-down adaptation is the reverse of a gain-up adaptation.

Vestibulo-Occular Reflex

The vestibulo-occular reflex is responsible for stabilising the eye during head movements. Artificial perturbations can be applied on this reflex by having a drum/screen around the head which rotates at different speed than that of the head.

Locomotor Adaptation

Locomotor adaptation refers to adapting the asymmetry of gait. The stride lengths are made to vary between left and right legs through distorted visual feedback or through the use of a split-belt treadmill.

B.2. Behavioural Properties of Adaptation

Table B.1: Behavioural characteristics of Sensorimotor Adaptation

Behavioural Properties of Sensorimotor Adaptation	
Adaptation Behaviour	**Description**
Savings	Savings is the faster re-adaptation from baseline behaviour to a perturbation that was previously experienced.
Spontaneous Recovery	Spontaneous Recovery from baseline behaviour after Error-Clamp Trials (in which error feedback is set to zero) following de-adaptation.
Rapid De-adaptation	Rapid De-adaptation to baseline behaviour when the perturbation is removed.
Accelerated Re-adaptation	Accelerated Re-adaptation to a downscaled version of a previously experienced perturbation.
Anterograde Interference	Slower adaptation from baseline behaviour to a perturbation in the opposite direction to that of a previously adapted perturbation.

C

Literature Review on Multiple Processes

This appendix a brief account of the literature review on the multiple processes of adaptation.

C.1. Finding Relevant Literature

Literature on the fast-slow and explicit-implicit dichotomies were gathered through database searches in Web of Science, Scopus and Pubmed. The structure of the search strings used are explained in Tables C.1 and C.2. From the results found, relevant articles were shortlisted as shown in Fig. C.1.

Table C.1: Search String Blocks for each research topic of interest

Blocks	Block Structure
Learning	(*motor NEAR/3 (learn* OR adapt*) OR ((*motor NEAR/3 skill*) AND (learn* OR adapt*)) OR (*motor NEAR/10 rehabilitation))
Neuro	(cortex OR *cortico* OR cerebellum OR cerebellar OR “basal ganglia” OR supraspinal OR neural* OR “subtangia nigra” OR striatum OR caudate OR putamen OR “globus pallidus” OR “ventral pallidum” OR “subthalamic nucleus” OR brain OR (Neurorehab* OR Neuro-rehab* OR Neuroscience OR Neurophysiol* OR Neurolog* OR Neuron*))
Temporal	(multirate OR multi-rate OR (slow OR fast) OR rate OR rates OR time-scale* OR timescale* OR time-constant* OR (implicit OR explicit))
Model	(model* OR computational OR “process” OR “processes”)
Memory	(retent* OR forget* OR sav* OR extinct* OR memory)

Table C.2: Search String Structure based on the search string blocks of Table C.1

Search String Structure
[Learning] AND [Neuro] AND [Temporal] AND [Model] AND [Memory] AND [([Temporal] NEAR [Process]) OR ([Temporal] NEAR (Learn* OR Adapt*))]

C.2. Literature Found

Table C.3: List of references that were included for the quantitative and qualitative analyses and whether they talked about the *Fast-Slow* or the *Explicit-Implicit* Dichotomies.

References for Qualitative and Quantitative Analyses				
Reference	**Adaptation Type**	**Fast-Slow Dichotomy**	**Explicit-Implicit Dichotomy**	**Used for Quantitative Analysis**
References From Database Searches				
Kojima et al. [2004]	Saccade			
Smith et al. [2006]	Saccade	●		●
Kording et al. [2007]	Sacccade	●		
C-Hemminger and Shadmehr [2008]	Force Field	●		●
Ethier et al. [2008]	Saccade	●		
Joiner and Smith [2008]	Force Field	●		●
Zarahn et al. [2008]	Visuomotor Rotation	●		●
Huang and Shadmehr [2009]	Force Field	●		●
Lee and Schweighofer [2009]	Visuomotor Rotation	●		●
Anguera et al. [2010]	Visuomotor Rotation			
Keisler and Shadmehr [2010]	Force Field	●	●	
Sing and Smith [2010]	Force Field	●		●
Anguera et al. [2011]	Visuomotor Rotation			
Berniker and Kording [2011]	Visuomotor Rotation			
Mandelblat-Cerf et al. [2011]	Force Field			
Turnham et al. [2012]	Visuomotor Rotation	●		●
Wong and Shelhamer [2013]	Saccade			
Herzfeld et al. [2014]	Force Field			
Taylor et al. [2014]	Visuomotor Rotation		●	
Trewartha et al. [2014]	Force Field	●	●	●
Colagiorgio et al. [2015]	Vestibulo Occular	●		●
Inoue et al. [2015]	Visuomotor Prism	●		●
Kim et al. [2015]	Visuomotor Rotation			
Kim et al. [2015]	Visuomotor Rotation	●		

Continued on next page

Table C.3 – continued from previous page

Reference	Adaptation Type	Fast-Slow Dichotomy	Explicit-Implicit Dichotomy	Used for Quantitative Analysis
Kim et al. [2015]	Locomotor		●	
Leukel et al. [2015]	Visuomotor Prism		●	
McDougle et al. [2015]	Force Field & Visuomotor Rotation	●	●	●
Morehead et al. [2015]	Visuomotor Rotation		●	
Werner et al. [2015]	Visuomotor Rotation		●	
Poh et al. [2016]	Visuomotor Rotation		●	
Thurer et al. [2016]	Force Field		●	
Butcher et al. [2017]	Visuomotor Rotation		●	
Mawase et al. [2017]	Locomotor			
McDougle et al. [2017]	Visuomotor Rotation	●	●	
Albert and Shadmehr [2018]	Visuomotor Rotation	●		●
Charalambous et al. [2018]	Locomotor	●		
de Brouwer et al. [2018]	Visuomotor Rotation		●	
French et al. [2018]	Locomotor		●	
Leow et al. [2018]	Visuomotor Rotation		●	
Liew et al. [2018]	Visuomotor Rotation		●	
Schween et al. [2018]	Visuomotor Rotation		●	
Coltman et al. [2019]	Force Field	●		●
van Es and Knapen [2019]	Saccade	●	●	
References From Other Sources				
Mazzoni and Krakauer [2006]	Visuomotor Rotation		●	
Werner et al. [2019]	Visuomotor Rotation		●	

C.3. Dichotomies of Adaptation Processes

Table C.4: Proposed Dichotomies of Adaptive Processes based on the Nature of Component Processes.

Dichotomy of Adaptive Processes	
Process Dichotomy	**Description**
Fast-Slow	Adaptive processes acting in different timescales (Smith et al. [2006]).
Explicit-Implicit	Awareness dependant components of adaptation (Mazzoni and Krakauer [2006]).
Body-World	Adaptive components for intrinsic vs extrinsic perturbations. (Kording et al. [2007], Berniker and Kording [2011]).

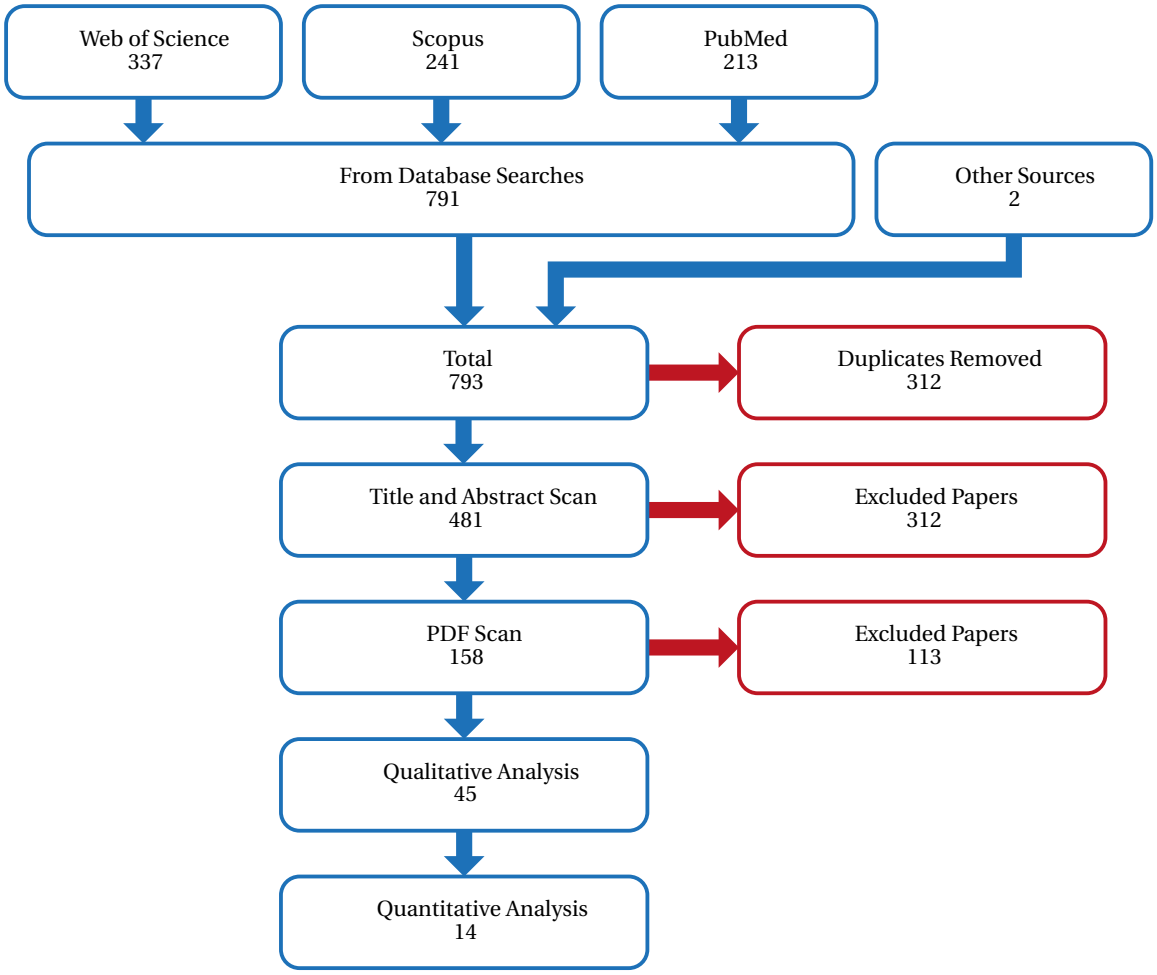

Figure C.1: Summary of the literature shortlisting process with the number of articles that were selected after each stage.

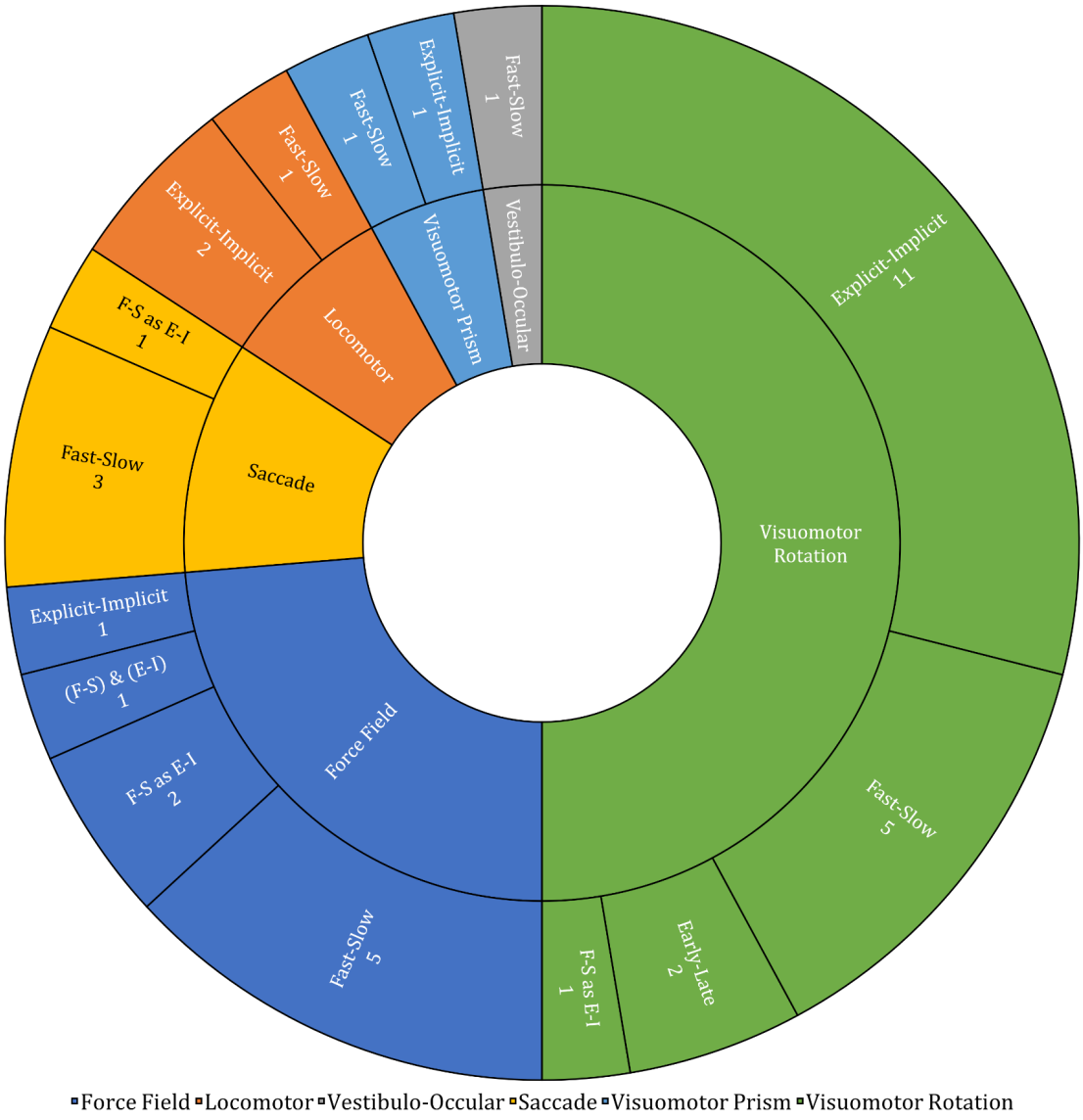

Figure C.2: Distribution of Adaptation Tasks and Dichotomies in the final selection of articles. **F-S as E-I** refers to those articles that talk of the fast process as the explicit process and the slow process as the implicit process. **(F-S) & (E-I)** refers to those articles that separately consider the *Fast-Slow* and *Explicit-Implicit* dichotomies without drawing any correlation between them.

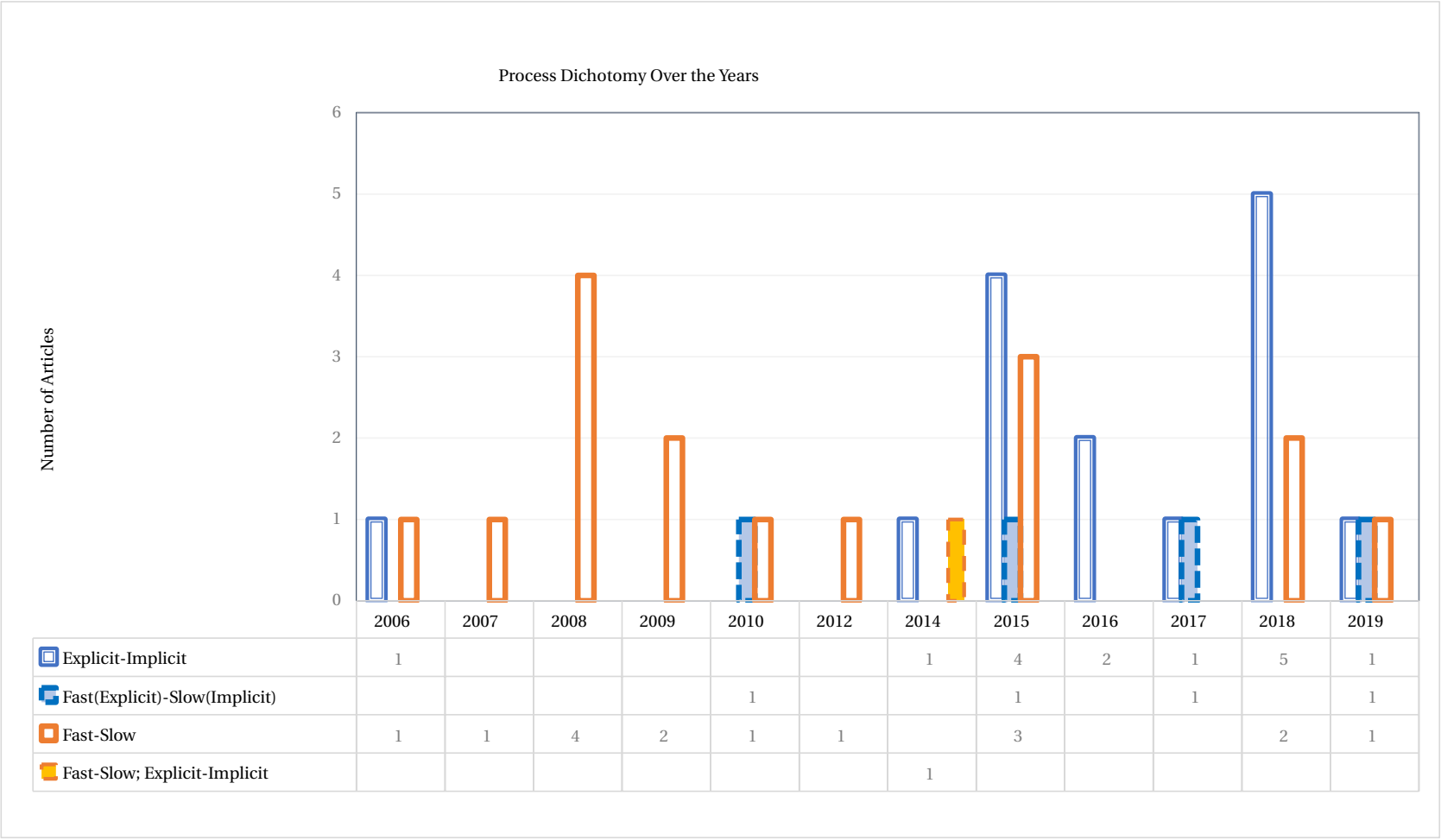

Figure C.3: Fast-Slow and Explicit-Implicit based process dichotomy in the included papers over the years. 'Fast(Explicit)-Slow(Implicit)' represents the articles that consider the explicit process as the fast process and the implicit process as the slow process. 'Fast-Slow; Explicit-Implicit' represents those papers that talk about both types of dichotomies without drawing a correlation between them.

C.4. List of Mathematical Models of Adaptation

Table C.5: Mathematical Models of Adaptation. For detailed descriptions of the various mathematical models please check appendix **??**

Mathematical Models of Adaptation		
Model	**Equations**	**Description**
2-rate Linear Time Invariant	$x_s(n+1) = a_s \cdot x_s(n) + b_s \cdot e(n)$ $x_f(n+1) = a_f \cdot x_f(n) + b_f \cdot e(n)$ $x(n) = x_s(n) + x_f(n)$ $b_s < b_f\ ,\ a_f < a_s$	Fast Process and Slow Process with unchanging parameters (Smith et al. [2006])
2-rate Varying Parameter	$x_s(n+1) = a_s(t) \cdot x_s(n) + b_s(t) \cdot e(n)$ $x_f(n+1) = a_f(t) \cdot x_f(n) + b_f(t) \cdot e(n)$ $x = x_s(n) + x_f(n)$ $b_s(t) < b_f(t)\ ,\ a_f(t) < a_s(t)$	Fast Process and Slow Process where parameters change according to previous experience of Perturbations (Zarahn et al. [2008])
3-rate Linear Time Invariant	$x_{us}(n+1) = a_{us} \cdot x_{us}(n) + b_{us} \cdot e(n)$ $x_s(n+1) = a_s \cdot x_s(n) + b_s \cdot e(n)$ $x_f(n+1) = a_f \cdot x_f(n) + b_f \cdot e(n)$ $x = x_s + x_f$ $b_{us} < b_s < b_f\ ,\ a_f < a_s < a_{us}$	Fast Process, Slow Process and Ultra-Slow Process with unchanging parameters (Inoue et al. [2015])
Context Based: 1-Fast N-Slow	$x_f(n+1) = a_f \cdot x_f(n) + b_f \cdot e(n)$ $\boldsymbol{x}_s(n+1) = \mathbf{A}_s \cdot \boldsymbol{x}_s(n) + \mathbf{B}_s \cdot e(n) \cdot \boldsymbol{c}(n)$ $x = \boldsymbol{x}_s + x_f$ $\mathbf{A}_s = \mathbf{I} \cdot a_s$ $\mathbf{B}_s = \mathbf{I} \cdot b_s$ $b_s < b_f\ ,\ a_f < a_s$	A single fast process shared with all contexts and n slow processes for n contexts. The slow process become active based in the context (Lee and Schweighofer [2009])
2-State Gain-Specific	$x_1(n+1) = min\,(0, a \cdot x_1(n) + b \cdot e(n))$ $x_2(n+1) = max\,(0, a \cdot x_2(n) + b \cdot e(n))$ $x = x_1 + x_2$	Two separate processes — one for increasing gain and the other for decreasing gain (Kojima et al. [2004]).

Continued on next page

Table C.5 – continued from previous page

Model	Equations	Description
Active-Inactive: Fast to Slow when Inactive	$\begin{bmatrix} x_s(n+1) \\ x_f(n+1) \end{bmatrix} = \mathbf{A} \cdot \begin{bmatrix} x_s(t) \\ x_f(t) \end{bmatrix} + \epsilon$ Active: $\mathbf{A} = \mathbf{A}_a = \begin{bmatrix} a_s & 0 \\ 0 & a_f \end{bmatrix}$ and $\epsilon = \epsilon_a$ Inactive: $\mathbf{A} = \mathbf{A}_i = \begin{bmatrix} a_s & a_{sf} \\ 0 & a_f \end{bmatrix}$ and $\epsilon = \epsilon_i$ $b_s < b_f$, $a_f < a_s$	Fast Process influences slow process when adaptation is inactive(environment is not observable). Fast and Slow uncoupled when active(when environment is observable) (C-Hemminger and Shadmehr [2008]).
Credit Assignment Model	$x_i(n+1) = \left(1 - \frac{1}{\tau_i}\right) \cdot x_i(n) + \epsilon_i$ $\hat{y}(n+1) = 1 + \sum_i x_i(n+1)$ $y = \hat{y} + \epsilon_y$ $\epsilon_i \sim \mathcal{N}(0, \sigma_i^2)$ $\sigma_i^2 = c\tau_i{}^{-}1$ $\epsilon_y \sim \mathcal{N}(0, \sigma_y^2)$	In the credit assignment model a range of timescales are considered and there is an adaptive state corresponding to each timescale. Observations on each trial are used to update the state estimates using a Kalman Filter (Kording et al. [2007]).
Regime Switching Model	Output $\hat{y}_{n+1} = \lambda_1 \cdot \hat{\mu}_n + \lambda_2 \cdot \hat{x}_n + \epsilon_y$ Mean Process $\hat{\mu}_{n+1} = \begin{cases} \beta_1 \cdot \hat{\mu}_n + \sum_{j=n-\tau+1}^{n} \phi_j \left(y_j - \hat{y}_j\right) + \epsilon_\mu \\ E_{\text{Cumulative}} \geq E_{\text{Thresh}} \\ \mu_n \\ \text{otherwise} \end{cases}$ Error-Correction Process $\hat{x}_{n+1} = \xi_1 \cdot \hat{x}_n + \xi_2 \cdot w_n \cdot \left(y_n - \hat{\mu}_i\right)$ Error-Tolerance Process Updates E_{Thresh} based on recent experience.	Keeps track of the mean of the perturbation on previous trials until the accumulated error passes a threshold. Once the accumulated error surpasses a threshold, regime switching ensues whereby all the information regarding the previous trials are discarded (Wong and Shelhamer [2013]).

Continued on next page

Table C.5 – continued from previous page

Model	Equations	Description
Body Rotation Vs World Rotation	$\begin{bmatrix}\hat{\theta}_{\mathrm{b}}(n+1)\\ \hat{\theta}_{\mathrm{w}}(n+1)\end{bmatrix} = \begin{bmatrix}a_{\mathrm{b}} & 0\\ 0 & a_{\mathrm{w}}\end{bmatrix} \cdot \begin{bmatrix}\hat{\theta}_{\mathrm{b}}(n)\\ \hat{\theta}_{\mathrm{w}}(n)\end{bmatrix} + \begin{bmatrix}1 & 0\\ 0 & P(\lambda = 1 \mid y)\end{bmatrix} \cdot K \cdot (y - \hat{y})$ $\lambda = \begin{cases}1 & \Longrightarrow \text{World rotation is present}\\ 0 & \Longrightarrow \text{World rotation is absent}\end{cases}$	Body Rotation is constantly updated while World Rotation is only activated if the predictions of Body Rotation alone cannot account for the observed sensory feedback (Berniker and Kording [2011]).

C.5. Neural Bases of Adaptation

Fast-Slow

Kim et al. [2015] correlated neural activity to states of adaptive processes operating at different timescales. They observed four principle components of neural activations related to different timescales — two fast, one intermediate and one slow. One of the fast components was related to activity in the prefrontal and parietal lobes. The other fast process was related to the posterior part of the cerebellum. The intermediate component was based in the inferior parietal region while the slow component was based in the anterior-medial cerebellum. Thus the cerebellum as a whole affects both fast and slow components of adaptation. The prefrontal and parietal regions contribute to fast and intermediate timescales of adaptation.

Mawase et al. [2017] studied how connectivity between different regions of the brain are related to adaptation. It was noted that long term behaviour was correlated with baseline activity in the cerebellar-thalamic-cortical network. The contribution of cerebellum, prefrontal cortex and the parietal lobe suggested by Kim et al. [2015] is in line with this observation as cerebellar-thalamic-cortical network connects the cerebellum, the prefrontal cortex and the parietal lobe. In addition to changes in the cerebellar-thalamic-cortical networks, adaptation was also observed to cause changes in the cerebellar-basal ganglia networks. The involvement of the basal ganglia could be contributing to reinforcement learning related to adaptation.

Explicit-Implicit

The results from Thurer et al. [2016] suggest that the prefrontal cortex is related to the explicit process. Liew et al. [2018] observed the effects of the prefrontal cortex and the cerebellum on the explicit and implicit processes respectively. Butcher et al. [2017] shows the contribution of the cerebellum towards both explicit and implicit processes.

In the early stages of adaptation the explicit process will be predominant and as adaptation progresses, the implicit process starts to dominate. Anguera et al. [2010] observed that prefrontal cortex and parietal lobules showed greater activity during the early stages of adaptation. In later stages, the activity shifted to the temporal gyrus and the cerebellum. Thurer et al. [2016] also noted higher activity in the prefrontal cortex during early adaptation.

Anguera et al. [2010] and Anguera et al. [2011] identified the correlation between neural activity in the prefrontal cortex and spatial working memory which was in turn associated with the explicit process.

In conclusion, the regions near the prefrontal cortex and the parietal lobule can be assumed to be contributing to the explicit process while the cerebellum contributes to both explicit and implicit components.

Fast-Slow as Explicit-Implicit

The explicit process is believed to be the fast process and the implicit process is believed to be the slow process. Studies on the neural bases of the *Fast-Slow* and *Explicit-Implicit* processes also seem to support this convergence.

Both the fast process and the explicit process are related to the prefrontal cortex and the parietal lobe. The cerebellum was found to influence both the explicit and implicit components of adaptation. It is interesting to note that Kim et al. [2015] related the cerebellum to one fast and one slow component of adaptation. Posterior part of the cerebellum was associated with the fast process whereas the anterior-medial cerebellum was

associated with the slow process. Based on the proposed relation between the *Fast-Slow* dichotomy with the *Explicit-Implicit* dichotomy, it is plausible to hypothesise that different parts of the cerebellum affect explicit and implicit processes.

D

Optimal Control - Addendum

This appendix provides a refresher for the derivation of Linear-Quadratic Tracking (LQT) control using Pontryagin's Minimum Principle.

D.1. Linear-Quadratic Tracking (LQT) Formulation

The goal of the controller design for the thesis is to formulate am *Optimal Tracking* controller for a *Linear System* which minimises *Quadratic Cost Function* of the tracking error and input. A controller with *Constrained Inputs* will also be studied. Only *Open-Loop* controllers will be considered as the intended experiments do not involve online feedback.

D.1.1. Linear System

Linear Continuous-Time Model

$$\dot{\boldsymbol{x}}(t) = \mathbf{A}(t)\boldsymbol{x}(t) + \mathbf{B}(t)\boldsymbol{u}(t) \tag{D.1}$$

Linear Discrete-Time Model

$$\boldsymbol{x}(k+1) = \mathbf{A}(k)\boldsymbol{x}(k) + \mathbf{B}(k)\boldsymbol{u}(k) \tag{D.2}$$

D.1.2. Quadratic Cost Function

A quadratic cost function is considered for formulating the optimal control problem. The cost function is quadratic in the states ($\boldsymbol{x}$) and input ($\boldsymbol{u}$). The cost is defined for initial time t_0 and final time t_f [1].The final state is represented in this chapter as $\boldsymbol{x}_\mathrm{f} = \boldsymbol{x}(t_\mathrm{f})$ for simplicity [2]. For a regulator problem the cost function penalises the value of the states ($\boldsymbol{x}$) Eq. (D.3). For a tracking problem, the cost function penalises the error ($\boldsymbol{e}$) of the output ($\boldsymbol{y}$) from a desired trajectory ($\boldsymbol{z}$) Eq. (D.7). Apart from the input, the cost function also depends on the initial conditions of the system (initial time t_0, and initial states $\boldsymbol{x}(t_0)$)

Cost function for the regulator problem:

$$J(\boldsymbol{x}(t_0), \boldsymbol{u}, t_0) = \frac{1}{2}\boldsymbol{x}^\mathsf{T}(t_\mathrm{f})\mathbf{F}(t_\mathrm{f})\boldsymbol{x}(t_\mathrm{f}) + \frac{1}{2}\int_{t_0}^{t_\mathrm{f}} \left[\boldsymbol{x}^\mathsf{T}(t)\mathbf{Q}(t)\boldsymbol{x}(t) + \boldsymbol{u}^\mathsf{T}(t)\mathbf{R}(t)\boldsymbol{u}(t)\right] \mathrm{d}t \tag{D.3}$$

Cost function for the tracking problem we consider the tracking error $\boldsymbol{e}(t) = \boldsymbol{z}(t) - \boldsymbol{x}(t)$:

$$\begin{aligned} J(\boldsymbol{x}(t_0), \boldsymbol{u}, t_0) &= \frac{1}{2}\boldsymbol{e}^\mathsf{T}(t_\mathrm{f})\mathbf{F}(t_\mathrm{f})\boldsymbol{e}(t_\mathrm{f}) + \frac{1}{2}\int_{t_0}^{t_\mathrm{f}} \left[\boldsymbol{e}^\mathsf{T}(t)\mathbf{Q}(t)\boldsymbol{e}(t) + \boldsymbol{u}^\mathsf{T}(t)\mathbf{R}(t)\boldsymbol{u}(t)\right] \mathrm{d}t \\ &= \frac{1}{2}\left[\boldsymbol{z}(t_\mathrm{f}) - \boldsymbol{y}(t_\mathrm{f})\right]^\mathsf{T}\mathbf{F}(t_\mathrm{f})\left[\boldsymbol{z}(t_\mathrm{f}) - \boldsymbol{y}(t_\mathrm{f})\right] \\ &\quad + \frac{1}{2}\int_{t_0}^{t_\mathrm{f}} \left[\left[\boldsymbol{z}(t) - \boldsymbol{y}(t)\right]^\mathsf{T}\mathbf{Q}(t)\left[\boldsymbol{z}(t) - \boldsymbol{y}(t)\right] + \boldsymbol{u}^\mathsf{T}(t)\mathbf{R}(t)\boldsymbol{u}(t)\right] \mathrm{d}t \end{aligned} \tag{D.4}$$

[1] NOTE: t_f refers to final time and is not related to the fast process.
[2] This is not to be confused with the fast process.

The output of the system $\boldsymbol{y}(t)$ is given by the relation:

$$\boldsymbol{y}(t) = \mathbf{C}(t)\boldsymbol{x}(t) \tag{D.5}$$

Substituting Eq. (D.5) into the relation for tracking error $\boldsymbol{e}(t)$ gives,

$$\boldsymbol{e}(t) = \boldsymbol{z}(t) - \boldsymbol{y}(t) = \boldsymbol{z}(t) - \mathbf{C}(t)\boldsymbol{x}(t) \tag{D.6}$$

From Eqs. (D.4) and (D.6) we ge the cost function in terms of the states $\boldsymbol{x}(t)$ as:

$$\begin{aligned} J(\boldsymbol{x}(t_0), \boldsymbol{u}, t_0) = &\frac{1}{2}\left[\boldsymbol{z}(t_\mathrm{f}) - \mathbf{C}(t)\boldsymbol{x}(t_\mathrm{f})\right]^\mathsf{T} \mathbf{F}(t_\mathrm{f})\left[\boldsymbol{z}(t_\mathrm{f}) - \mathbf{C}(t)\boldsymbol{x}(t_\mathrm{f})\right] \\ &+ \frac{1}{2}\int_{t_0}^{t_\mathrm{f}} \left[\left[\boldsymbol{z}(t) - \mathbf{C}(t)\boldsymbol{x}(t)\right]^\mathsf{T} \mathbf{Q}(t)\left[\boldsymbol{z}(t) - \mathbf{C}(t)\boldsymbol{x}(t)\right] + \boldsymbol{u}^\mathsf{T}(t)\mathbf{R}(t)\boldsymbol{u}(t)\right] \mathrm{d}t \end{aligned} \tag{D.7}$$

The cost functions mentioned above are for continuous-time control. For discrete-time control, the integration in the cost function is replaced by a summation.

Thus the cost function for a discrete-time regulator is:

$$J(\boldsymbol{x}(k_0), \boldsymbol{u}, k_0) = \frac{1}{2}\boldsymbol{x}^\mathsf{T}(k_\mathrm{T})\mathbf{F}(k_\mathrm{T})\boldsymbol{x}(k_\mathrm{T}) + \frac{1}{2}\sum_{k=k_0}^{k_\mathrm{T}-1}\left[\boldsymbol{x}^\mathsf{T}(k)\mathbf{Q}(k)\boldsymbol{x}(k) + \boldsymbol{u}^\mathsf{T}(k)\mathbf{R}(k)\boldsymbol{u}(k)\right] \tag{D.8}$$

And, the cost function for a discrete-time tracking controller is :

$$\begin{aligned} J(\boldsymbol{x}(k_0), \boldsymbol{u}, k_0) = &\frac{1}{2}\left[\boldsymbol{z}(k_\mathrm{T}) - \mathbf{C}(k)\boldsymbol{x}(k_\mathrm{T})\right]^\mathsf{T} \mathbf{F}(k_\mathrm{T})\left[\boldsymbol{z}(k_\mathrm{T}) - \mathbf{C}(k)\boldsymbol{x}(k_\mathrm{T})\right] \\ &+ \frac{1}{2}\sum_{k=k_0}^{k_\mathrm{T}-1}\left[\left[\boldsymbol{z}(k) - \mathbf{C}(k)\boldsymbol{x}(k)\right]^\mathsf{T} \mathbf{Q}(k)\left[\boldsymbol{z}(k) - \mathbf{C}(k)\boldsymbol{x}(k)\right] + \boldsymbol{u}^\mathsf{T}(k)\mathbf{R}(k)\boldsymbol{u}(k)\right] \end{aligned} \tag{D.9}$$

D.1.3. Input Constraints

In some cases the inputs ($\boldsymbol{u}(t)$) are constrained. Here the only type of input constraints considered is of the type:

$$\boldsymbol{U}^- \leq \boldsymbol{u}(t) \leq \boldsymbol{U}^+ \rightarrow |\boldsymbol{u}(t)| \leq \boldsymbol{U} \tag{D.10}$$

For simplicity the inputs can also be represented by normalising the inputs with $\boldsymbol{U}$ as :

$$-\mathbf{1} \leq \boldsymbol{u}(t) \leq +\mathbf{1} \rightarrow |\boldsymbol{u}(t)| \leq \mathbf{1} \tag{D.11}$$

or component-wise

$$\left|u_j(t)\right| \leq 1 \quad j = 1, 2, \ldots, r \tag{D.12}$$

D.2. Pontryagin Minimum Principle

Pontryagin principle states that for a plant as described by:

$$\dot{\boldsymbol{x}}(t) = f(\boldsymbol{x}(t), \boldsymbol{u}(t), t) \tag{D.13}$$

, a cost function (performance index) as:

$$J(\boldsymbol{x}(t_0), \boldsymbol{u}, t_0) = S(\boldsymbol{x}(t_\mathrm{f}), t_\mathrm{f}) + \frac{1}{2}\int_{t_0}^{t_\mathrm{f}} V(\boldsymbol{x}(t), \boldsymbol{u}(t), t)\,\mathrm{d}t \tag{D.14}$$

and with fixed initial conditions ($\boldsymbol{x}(t_0) = \boldsymbol{x}_0$) and free final conditions ($t_\mathrm{f}, \boldsymbol{x}(t_\mathrm{f}) = \boldsymbol{x}_\mathrm{f}$), the optimal control is obatined by formulating the Hamiltoninan $\mathscr{H}$ as:

$$\mathscr{H}(\boldsymbol{x}(t), \boldsymbol{u}(t), \boldsymbol{\lambda}(t), t) = V(\boldsymbol{x}(t), \boldsymbol{u}(t), t) + \boldsymbol{\lambda}^\mathsf{T}(t) f(\boldsymbol{x}(t), \boldsymbol{u}(t), t) \tag{D.15}$$

and minimising it with respect to the input $\boldsymbol{u}(t)$:

$$\mathscr{H}\left(\boldsymbol{x}^*(t), \boldsymbol{u}^*(t), \boldsymbol{\lambda}^*(t), t\right) \leq \mathscr{H}\left(\boldsymbol{x}^*(t), \boldsymbol{u}(t), \boldsymbol{\lambda}^*(t), t\right) \tag{D.16}$$

The optimal state trajectories can be calculated by solving the state and costate equations:

$$\dot{\boldsymbol{x}}^*(t) = +\left(\frac{\partial \mathscr{H}}{\partial \boldsymbol{\lambda}}\right)_* \tag{D.17}$$

$$\dot{\boldsymbol{\lambda}}^*(t) = -\left(\frac{\partial \mathscr{H}}{\partial \boldsymbol{x}}\right)_* \tag{D.18}$$

with the boundary conditions $\boldsymbol{x}_0$ and

$$\left[\mathscr{H}^* + \left(\frac{\partial S}{\partial t}\right)\right]_{t_\mathrm{f}} \delta t_\mathrm{f} + \left[\left(\frac{\partial S}{\partial \boldsymbol{x}}\right)_* - \boldsymbol{\lambda}^*(t)\right]_{t_\mathrm{f}}^\mathsf{T} \delta \boldsymbol{x}_\mathrm{f} = 0 \tag{D.19}$$

Eq. (D.16) is a general condition for optimality. For unconstrained systems, this can be reduced to the necessary condition:

$$\left(\frac{\partial \mathscr{H}}{\partial \boldsymbol{u}}\right)_* = \boldsymbol{0} \tag{D.20}$$

and the sufficient condition:

$$\left(\frac{\partial^2 \mathscr{H}}{\partial \boldsymbol{u}^2}\right)_* > \boldsymbol{0} \tag{D.21}$$

The Pontryagin principle for unconstrained and constrained input have been summarised in Tables D.1 and D.2 respectively. The Pontryagin principle for discrete-time control is summarised in Table D.3

Table D.1: Unconstrained Optimal Control Formulation using Pontryagin Minimum Principle

Optimal Control Formulation — Unconstrained

Plant Model

$$\dot{\boldsymbol{x}}(t) = f(\boldsymbol{x}(t), \boldsymbol{u}(t), t)$$

Cost Function

$$J(\boldsymbol{x}(t_0), \boldsymbol{u}, t_0) = S(\boldsymbol{x}(t_\mathrm{f}), t_\mathrm{f}) + \int_{t_0}^{t_\mathrm{f}} V(\boldsymbol{x}(t), \boldsymbol{u}(t), t)\,\mathrm{d}t$$

Hamiltonian

$$\mathscr{H}(\boldsymbol{x}(t), \boldsymbol{u}(t), \boldsymbol{\lambda}(t), t) = V(\boldsymbol{x}(t), \boldsymbol{u}(t), t) + \boldsymbol{\lambda}^\mathsf{T}(t) f(\boldsymbol{x}(t), \boldsymbol{u}(t), t)$$

Optimal Control

$$\left(\frac{\partial \mathscr{H}}{\partial \boldsymbol{u}}\right)_* = \mathbf{0}$$

Canonical System

$$\dot{\boldsymbol{x}}^*(t) = +\left(\frac{\partial \mathscr{H}}{\partial \boldsymbol{\lambda}}\right)_*$$

$$\dot{\boldsymbol{\lambda}}^*(t) = -\left(\frac{\partial \mathscr{H}}{\partial \boldsymbol{x}}\right)_*$$

Boundary Conditions

$$\left[\mathscr{H}^* + \left(\frac{\partial S}{\partial t}\right)\right]_{t_\mathrm{f}} \delta t_\mathrm{f} + \left[\left(\frac{\partial S}{\partial \boldsymbol{x}}\right)_* - \boldsymbol{\lambda}^*(t)\right]_{t_\mathrm{f}}^\mathsf{T} \delta \boldsymbol{x}_\mathrm{f} = 0$$

D.3. Unconstrained Linear-Quadratic Tracking (LQT) — Discrete-Time

From Naidu [2002].

This section looks at the design of a tracking controller for a discrete-time model as in Eq. (D.2) but a time invariant version as:

$$\boldsymbol{x}(k+1) = \mathbf{A}\boldsymbol{x}(k) + \mathbf{B}\boldsymbol{u}(k) \tag{D.22}$$

and a cost function as in Eq. (D.9):

$$\begin{aligned} J(\boldsymbol{x}(k_0), \boldsymbol{u}, k_0) = {} & \frac{1}{2}\left[\boldsymbol{z}(k_\mathrm{T}) - \mathbf{C}\boldsymbol{x}(k_\mathrm{T})\right]^\mathsf{T} \mathbf{F}\left[\boldsymbol{z}(k_\mathrm{T}) - \mathbf{C}\boldsymbol{x}(k_\mathrm{T})\right] \\ & + \frac{1}{2}\sum_{k=k_0}^{k_\mathrm{T}-1}\left[\left[\boldsymbol{z}(k) - \mathbf{C}\boldsymbol{x}(k)\right]^\mathsf{T} \mathbf{Q}\left[\boldsymbol{z}(k) - \mathbf{C}\boldsymbol{x}(k)\right] + \boldsymbol{u}^\mathsf{T}(k)\mathbf{R}\boldsymbol{u}(k)\right] \end{aligned} \tag{D.23}$$

D.3.1. Hamiltonian

The Hamiltonian for the system in Eq. (D.1) with the cost function Eq. (D.7) is :

Table D.2: Constrained Optimal Control Formulation using Pontryagin Minimum Principle

Optimal Control Formulation — Constrained

Plant Model

$$\dot{\boldsymbol{x}}(t) = f\left(\boldsymbol{x}(t), \boldsymbol{u}(t), t\right)$$

Cost Function

$$J\left(\boldsymbol{x}(t_0), \boldsymbol{u}, t_0\right) = S\left(\boldsymbol{x}(t_\mathrm{f}), t_\mathrm{f}\right) + \int_{t_0}^{t_\mathrm{f}} V\left(\boldsymbol{x}(t), \boldsymbol{u}(t), t\right) \mathrm{d}t$$

Hamiltonian

$$\mathscr{H}\left(\boldsymbol{x}(t), \boldsymbol{u}(t), \boldsymbol{\lambda}(t), t\right) = V\left(\boldsymbol{x}(t), \boldsymbol{u}(t), t\right) + \boldsymbol{\lambda}^\mathsf{T}(t) f\left(\boldsymbol{x}(t), \boldsymbol{u}(t), t\right)$$

Optimal Control

$$\mathscr{H}\left(\boldsymbol{x}^*(t), \boldsymbol{u}^*(t), \boldsymbol{\lambda}^*(t), t\right) \leq \mathscr{H}\left(\boldsymbol{x}^*(t), \boldsymbol{u}(t), \boldsymbol{\lambda}^*(t), t\right)$$

Canonical System

$$\dot{\boldsymbol{x}}^*(t) = +\left(\frac{\partial \mathscr{H}}{\partial \boldsymbol{\lambda}}\right)_*$$

$$\dot{\boldsymbol{\lambda}}^*(t) = -\left(\frac{\partial \mathscr{H}}{\partial \boldsymbol{x}}\right)_*$$

Boundary Conditions

$$\left[\mathscr{H}^* + \left(\frac{\partial S}{\partial t}\right)\right]_{t_\mathrm{f}} \delta t_\mathrm{f} + \left[\left(\frac{\partial S}{\partial \boldsymbol{x}}\right)_* - \boldsymbol{\lambda}^*(t)\right]_{t_\mathrm{f}}^\mathsf{T} \delta \boldsymbol{x}_\mathrm{f} = 0$$

$$\begin{aligned}\mathscr{H}\left(\boldsymbol{x}(k), \boldsymbol{u}(k), \boldsymbol{\lambda}(k+1)\right) = \frac{1}{2}\left[\boldsymbol{z}(k) - \mathbf{C}\boldsymbol{x}(k)\right]^\mathsf{T} \mathbf{Q}\left[\boldsymbol{z}(k) - \mathbf{C}\boldsymbol{x}(k)\right] + \frac{1}{2}\boldsymbol{u}^\mathsf{T}(k)\mathbf{R}\boldsymbol{u}(k) \\ + \boldsymbol{\lambda}^\mathsf{T}(k+1)\left[\mathbf{A}\boldsymbol{x}(k) + \mathbf{B}\boldsymbol{u}(k)\right]\end{aligned} \tag{D.24}$$

D.3.2. Optimal Control

The realtion for optimal control for the unconstrained discrete-time tracking problem with the hamiltonian Eq. (D.24) is :

$$\left(\frac{\partial \mathscr{H}}{\partial \boldsymbol{u}}\right)_* = \mathbf{0} \implies \mathbf{R}\boldsymbol{u}(k) + \mathbf{B}^\mathsf{T}\boldsymbol{\lambda}(K+1) = 0 \tag{D.25}$$

So the optimal input is:

$$\boldsymbol{u}^*(k) = -\mathbf{R}^{-1}\mathbf{B}^\mathsf{T}\boldsymbol{\lambda}^*(k+1) \tag{D.26}$$

D.3.3. Canonical System

The state relation for the optimal solution is obtained from the Hamiltonian as:

Table D.3: Unconstrained Discrete-Time Optimal Control Formulation using Pontryagin Minimum Principle

Discrete-Time Optimal Control Formulation — Unconstrained

Plant Model

$$\boldsymbol{x}(k+1) = f\left(\boldsymbol{x}(k), \boldsymbol{u}(k), k\right)$$

Cost Function

$$J\left(\boldsymbol{x}(k_0), \boldsymbol{u}, k_0\right) = S\left(\boldsymbol{x}(k_\mathrm{T}), k_\mathrm{T}\right) + \sum_{k=k_0}^{k_\mathrm{T}-1} V\left(\boldsymbol{x}(k), \boldsymbol{u}(k), k\right)$$

Hamiltonian

$$\mathscr{H}\left(\boldsymbol{x}(k), \boldsymbol{u}(k), \boldsymbol{\lambda}(k+1), k\right) = V\left(\boldsymbol{x}(k), \boldsymbol{u}(k), k\right) + \boldsymbol{\lambda}^\mathsf{T}(k+1) f\left(\boldsymbol{x}(k), \boldsymbol{u}(k), k\right)$$

Optimal Control

$$\left(\frac{\partial \mathscr{H}}{\partial \boldsymbol{u}(k)}\right)_* = \boldsymbol{0}$$

Canonical System

$$\boldsymbol{x}^*(k+1) = \left(\frac{\partial \mathscr{H}^*}{\partial \boldsymbol{\lambda}^*(k+1)}\right)$$

$$\dot{\boldsymbol{\lambda}}^*(k) = \left(\frac{\partial \mathscr{H}^*}{\partial \boldsymbol{x}^*(k)}\right)$$

Boundary Conditions for free x_f and fixed k_T

$$\left[\left(\frac{\partial S\left(\boldsymbol{x}^*(k), k\right)}{\partial \boldsymbol{x}^*(k)}\right) - \boldsymbol{\lambda}^*(k)\right]_{k_\mathrm{T}}^\mathsf{T} \delta \boldsymbol{x}_\mathrm{f} = 0$$

$$\boldsymbol{x}^*(k+1) = \frac{\partial \mathscr{H}}{\partial \boldsymbol{\lambda}^*(k+1)} = \mathbf{A}\boldsymbol{x}^*(k) + \mathbf{B}\boldsymbol{u}^*(k) \tag{D.27}$$

Substituting for the optimal input $\boldsymbol{u}^*(t)$ from Eq. (D.26), gives:

$$\boldsymbol{x}^*(k+1) = \mathbf{A}\boldsymbol{x}^*(k) - \mathbf{B}\mathbf{R}^{-1}\mathbf{B}^\mathsf{T}\boldsymbol{\lambda}^*(k+1) \tag{D.28}$$

The costate relation is obtained from the Hamiltonian as:

$$\boldsymbol{\lambda}^*(k) = \frac{\partial \mathscr{H}}{\partial \boldsymbol{x}^*(k)} = \mathbf{A}^\mathsf{T}\boldsymbol{\lambda}^*(k+1) + \mathbf{C}^\mathsf{T}\mathbf{Q}\mathbf{C}\boldsymbol{x}^*(k) - \mathbf{C}^\mathsf{T}\mathbf{Q}\boldsymbol{z}(k) \tag{D.29}$$

Thus Eqs. (D.28) and (D.29) give the canonical system:

$$\begin{bmatrix} \boldsymbol{x}^*(k+1) \\ \boldsymbol{\lambda}^*(k) \end{bmatrix} = \begin{bmatrix} \mathbf{A} & -\mathbf{E} \\ \mathbf{V} & \mathbf{A}^\mathsf{T} \end{bmatrix} \begin{bmatrix} \boldsymbol{x}^*(k) \\ \boldsymbol{\lambda}^*(k+1) \end{bmatrix} + \begin{bmatrix} \mathbf{0} \\ -\mathbf{W}(t) \end{bmatrix} \boldsymbol{z}(t) \tag{D.30}$$

where,

$$\mathbf{E} = \mathbf{B}\mathbf{R}^{-1}\mathbf{B}^\mathsf{T} \qquad \mathbf{V} = \mathbf{C}^\mathsf{T}\mathbf{Q}\mathbf{C} \qquad \mathbf{W} = \mathbf{C}^\mathsf{T}\mathbf{Q} \tag{D.31}$$

The solution for the state must satisfy the boundary condition ($\boldsymbol{x}(t_0) = \boldsymbol{x}_0$). Since the final time is fixed and the final state is free, the solution for the costate must satisfy the boundary condition:

$$\begin{aligned} \boldsymbol{\lambda}^*(k_\mathrm{T}) &= \left(\frac{\partial S(\boldsymbol{x}^*(k), k)}{\partial \boldsymbol{x}^*(k)} \right) \\ &= \left(\frac{\partial \left[\frac{1}{2} [\boldsymbol{z}(k_\mathrm{T}) - \mathbf{C}\boldsymbol{x}(k_\mathrm{T})]^\mathsf{T} \mathbf{F} [\boldsymbol{z}(k_\mathrm{T}) - \mathbf{C}\boldsymbol{x}(k_\mathrm{T})] \right]}{\partial \boldsymbol{x}(k_\mathrm{T})} \right) \\ &= \mathbf{C}^\mathsf{T}\mathbf{F}\mathbf{C}\boldsymbol{x}^*(k_\mathrm{T}) - \mathbf{C}^\mathsf{T}\mathbf{F}\boldsymbol{z}(t_\mathrm{f}) \end{aligned} \tag{D.32}$$

D.3.4. Matrix Difference Riccati Equation and Vector Difference Equation

Let us assume a transformation between the states and costates as:

$$\boldsymbol{\lambda}^*(k) = \mathbf{P}(k)\boldsymbol{x}^*(k) - \boldsymbol{g}(k) \tag{D.33}$$

This transform is inspired from the structure of the boundary condition Eq. (D.32).
Eliminating $\boldsymbol{\lambda}^*$ from the expression for $\boldsymbol{x}^*$ from Eq. (D.30) using Eq. (D.33) gives:

$$\boldsymbol{x}^*(k+1) = \mathbf{A}\boldsymbol{x}^*(k) - \mathbf{E}\mathbf{P}(k+1)\boldsymbol{x}^*(k+1) + \mathbf{E}\boldsymbol{g}(k+1) \tag{D.34}$$

Collecting all the terms with $\boldsymbol{x}^*(k+1)$,

$$[\mathbf{I} + \mathbf{E}\mathbf{P}(k+1)]\,\boldsymbol{x}^*(k+1) = \mathbf{A}\boldsymbol{x}^*(k) + \mathbf{E}\boldsymbol{g}(k+1) \tag{D.35}$$

Solving for $\boldsymbol{x}^*(k+1)$,

$$\boldsymbol{x}^*(k+1) = [\mathbf{I} + \mathbf{E}\mathbf{P}(k+1)]^{-1} \left[\mathbf{A}\boldsymbol{x}^*(k) + \mathbf{E}\boldsymbol{g}(k+1) \right] \tag{D.36}$$

Substituting for $\boldsymbol{x}^*(k+1)$ and $\boldsymbol{\lambda}^*(k+1)$ from Eqs. (D.33) and (D.36) into the co-state relation from Eq. (D.30):

$$\begin{aligned} \mathbf{P}(k)\boldsymbol{x}^*(k) - \boldsymbol{g}(k) &= \mathbf{V}\boldsymbol{x}^*(k) + \mathbf{A}^\mathsf{T}\left[\mathbf{P}(k+1)\boldsymbol{x}^*(k+1) - \boldsymbol{g}(k+1) \right] - \mathbf{W}\boldsymbol{z}(k) \\ &= \mathbf{V}\boldsymbol{x}^*(k) + \mathbf{A}^\mathsf{T}\mathbf{P}(k+1)\boldsymbol{x}^*(k+1) - \mathbf{A}^\mathsf{T}\boldsymbol{g}(k+1) - \mathbf{W}\boldsymbol{z}(k) \\ &= \mathbf{V}\boldsymbol{x}^*(k) + \mathbf{A}^\mathsf{T}\mathbf{P}(k+1)\,[\mathbf{I} + \mathbf{E}\mathbf{P}(k+1)]^{-1} \left[\mathbf{A}\boldsymbol{x}^*(k) + \mathbf{E}\boldsymbol{g}(k+1) \right] \\ &\quad - \mathbf{A}^\mathsf{T}\boldsymbol{g}(k+1) - \mathbf{W}\boldsymbol{z}(k) \end{aligned} \tag{D.37}$$

Rearranging,

$$\begin{aligned} \left[-\mathbf{P}(k) + \mathbf{A}^\mathsf{T}\mathbf{P}(k+1)\,[\mathbf{I} + \mathbf{E}\mathbf{P}(k+1)]^{-1}\mathbf{A} + \mathbf{V} \right] \boldsymbol{x}^*(k) \quad + \\ \left[\boldsymbol{g}(k) + \mathbf{A}^\mathsf{T}\mathbf{P}(k+1)\,[\mathbf{I} + \mathbf{E}\mathbf{P}(k+1)]^{-1}\mathbf{E}\boldsymbol{g}(k+1) - \mathbf{A}^\mathsf{T}\boldsymbol{g}(k+1) - \mathbf{W}\boldsymbol{z}(k) \right] \quad = \mathbf{0} \end{aligned} \tag{D.38}$$

Which can be simplifed as:

$$\begin{aligned}\left[-\mathbf{P}(k)+\mathbf{A}^{\mathsf{T}}\left[\mathbf{P}^{-1}(k+1)+\mathbf{E}\right]^{-1}\mathbf{A}+\mathbf{V}\right]\boldsymbol{x}^{*}(k) \quad + \\ \left[\boldsymbol{g}(k)+\mathbf{A}^{\mathsf{T}}\left[\mathbf{P}^{-1}(k+1)+\mathbf{E}\right]^{-1}\mathbf{E}\boldsymbol{g}(k+1)-\mathbf{A}^{\mathsf{T}}\boldsymbol{g}(k+1)-\mathbf{W}\boldsymbol{z}(k)\right] \quad =\mathbf{0}\end{aligned} \tag{D.39}$$

Now Eq. (D.39) should hold for all $\boldsymbol{x}^{*}(k)$, $\boldsymbol{z}(k)$ and k. This condition leads to the matrix difference equation:

$$\boxed{\mathbf{P}(k)=\mathbf{A}^{\mathsf{T}}\left[\mathbf{P}^{-1}(k+1)+\mathbf{E}\right]^{-1}\mathbf{A}+\mathbf{V}} \tag{D.40}$$

and the vector difference equation:

$$\boxed{\boldsymbol{g}(k)=\mathbf{A}^{\mathsf{T}}\left\{\mathbf{I}-\left[\mathbf{P}^{-1}(k+1)+\mathbf{E}\right]^{-1}\mathbf{E}\right\}\boldsymbol{g}(k+1)+\mathbf{W}\boldsymbol{z}(k)} \tag{D.41}$$

From Eq. (D.33), the boundary condition at k_{T} is :

$$\boldsymbol{\lambda}^{*}(k_{\mathrm{T}})=\mathbf{P}(k_{\mathrm{T}})\boldsymbol{x}^{*}(k_{\mathrm{T}})-\boldsymbol{g}(k_{\mathrm{T}}) \tag{D.42}$$

Comparing Eqs. (D.32) and (D.42) gives the following boundary conditions of $\mathbf{P}(k_{\mathrm{T}})$ and $\boldsymbol{g}(k_{\mathrm{T}})$ for all $\boldsymbol{x}(k_{\mathrm{T}})$ and $\boldsymbol{z}(k_{\mathrm{T}})$:

$$\boxed{\mathbf{P}(k_{\mathrm{T}})=\mathbf{C}^{\mathsf{T}}\mathbf{F}\mathbf{C}} \tag{D.43}$$

$$\boxed{\boldsymbol{g}(k_{\mathrm{T}})=\mathbf{C}^{\mathsf{T}}\mathbf{F}\boldsymbol{z}(k_{\mathrm{T}})} \tag{D.44}$$

From Eqs. (D.26) and (D.33), the optimal input is :

$$\boldsymbol{u}^{*}(t)=-\mathbf{R}^{-1}\mathbf{B}^{\mathsf{T}}\mathbf{P}(k+1)\boldsymbol{x}^{*}(k+1)+\mathbf{R}^{-1}\mathbf{B}^{\mathsf{T}}\boldsymbol{g}(k+1) \tag{D.45}$$

Substituting for $\boldsymbol{x}^{*}(k+1)$ from Eq. (D.27) gives:

$$\boldsymbol{u}^{*}(t)=-\mathbf{R}^{-1}\mathbf{B}^{\mathsf{T}}\mathbf{P}(k+1)\left[\mathbf{A}\boldsymbol{x}^{*}(k)+\mathbf{B}\boldsymbol{u}^{*}(k)\right]+\mathbf{R}^{-1}\mathbf{B}^{\mathsf{T}}\boldsymbol{g}(k+1) \tag{D.46}$$

Premultiplying by $\mathbf{R}$ and rearranging :

$$\boldsymbol{u}^{*}(t)\left[\mathbf{R}+\mathbf{B}^{\mathsf{T}}\mathbf{P}(k+1)\mathbf{B}\right]=-\mathbf{B}^{\mathsf{T}}\mathbf{P}(k+1)\mathbf{A}\boldsymbol{x}^{*}(k)+\mathbf{B}^{\mathsf{T}}\boldsymbol{g}(k+1) \tag{D.47}$$

This gives the relation for the optimal input $\boldsymbol{u}^{*}(k)$ as:

$$\boxed{\boldsymbol{u}^{*}(t)=-\mathbf{L}(k)\boldsymbol{x}^{*}(k)+\mathbf{L}_{g}(k)\boldsymbol{g}(k+1)} \tag{D.48}$$

where,

$$\mathbf{L}(k)=\left[\mathbf{R}+\mathbf{B}^{\mathsf{T}}\mathbf{P}(k+1)\mathbf{B}\right]^{-1}\mathbf{B}^{\mathsf{T}}\mathbf{P}(k+1)\mathbf{A} \tag{D.49}$$

$$\mathbf{L}_{g}(k)=\left[\mathbf{R}+\mathbf{B}^{\mathsf{T}}\mathbf{P}(k+1)\mathbf{B}\right]^{-1}\mathbf{B}^{\mathsf{T}} \tag{D.50}$$

Substituting for $\boldsymbol{u}^{*}(t)$ from Eq. (D.48) into Eq. (D.27), gives:

$$\boxed{\boldsymbol{x}^{*}(k+1)=\left[\mathbf{A}-\mathbf{B}\mathbf{L}(k)\right]\boldsymbol{x}^{*}(k)+\mathbf{B}\mathbf{L}_{g}(k)\boldsymbol{g}(k+1)} \tag{D.51}$$

Table D.4: Steps for Discrete-Time Linear Quadratic Tracking with Unconstrained Input

Discrete-Time Linear Quadratic Tracking with Unconstrained Input

Step 1:

Solve the matrix difference Riccati equation Eq. (D.40)

$$\mathbf{P}(k) = \mathbf{A}^{\mathsf{T}} \left[\mathbf{P}^{-1}(k+1) + \mathbf{E}\right]^{-1} \mathbf{A} + \mathbf{V}$$

with final condition Eq. (D.43)

$$\mathbf{P}(k_{\mathrm{T}}) = \mathbf{C}^{\mathsf{T}} \mathbf{F} \mathbf{C}$$

and the vector difference equation Eq. (D.41)

$$\boldsymbol{g}(k) = \mathbf{A}^{\mathsf{T}} \left\{\mathbf{I} - \left[\mathbf{P}^{-1}(k+1) + \mathbf{E}\right]^{-1} \mathbf{E}\right\} \boldsymbol{g}(k+1) + \mathbf{W}\boldsymbol{z}(k)$$

with the boundary condition Eq. (D.44):

$$\boldsymbol{g}(k_{\mathrm{T}}) = \mathbf{C}^{\mathsf{T}} \mathbf{F} \boldsymbol{z}(k_{\mathrm{T}})$$

where,

$$\mathbf{E} = \mathbf{B}\mathbf{R}^{-1}\mathbf{B}^{\mathsf{T}} \quad \mathbf{V} = \mathbf{C}^{\mathsf{T}}\mathbf{Q}\mathbf{C} \quad \mathbf{W} = \mathbf{C}^{\mathsf{T}}\mathbf{Q}$$

Step 2:

Solve for the optimal state $\boldsymbol{x}^*(t)$ from Eq. (D.51):

$$\boldsymbol{x}^*(k+1) = [\mathbf{A} - \mathbf{B}\mathbf{L}(k)]\, \boldsymbol{x}^*(k) + \mathbf{B}\mathbf{L}_g(k)\boldsymbol{g}(k+1)$$

with the initial condition

$$\boldsymbol{x}(t_0) = \boldsymbol{x}_0$$

where,

$$\mathbf{L}(k) = \left[\mathbf{R} + \mathbf{B}^{\mathsf{T}}\mathbf{P}(k+1)\mathbf{B}\right]^{-1} \mathbf{B}^{\mathsf{T}}\mathbf{P}(k+1)\mathbf{A}$$
$$\mathbf{L}_g(k) = \left[\mathbf{R} + \mathbf{B}^{\mathsf{T}}\mathbf{P}(k+1)\mathbf{B}\right]^{-1} \mathbf{B}^{\mathsf{T}}$$

Step 3:

The optimal control $\boldsymbol{u}^*(t)$ is obtained from Eq. (D.48) as :

$$\boldsymbol{u}^*(t) = -\mathbf{L}(k)\boldsymbol{x}^*(k) + \mathbf{L}_g(k)\boldsymbol{g}(k+1)$$

E

Experimental Results - Addendum

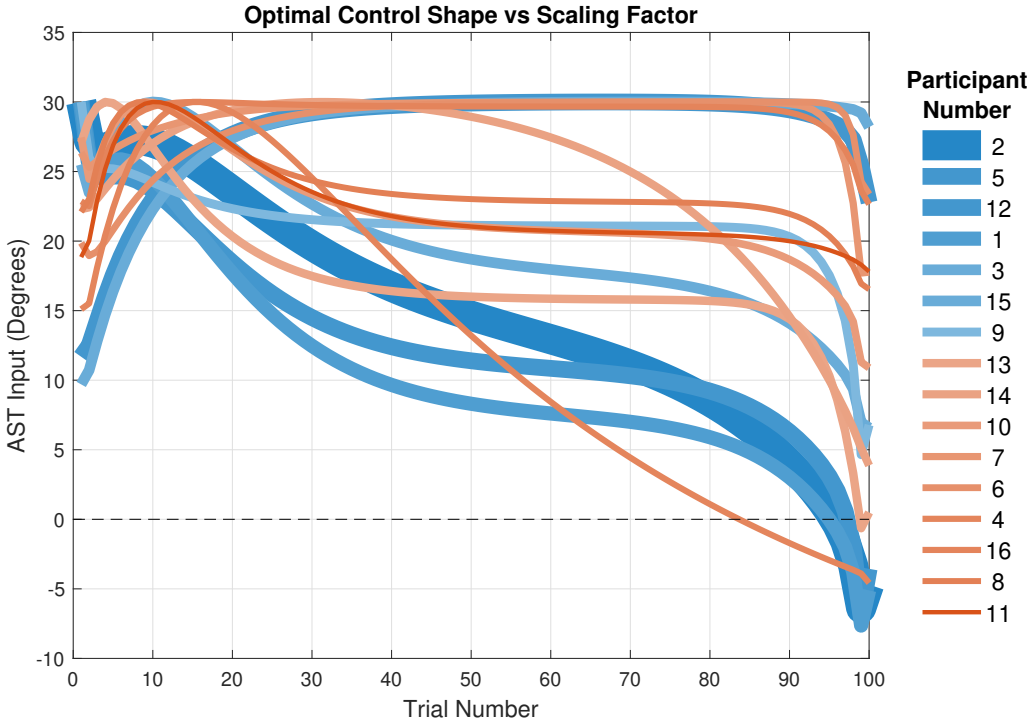

Figure E.1: AST Input vs Scaling. The participants are sorted in ascending order of the scaling factor (with Participant 2 having the smallest scaling factor). The thickness of each line is inversely proportional to the scaling factor.

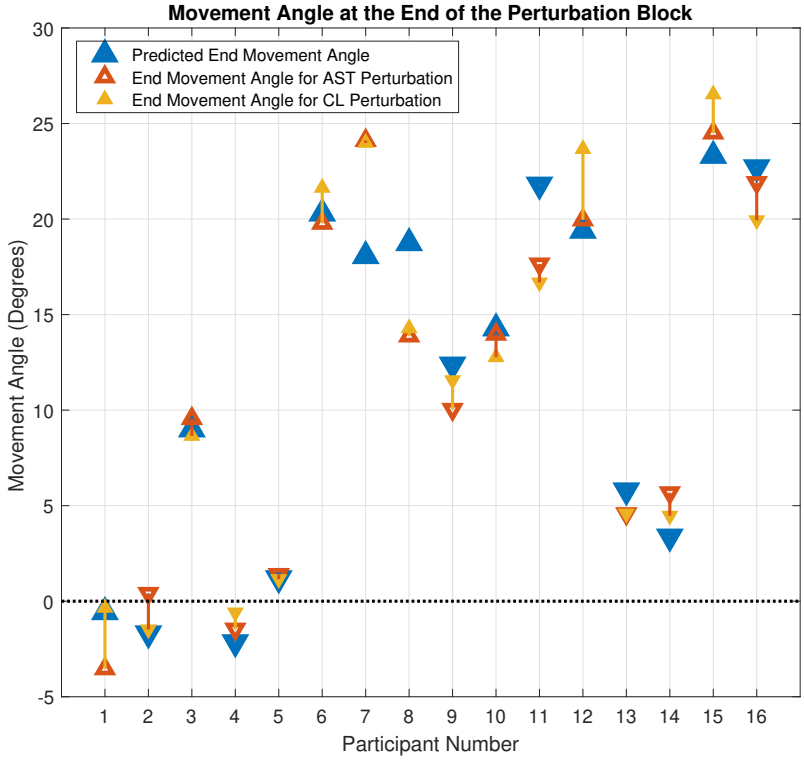

Figure E.2: End Movement Angles (Predicted and Actual)

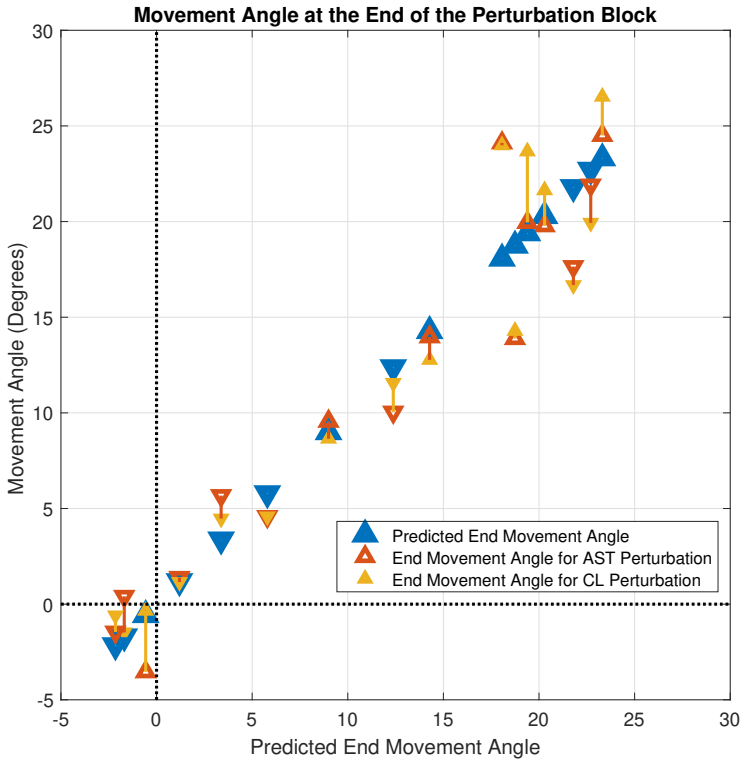

Figure E.3: End Movement Angles Vs Predicted End Movement Angles

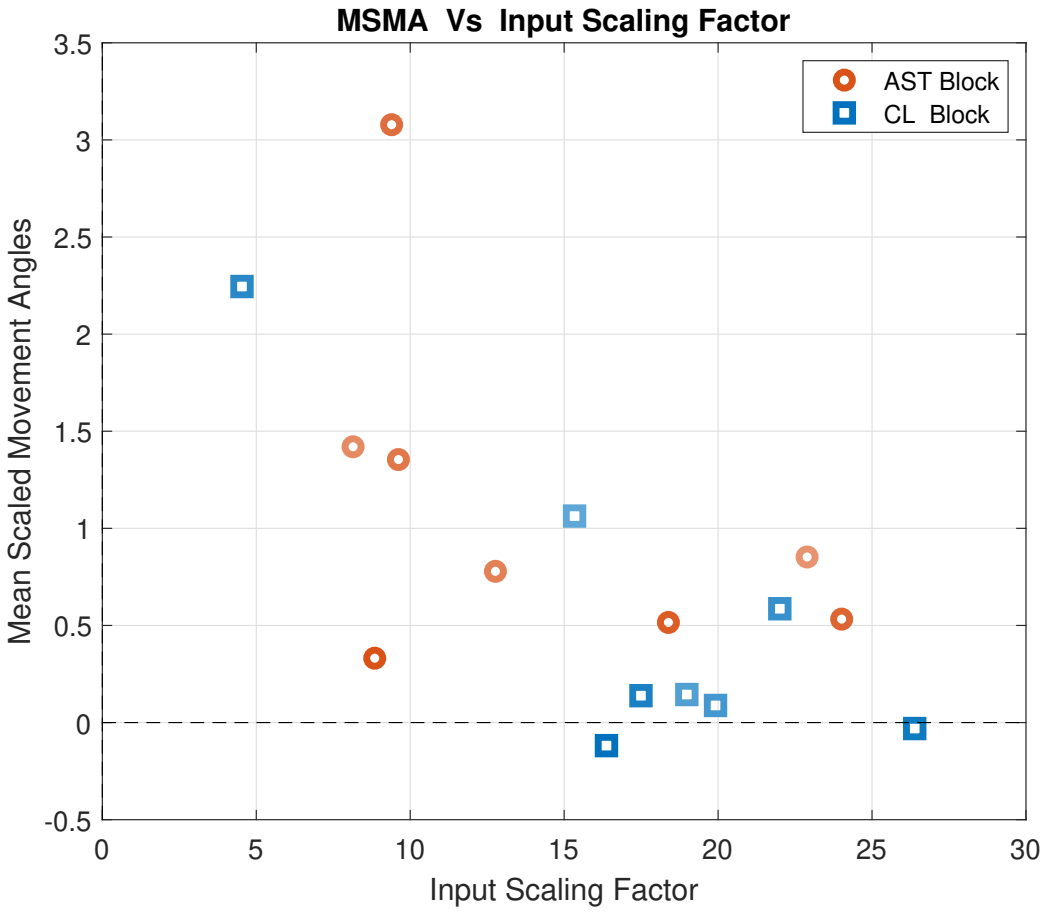

Figure E.4: MSMA Vs Input Scaling Factor

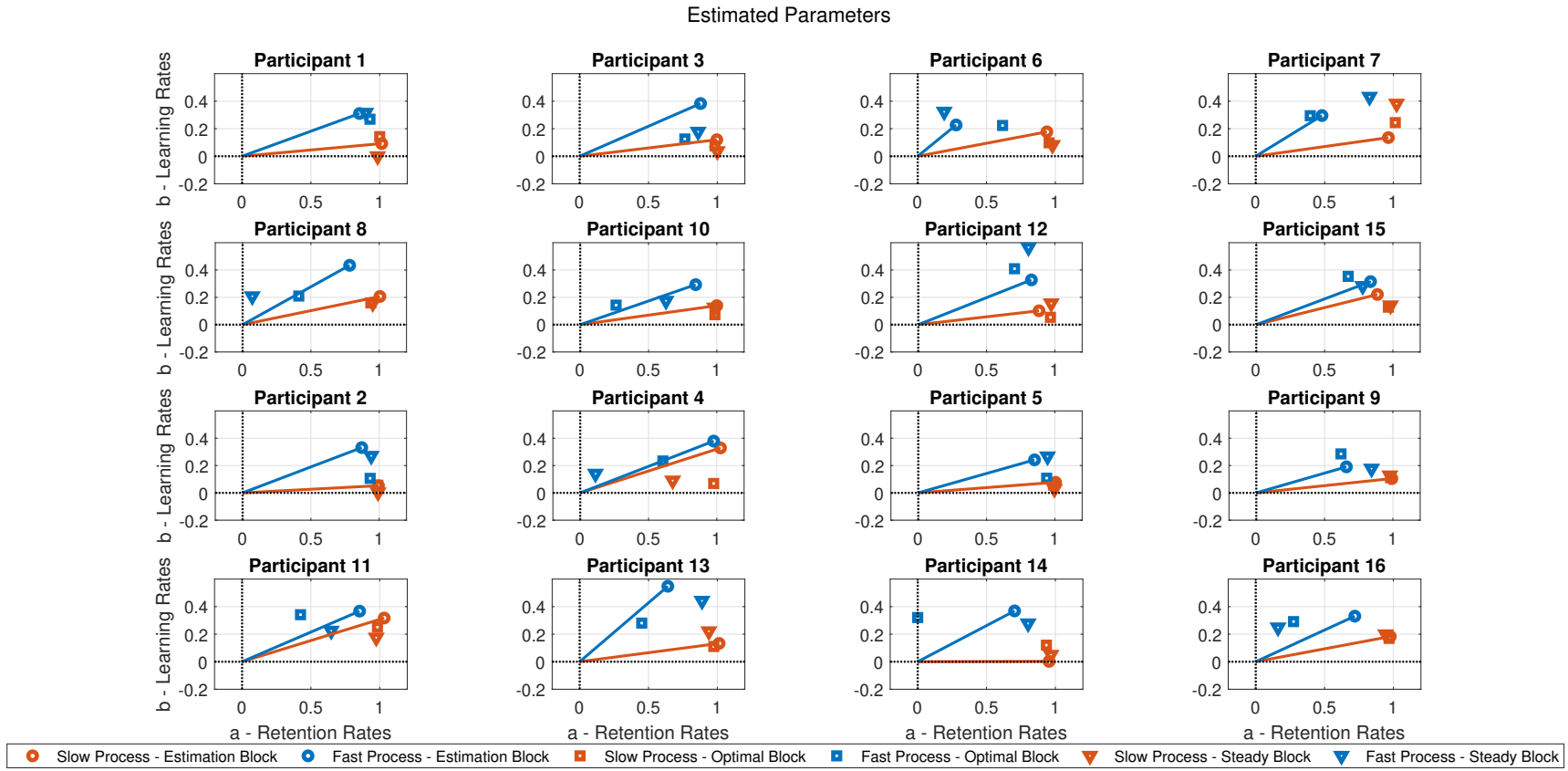

Figure E.5: Estimated Parameters

Acknowledgements

Thanks to God Almighty for all the nudges toward the global optimum.

I want to express my heartfelt gratitude to my parents, grandparents, and brother for being a constant source of support and motivation.

I am deeply indebted to Prof. Heike Vallery for giving me the opportunity to work on this exciting topic and for all the guidance throughout the project. Her feedback was instrumental for the formulation of the optimal control. I am also immensely grateful to Prof. Maarten Frens for giving me access to the facilities at Erasmus MC Rotterdam where the experiments were conducted and for providing valuable insights regarding the neuroscientific aspects of the research. Zeb Jonker played a major role in the initial stages of the research when I was trying to understand the neuroscience related to rehabilitation. His help in designing and conducting experiments was invaluable. I am extremely grateful for these. My sincere gratitude to Andrew Berry for the time he spent in reviewing my manuscript. I am also thankful for all the suggestions regarding the control side of the project and all the timely feedback pertaining to administrative matters throughout the whole graduation project. I am grateful to Dr. Thomas Jan Hulst, Carolin Gaiser and Rick van der Vliet for the help in conducting experiments and data processing. A big thanks to all the participants in the experiment, many of whom commuted to Rotterdam to be a part of the experiment.

I want to express my gratitude to Aneesh Ashok Kumar for all the help, support, motivation, and the sense of camaraderie throughout my master's programme in BioRobotics. I am also grateful to Rahul Ramesh for all the wonderful conversations we had regarding research in BioRobotics and other exciting matters. Both Aneesh and Rahul played a major role in reviewing the initial drafts of the manuscript. Thank you Aneesh and Rahul for all the help and the wonderful discussions which were a constant source of motivation. To all my friends from BioMechanical Design, BioMedical Engineering, the library and the Malayalee community, you guys made my time in Delft colourful and vibrant. I am much obliged. A word of thanks to Hari Prasanth, Aswin Muralidharan, Govind Rajanbabu Nharekkat, Aruna Nair and Albin Prince John for many uplifting talks and for making me passionate about research. Thank you, Sachin Menon and Jitin Gopakumar, for being wonderful housemates and for replenishing my disposition with loads of soul food, card games and movies (especially during the great lockdown of 2020).

Ashwin George
Delft, July 2020